

**Universidade de Évora - Instituto de Investigação e Formação Avançada
Università di Roma La Sapienza Aristotle University of Thessaloniki**

Mestrado em Ciência dos Materiais Arqueológicos (ARCHMAT)

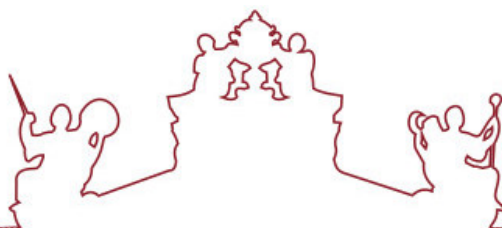
Dissertação

ISLAMIC CERAMICS: TRADE AND TECHNOLOGY IN THE SOUTHERN GARB AL-ANDALUS (X-XI CENTURY)

Carlos Andrés Camara Vela

Orientador(es) | Jose Mirao
Massimo Beltrame
Susana Gómez Martínez

Évora 2021



**Universidade de Évora - Instituto de Investigação e Formação Avançada
Università di Roma La Sapienza Aristotle University of Thessaloniki**

Mestrado em Ciência dos Materiais Arqueológicos (ARCHMAT)

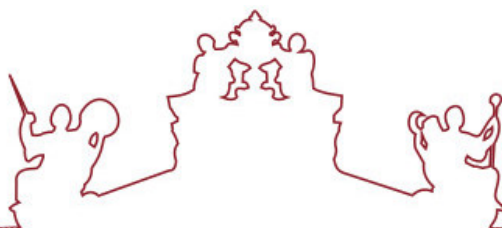
Dissertação

ISLAMIC CERAMICS: TRADE AND TECHNOLOGY IN THE SOUTHERN GARB AL-ANDALUS (X-XI CENTURY)

Carlos Andrés Camara Vela

Orientador(es) | Jose Mirao
Massimo Beltrame
Susana Gómez Martínez

Évora 2021



A dissertação foi objeto de apreciação e discussão pública pelo seguinte júri nomeado pelo Diretor do Instituto de Investigação e Formação Avançada:

Presidente | Nicola Schiavon (Universidade de Évora)

Vogais | Christos Karydis (Aristotle University of Thessaloniki)
Georgios Zachariadis (Aristotle University of Thessaloniki)
Jose Mirao (Universidade de Évora) (Orientador)
Marcello Vitale (Università di Roma La Sapienza)
Mathilda Coutinho (Universidade de Évora) (Arguente)
Susana Gómez Martínez (Universidade de Évora) (Orientador)

**Islamic ceramics: trade and technology in the southern
Garb al-Andalus (X-XI century)**

Carlos Andrés Camara Vela

RESUMO

Cerâmica Islâmica: comércio e tecnologia no sul do Gharb al-Andalus (Seculos X-XI)

A produção de cerâmica vidrada na Península Ibérica foi generalizada durante o período islâmico. Durante este período, a técnica do vidrado era caracterizada pelo uso de chumbo como principal fundente, para além de coexistirem outras práticas tais como a utilização de fritas e aplicação de soluções de esmalte sobre os corpos cerâmicos calcários cozidos. O principal objetivo do presente estudo é comparar a produção de cerâmica vidrada em Évora com outras cidades, tais como Mértola e Silves, a fim de identificar padrões de produção, contactos regionais e a proveniência dos materiais durante a ocupação Islâmica. Assim, seleccionou-se um conjunto de exemplares constituídos por vidrados monocromáticos e de decoração melada e manganês desses três locais, sendo este submetido a análises multi-elementares. Microscopia ótica (OM), difração raio-X (XRD) e fluorescência de raio-X (XRF) foram as análises aplicadas para determinar as características das pastas cerâmicas, assim como o processo de produção e a proveniência das matérias-primas. O recurso ao Microscópio Eletrónico de Varrimento acoplado a um Espectrómetro Dispersivo de Energia (SEM-EDS) foi crucial para determinar a microestrutura e a composição química do vidrado e da decoração a manganês, a fim de avaliar a técnica de produção do vidrado.

Palavras-chave: período Islâmico, produção de cerâmica vidrada, contactos regionais, proveniência.

ABSTRACT

Islamic ceramics: trade and technology in the southern Gharb al-Andalus (X-XI century)

Glazed pottery production in the Iberian Peninsula was widespread during the Islamic period. During this time, the glaze recipe was characterized for the main use of lead as flux, besides other common practice such as the employment of frits and the application of the glaze suspension over biscuit-fired calcareous ceramic bodies. The main goal of the present study is to compare the glazed pottery production in Évora with other cities, such as Mértola and Silves, for identifying patterns of production, regional contacts and provenance of the products during the Islamic occupation. Thereby, a set of specimens which consist of monochromatic and black-decorated dichromatic honey glazes and coarsewares were retrieved from those three places and subjected to multi-elemental analysis. Optical Microscopy (OM), X-ray Diffraction (XRD), X-ray Fluorescence (XRF) analyses were applied to determine the ceramic bodies characteristics, shedding light on the production process and the provenance of the raw materials. Scanning Electron Microscope coupled to an Energy Dispersive Spectrometer (SEM-EDS) analysis were used to determine the microstructure and the chemical composition of the glaze and black decoration to evaluate glaze technology.

Keywords: Islamic period, glazed pottery production, regional contacts, provenance.

ACKNOWLEDGEMENTS

This M. A. thesis would not have been possible without the constant support and motivation of my family, colleagues and friends.

I would like to thank my main supervisors for their valuable advices when they were required. My knowledge about glazed ceramic and the Islamic world was filled profoundly from their suggestions and directions during this time of the thesis elaboration, full of questions and doubts. I am extremely grateful to prof. José Antonio Paulo Mirão for sharing important information about petrography analysis and analytical techniques, two themes in which I am more familiar now. My great thanks go to prof. Susana Gómez Martínez for introducing me into the current Islamic glazed pottery production debate in the Iberian Peninsula, for supporting me and gave me the opportunity to visit the Parque Arqueológico of Mértola and checking essential references. Last but not least, I would like to thank to Massimo Beltrame, every step of this thesis process, from the arduous specimen preparation to the interpretation of the results and discussion, was monitored through his constant correction and advice. I appreciate a lot.

I would also like to thank Prof. Nick Schiavon and the ARCHMAT EMMC International Selection Committee for accepting me in this master programme and all the professors that contribute to acquire the knowledge and to develop the skills required for archaeometric research.

As well, during this process valuable people crossed my way and contributed essentially from their particular point of view about different topics. From the very beginning when I started drawing the ceramic pieces in the archaeological lab, the presence of Inês Amaral was really supportive and friendly. Researchers from Hercules Lab such as Pedro Barrulas, Mafalda Costa, Luis Diaz, Ana Cardoso, Silvia Scardina and Fabio Sitzia, with whom I shared small talks about chemistry, were part of this process and I will be totally grateful for meeting them. I am also deeply grateful to all my friends from Perú and buddies from all over the world, whom I met in this ARCHMAT master programme, for their constant encouragement and backing.

TABLE OF CONTENTS

List of Illustrations.....	<i>I</i>
List of Tables.....	<i>V</i>
Chapter 1: Introduction	1
1.1 Main Objectives.....	2
Chapter 2: Research Background	3
2.1 Historical Context.....	3
2.2 Geological Setting.....	5
2.2.1 Évora.....	5
2.2.2 Mértola.....	6
2.2.3 Silves.....	7
2.3 Glazed Pottery Production During Islamic Period.....	8
2.3.1 Ceramic Technology.....	8
2.3.2 Glazed Ceramic Technology.....	10
2.3.3 Black Decoration.....	14
2.3.4 Archaeological Evidences.....	14
Chapter 3: Typology and Chronology	19
3.1 Archaeological Contexts and Materials.....	19
Chapter 4: Instrumentation	36
4.1 Optical Microscopy (OM).....	36
4.2 X-Ray Diffraction (XRD).....	37
4.3 X-Ray Fluorescence Spectroscopy (XRF).....	39
4.4 Scanning Electron Microscope coupled to an Energy Dispersive Spectrometer (SEM-EDS).....	41
Chapter 5: Methods	43
5.1 Specimen Preparation Process.....	43
5.2 Instrumental Conditions and Methods.....	50
Chapter 6: Results and Discussion	52
6.1 Chronology and Typology.....	52
6.2 Optical Microscopy (OM).....	54
6.3 X-Ray Diffraction (XRD).....	66
6.4 X-Ray Fluorescence (XRF).....	70
6.5 SEM-EDS.....	73
Chapter 7: Final Remarks	92
Chapter 8: Appendices	95
8.1 Appendix I.....	95
Chapter 9: References	107

LIST OF ILLUSTRATIONS

Figure 1: The western expansion of Islam during the first decades of 8 th century.	3
Figure 2: Map of the Iberian Peninsula and the geographical location of the cities from where the analysed materials were retrieved.	5
Figure 3: Localization of Ossa-Morena Zone within the Iberian Massif and geological map of Évora massif.	5
Figure 4: Simplified Mértola region geology.	6
Figure 5: Geological map of the Algarve basin with the location of Silves and the above-mentioned three zones.	7
Figure 6: Ceramic fragments corresponding to a cooking pot.	20
Figure 7: Ceramic fragments corresponding to a cooking pot.	20
Figure 8: Ceramic fragments corresponding to a cooking pot.	21
Figure 9: Ceramic fragment corresponding to a casserole.	21
Figure 10: Ceramic fragment corresponding to a small jug.	22
Figure 11: Ceramic fragment corresponding to a small jug.	22
Figure 12: Ceramic fragment corresponding to a bowl.	23
Figure 13: Ceramic fragment corresponding to a small jug.	24
Figure 14: Ceramic fragment corresponding to a small jug.	24
Figure 15: Ceramic fragments corresponding to a casserole.	25
Figure 16: Partially completed ceramic object corresponding to a tripod stand – stilt.	26
Figure 17: Ceramic fragments corresponding to a bowl.	26
Figure 18: Ceramic fragment corresponding to a bowl.	27
Figure 19: Ceramic fragments corresponding to a bowl.	27
Figure 20: Partially completed ceramic object corresponding to an oil lamp.	28
Figure 21: Partially completed ceramic object corresponding to an oil lamp.	28
Figure 22: Ceramic fragments corresponding to a bowl.	29
Figure 23: Ceramic fragments corresponding to a bowl.	29
Figure 24: Ceramic fragment corresponding to a bowl.	30
Figure 25: Ceramic fragment corresponding to a small bottle.	30
Figure 26: Ceramic fragment corresponding to a bowl.	31
Figure 27: Ceramic fragment corresponding to a bowl.	31
Figure 28: Ceramic fragment corresponding to a small jug.	32
Figure 29: Ceramic fragment corresponding to an oil lamp.	32
Figure 30: Ceramic fragment corresponding to a tureen.	33
Figure 31: Ceramic fragment corresponding to a small bowl.	33
Figure 32: Ceramic fragment corresponding to a small bowl.	34
Figure 33: Ceramic fragment corresponding to a small bowl.	34

Figure 34: Ceramic fragment corresponding to a small bowl.	35
Figure 35. A typical petrographic microscope and its component parts.	37
Figure 36: Fundamental Bragg's condition depicted by X-ray incident radiations	39
Figure 37: The electromagnetic spectrum, showing the X-ray area overlapping the ultraviolet and gamma regions.	40
Figure 38: Photoelectric ionization.	40
Figure 39: Schematic drawing showing the X-ray source and other components of a common benchtop XRF spectrometer.	41
Figure 40: A) Schematic diagram of SEM with both electron and X-ray detection (EDS). B) the result of the interaction between a primary electron beam and a solid sample.	42
Figures 41. Process of cutting off the bulk samples.	44
Figures 42. Displaying of the sectioned ceramic pieces.	44
Figures 43. Drying chamber where were kept the chips after sectioning procedure.	44
Figures 44. Use of a agate mortar for the first hand-crushing.	45
Figures 45. A full ground by means of an automatically mill machine.	45
Figures 46. Solid ceramic balls inside a drum are involved in the ground process.	45
Figures 47. Fine powder specimens preserved in small plastic containers and labelled.	45
Figures 48. A certain amount of lithium tetraborate-metaborate-iodide and fine powder specimen are mixed for making glass beads.	46
Figures 49. Claisse LeNeo® fusion furnace and crucible inside.	46
Figures 50. Ceramic crucibles inside the furnace for the calcination.	46
Figures 51. Furnace where the calcination of fine powder specimens were carried out.	46
Figures 52. Desiccator with silica gel and crucibles getting cold inside in a dry environment.	46
Figures 53. Measuring of the respective weights of crucibles and specimens.	46
Figures 54. A particular resin and hardener mixed together for making the epoxy resin.	48
Figures 55. Epoxy resin was poured into a small cups with the chips inside.	48
Figures 56. Process of hand-polishing for removing resin remnants.	48
Figures 57. A semi-automatically polishing-lapping machine with a coupled rotary platform for the finishing polishing onto a velvet-coated magnetic foil.	48
Figures 58. Hand polishing of polish block using a SiC grit, water and a flat, thick glass.	49
Figures 59. A semi-automatically polishing-lapping device was used in the process.	49
Figures 60. Glass slides attached to the resin blocks ready for polishing.	49
Figures 61. Mechanical polishing of glass slides by means of a diamond-covered rotating wheel.	49
Figures 62. Leveling of the glass slides were checked out through the interference colour pattern using and microscope.	49
Figure 63: A representative microphotograph (XPL) of the Pottery Fabric 1 belonging to the specimen EVR 6.	56
Figure 64: A representative microphotograph (XPL) of the Pottery Fabric 2 belonging to the specimen EVR 18.	57

- Figure 65: A representative microphotograph (XPL) of the Pottery Fabric 2 belonging to the specimen SIL 27. **57**
- Figure 66: A representative microphotograph (XPL) of the Pottery Fabric 2 belonging to the specimen SIL 27. **58**
- Figure 67: A representative microphotograph (XPL) of the Pottery Fabric 3 belonging to the specimen SIL 26. **59**
- Figure 68: A representative microphotograph (XPL) of the Pottery Fabric 3 belonging to the specimen EVR 13. **59**
- Figure 69: A representative microphotograph (XPL) of the Pottery Fabric 4 belonging to the specimen EVR 12. **60**
- Figure 70: A representative microphotograph (XPL) of the Pottery Fabric 5 belonging to the specimen EVR 16. **61**
- Figure 71: A representative microphotograph (XPL) of the Pottery Fabric 6 belonging to the specimen EVR 2. **62**
- Figure 72: A representative microphotograph (XPL) of the Pottery Fabric 6 belonging to the specimen MER 20. **62**
- Figure 73: Representative XRD pattern from EVR 8 specimen depicting the mineralogical composition of the Subgroup 1 coarse wares. **67**
- Figure 74: Representative XRD pattern from MER 23 specimen depicting the mineralogical composition of the Subgroup 2A glazed wares. **68**
- Figure 75: Representative XRD pattern from EVR 12 specimen depicting the mineralogical composition of the Subgroup 2B glazed wares. **69**
- Figure 76: Évora specimens plotted on the ternary (CaO+MgO)–Al₂O₃–SiO₂. Considering glazed decoration types (A) and XRD groups (B). **70**
- Figure 77: Mértola specimens plotted on the ternary (CaO+MgO)–Al₂O₃–SiO₂. Considering glazed decoration types (A) and XRD groups (B). **71**
- Figure 78: Silves specimens plotted on the ternary (CaO+MgO)–Al₂O₃–SiO₂. Considering glazed decoration types (A) and XRD groups (B). **71**
- Figure 79: Provenance analysis depicted by the binary plots Na₂O/K₂O vs CaO (A-B) and Al₂O₃ vs CaO (C-D). **72**
- Figure 80: Provenance analysis depicted by the binary plot SiO₂ vs CaO in which all the specimen collection are differentiated owing to the SiO₂ content. **73**
- Figure 81: A) SIL 25 (Inner surface). Honey-glazed monochromatic ceramic. B) EVR 11 (Inner surface). Black-decorated honey-glazed ceramic. C) EVR 9 (Outer surface). Green-glazed drop. D) MER 20 (Outer surface). White glaze. **74**
- Figure 82: A) EVR 2 (Inner surface). Honey-glazed section of the specimen displaying a limited glaze-body interaction layer and homogeneous and uniform glaze. B) EVR 12 (Inner surface). Honey-glazed section of the specimen characterized by high alkali content. The image displays an absent glaze-body interaction layer and crazing due to the glaze's high thermal expansion. C) SIL 29 (Inner surface). Honey-glazed section of the specimen displaying undissolved Fe-bearing particles. **75**
- Figure 83: SIL 29 (Inner surface). A) BSE images of the black-decorated section of the specimen displaying new crystallites formation growing from a limited glaze-body interaction layer. B) SE electron images plus elemental mapping of the black-decorated section displaying the chemical distribution of Na, K and Ca over the glaze, the ceramic body and crystallites. C) Elemental mapping of the black-decorated section displaying the chemical distribution of Na, K and Ca but with SE image as background. **76**

Figure 84: Plots A-B) Al_2O_3 ceramic paste/ Al_2O_3 glaze biplots from the inner and outer surfaces of each glazed specimen. Plots C-D) SiO_2 ceramic paste/ SiO_2 glaze biplots from the inner and outer surfaces of each glazed specimen. **77**

Figure 85: SiO_2/PbO biplots from the inner and outer glazed surface of each specimen. A-B) SiO_2/PbO biplots displaying the distribution pattern of specimens according to their decorations. C-D) SiO_2/PbO biplots displaying the distribution pattern of specimens according to their chronologies. E-F) SiO_2/PbO biplots displaying the distribution pattern of specimens according to their pottery fabrics. **80**

Figure 86: $\text{Na}_2\text{O}+\text{K}_2\text{O}/\text{SiO}_2\text{-PbO}$ biplots from the inner and outer glazed surface of each specimen. A-B) $\text{Na}_2\text{O}+\text{K}_2\text{O}/\text{SiO}_2\text{-PbO}$ biplots displaying the groupings of high alkali-content specimens EVR 12, 17, MER 20 and 24, according to their decorations. C-D) $\text{Na}_2\text{O}+\text{K}_2\text{O}/\text{SiO}_2\text{-PbO}$ biplots displaying the groupings of high alkali-content specimens EVR 12, 17, MER 20 and 24, according to their chronologies. E-F) $\text{Na}_2\text{O}+\text{K}_2\text{O}/\text{SiO}_2\text{-PbO}$ biplots displaying the groupings of high alkali-content specimens EVR 12, 17, MER 20 and 24, according to their pottery fabrics. **82**

Figure 87: $\text{Al}_2\text{O}_3/\text{FeO}$ biplot displaying the linear correlation between the chemical elements. **84**

Figure 88: MER 19 displaying the absence of crystallites due to they were dissolved into the glaze (A-C). SIL 26 displaying Fe- and Mg-bearing crystallites undissolved into the glaze (B-D). **87**

Figure 89: EVR 2, Mn-bearing components present in high amount within the black decoration as they did not dissolved during the firing process, developing new crystalline compounds (A-C). EVR 11, Fe-bearing components as a main mineral pigment for black decoration colouring (i.e. hematite) (B-D). The mineral colourants were applied overglaze and grew towards the glaze-body interface during the firing process. **89**

Figure 90: SIL 25 possibly displaying undissolved particles of the raw materials and from the Fe-bearing metallic pigments (A-C). SIL 26 displaying Fe-bearing undissolved particles (i.e. Hematite) (B-D). **90**

LIST OF TABLES

Table 1: Provenance, morphology, decoration and relative chronology of the specimen collection.	35
Table 2: Ceramic paste analysis.	63
Table 3: Temper material description of the mineral, rock fragments and distinctive inclusion particulates identified by Optical Microscopy.	64
Table 4. Semi-quantitative determination of the mineralogical phase's abundance identified by XRD. (Legend: TR, traces; X, scarce; XX, moderate; XXX, frequent; XXXX, abundant).	69
Table 5. Pottery fabrics and XRD groups related to the inner/outer glazed-colour decoration of the collection.	73
Table 6: Calculate Medium Values (Avr.) with Standard Deviation (SD). Inner glazed surface. Oxides Wt%.	84
Table 7: Calculate Medium Values (Avr.) with Standard Deviation (SD). Outer glazed surface. Oxides Wt%.	85
Table 8: Renormalized values of the ceramic paste without PbO. Medium values in weight percent (wt%).	78
Table 9A: Renormalized values of the inner glazes without PbO. Medium values in weight percent (wt%).	78
Table 9B: Renormalized values of the outer glazes without PbO. Medium values in weight percent (wt%).	79
Table 10: Comparative chemical elements. Medium values in weight percent (wt%).	82
Table 11: Medium values of the chemical composition of the black decoration.	87
Table 12: Chemical composition of analysed crystallites by means of spot analysis.	91

CHAPTER 1: INTRODUCTION

The current Master Thesis is addressed to the archaeometric analysis of Islamic glazed pottery retrieved in Évora, Mértola and Silves, with a chronology comprised mainly from 10th to 11th centuries AD, and reference materials that expand to the mid-13th century AD.

The ceramic assemblage includes twenty-nine (29) ceramic specimens in total. Eight (8) specimens are monochromatic glazed ceramics, twelve (12) are represented by honey and black glazed ceramics, a (1) kiln tool (i.e. tripod stand) with some glaze drop on top, a (1) white glazed ceramic, and eight (8) unglazed coarse wares.

The following description is a reflection of how the Master Thesis is arranged to understand, from the historical and archaeological context to the multi-analytical analysis, the characteristic production technology, the provenance and regional contacts (i.e. trading) of the considered ceramic assemblage.

The Main Objectives in the next section, state the aims to achieve with the Master Thesis. In the Research Background, section number two, three different parts have been included. The first one describes the Historical Context where glazed pottery production developed in the *al-Andalus*. The historical time-lapse goes from the Islamic conquest of the Iberian Peninsula in 711 AD to the fell down of the second African kingdom of Almohad in 1248 AD.

The Geological Setting of the cities of Évora, Mértola and Silves are explained in detail in the second part, to understand ceramic compatibility with the local geology in each case.

Glazed Pottery Production is described in the third part, in addition to the description of the main iron (Fe) and manganese (Mn) pigments associated with black decoration in honey and black glazed ceramics. The exploitation of calcareous and non-calcareous clay materials for glazed ceramic production is also briefly discussed. Additionally, the more outstanding evidences concerning the glazed pottery production in the Andalusian territory is summarized thoroughly.

Ceramic Typology and Chronology are given in section three with morphofunctional description of the shards. Information regarding the sample origin and the archaeological context are also provided.

The analytical techniques employed during glazed ceramic analyses are described in section four, Instrumentation. The section also includes the explanation of basic principles of each analysis method (i.e. Optical Microscopy, X-ray Diffraction, X-ray Fluorescence and Scanning

Electron Microscope coupled to an Energy Dispersive Spectrometer), and their utility in the study of archaeological materials such as pottery and glaze.

Methods in the section five include the instrumental condition applied. A thorough description of the sample preparation procedure in each case is explained.

In the section six of Results and Discussion, the results obtained by the Master Thesis are presented and discussed with the aid of tables, plots and diagrams. Data obtained are further compared with the existing bibliography.

At the end, in the section seven of Final Remarks a series of conclusions are delineated according to the obtained data. Furthermore, complementary images such as drawings of the ceramic pieces can be found in the section eight, Appendices.

1.1 MAIN OBJECTIVES

The knowledge of the mechanisms involved in the glazed pottery production, consumption and distribution in the city of Évora during the Islamic period is analysed by the application of multi-elemental analyses. The comparison with glazed pottery retrieved in the cities of Mértola and Silves provides a great opportunity for comparing not only the materials, their procurement and the techniques applied, but also the choices of ceramists (i.e. technology) and regional contacts (i.e. trading). These methodological concepts are the ground of the present study, which will be raised up from the main objectives.

Optical Microscopy (OM), X-ray Diffraction (XRD), X-ray Fluorescence (XRF) analyses were applied to determine the ceramic bodies characteristics, shedding light on the production process and the provenance of the raw materials. Scanning Electron Microscope coupled to an Energy Dispersive Spectrometer (SEM-EDS) analysis was used for the determination of the microstructure and the chemical composition of the glaze and black decoration to evaluate glaze technology.

The above-mentioned analyses were directed to answer the following archaeological demands:

1. To establish whether monochromatic and honey and black ceramics were produced in the city of Évora during the Islamic time or were imported into the city.
2. To analyse glazed ceramic production recovered in the city of Silves and Mértola to establish whether monochromatic and/or honey and black ceramic show similar characteristics to Évora glazed ceramics.
3. To establish whether some glazed ceramics were imported from a different area of the *al-Andalus*.
4. To evaluate glaze technology during time.

CHAPTER 2: RESEARCH BACKGROUND

2.1 HISTORICAL CONTEXT

By the year 711 AD, when Toledo was the capital of the Visigoth kingdom, the Arab *Tariq ibn Ziyad*, envoy of the Umayyad governor, *Musa ibn Nusayr*, arrived to *Baetica* from North Africa. After a bloody battle in which the Visigoth king Rodrigo died, the Arab army was able to advance further in the territory (Robinson, 2011).

Musa ibn Nusayr, the Umayyad governor, who had sent Tariq, travelled with more armies to the new territories, taking Toledo in 712 AD. A few years later, Musa's son, Abd al-Aziz and Tariq ibn Ziyad, had already managed to invade several more Visigoth territories (Ibid.).

After invading Toledo, the Arab advance and invasion towards the peripheral regions was rapid and, in most cases, simple. The Arab leaders had managed to occupy most of the Iberian Peninsula and part of southern France, including the new lands under the Umayyad Empire of Damascus. (Figure 1) (Ibid.).

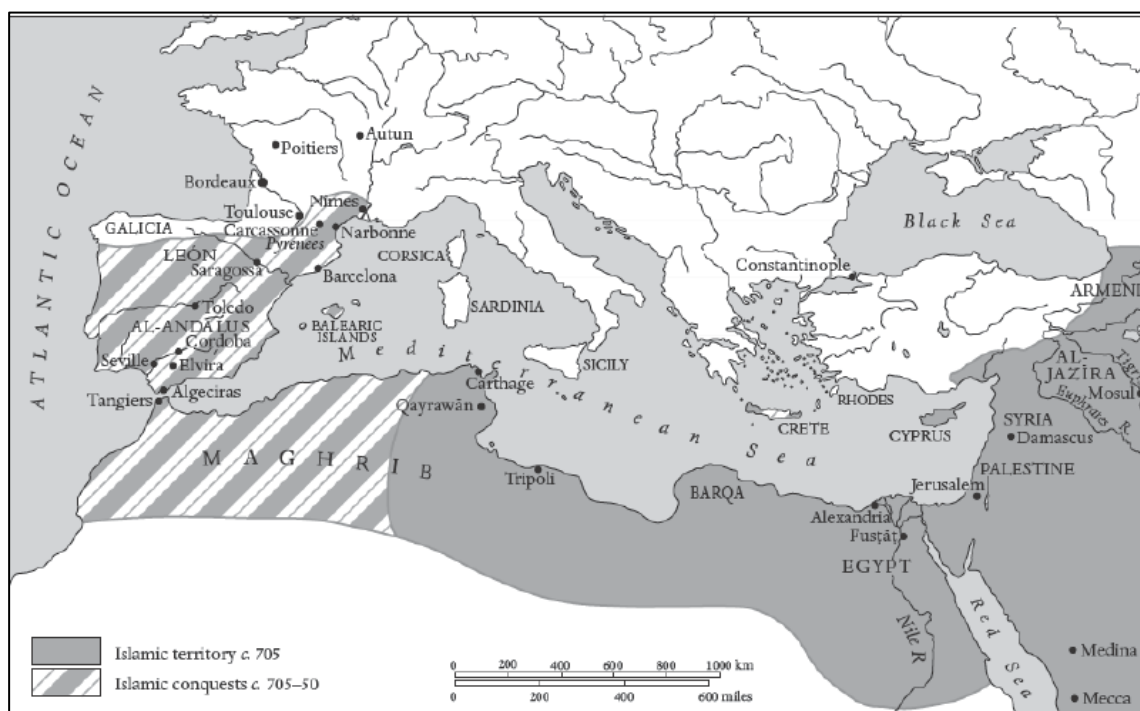


Figure 1. The western expansion of Islam during the first decades of 8th century (Robinson, 2011).

After a long period, the *al-Andalus* was considered as Umayyad territory. Around the year 730 AD, the Umayyad empire was weakened by various disputes, such as a Berber revolt and fights

between Syrian and Arabs, which finally led to the triumph of the Abbasids, a Persian dynasty, who took Baghdad as capital (Ibid.).

The Umayyad were the object of constant persecution and murder, but, the prince *Abd al-Rahman I*, managed to escape and settle in Cordoba, establishing an independent Emirate. That, despite the siege and internal conflicts, survived until the end of the 10th century AD. The subsequent periods the *al-Andalus* peace and quietness reigned during 64 years when two of the most outstanding Umayyad rulers Abd al-Rahman III and al-Hakem II seized the power (Ibid.).

After the death of Al-Hakem II in 976 AD, a twelve-year-old son as successor, left the whole power to the prime minister al-Mansur, being a puppet and obeying his orders (Ibid.).

Once al-Mansur was in command of the entire Andalusian territory, established his own form of government and, using his own military skills, managed to conquer Christian territories to the north and much of the south, to the Maghrib. Even though the connection with the Berber troops from Morocco, a series of bloody revolts and attacks with this group occurred, bringing a tense situation in the Andalus territory that ended up with its disintegration at the beginning of the 11th century AD (Ibid.).

This event generated political instability, in which finally the territory was divided into several *taifas* for a short time. Afterwards, in the west of *al-Andalus*, those that finally predominated were mainly the *taifas* of Badajoz and Seville, and four small ones: Faro, Mértola, Silves and Huelva. In the middle of the 11th century AD, the two main *taifas* Badajoz and Seville absorbed the rest (Ibid.).

Subsequently to the death of al-Mansur, the Christian kingdoms from the north started attacking Muslim territories, managing to get some *taifa* realms to give them tributes and money, during a time-lapse called *párias*, a system that became popular until Toledo was occupied by the Castilians in 1085 AD. This episode triggered the alliance between the *taifas* with the Almoravids, a militant Islamic dynasty that had occupied Morocco. The Almoravids managed to get close to Badajoz, but after just over 100 years, they lost power in Morocco and finally left the Andalus territory by the 1120s AD (Ibid.).

The Almoravids were overthrown by a new Berber Muslim movement, known as the Almohads, who by 1172 AD, extended their dominions throughout the Maghrib, as well as North Africa and Islamic Iberia. Their rule lasted until 1212 AD, when they were defeated by an alliance of Christian princes from Castile, Aragon, Navarra, and Portugal, making fell down the Islamic capitals of Cordoba and Seville by the years of 1236 and 1248, respectively (Ibid.).

2.2 GEOLOGICAL SETTING

The cities of Évora, Mértola and Silves are located in the southwestern section of the Iberian Peninsula (Figure 2). The geological setting is different in each case.



Figure 2: Map of the Iberian Peninsula and the geographical location of the cities from where the analysed materials were retrieved (elaborated by Beltrame M.).

2.2.1 Évora

The city of Évora (Figure 3) is located in the Évora Massif (Iberian Variscan Orogen), a geological unit within the Ossa-Morena Zone, identified between the cities of Évora and Montemor-o-Novo. It is composed of different Neoproterozoic – Lower Palaeozoic geological units (Ediacaran to Ordovician), affected by medium to high-grade metamorphism. The city of Évora lies in an area where the bedrocks are mainly composed of schists, migmatites and gneiss intruded by Variscan plutonic rocks. The composition ranges from gabbro to granite, being mainly represented by tonalites and granodiorites (Moita, 2008; Moita et al., 2009).

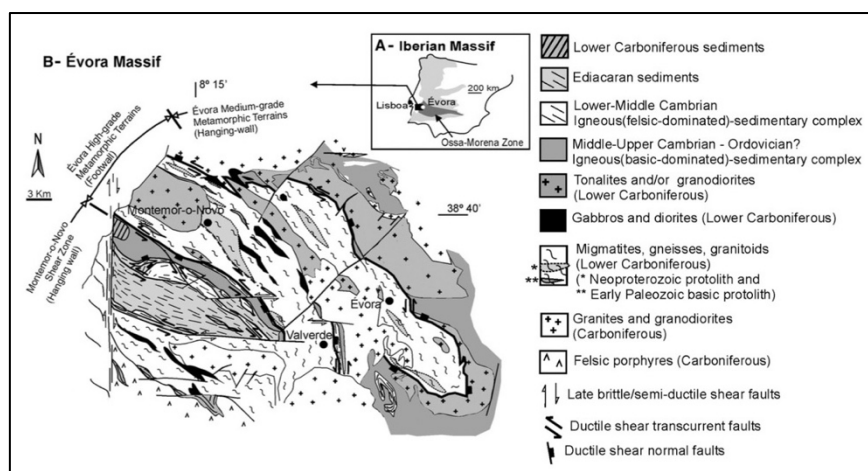


Figure 3: Localization of Ossa-Morena Zone within the Iberian Massif and geological map of Évora massif (adapted from Moita et al., 2009, p. 127).

2.2.2 Mértola

The city of Mértola (Figure 4) is located in the South Portuguese Zone (SPZ), the southernmost segment of the Iberian Variscan Massif, with rocks characteristics of the Iberian Pyrite Belt. The stratigraphic succession of the IPB is subdivided into three major Upper Palaeozoic (Givetian-Visean) sedimentary and igneous rocks lithostratigraphic units. They are the Phyllite/Slate–Quartzite Group (PQ Group), the Volcano-Sedimentary Complex (VS) and a thick post-volcanic turbiditic succession called Baixo Alentejo Flysch group. The stratigraphic limits of each unit are depositional. The PQ group is dominated by slate interlayered by fine-grained quartzite and siltstones. Quartz-rich greywackes, rare conglomerates, and jaspers lenses can also be found. The VS complex is represented by clay-rich and quartz-rich slates, siltstone, jaspers and cherts, mafic and felsic igneous rocks (mostly volcanic) and tuff with nodules of manganese and iron oxides. The different lithologies appear as lenticular outcrops with variable extensions. The Baixo Alentejo Flysch in this region is known as the Mértola Formation (MT). It is a turbiditic succession of pelitic deposits (i.e. slates) and bedded turbidites (i.e. greywackes). Some occurrences of carbonate-rich nodules can be observed (Schermerhorn, 1971; Gómez, 2004; Oliveira & Silva, 2007).

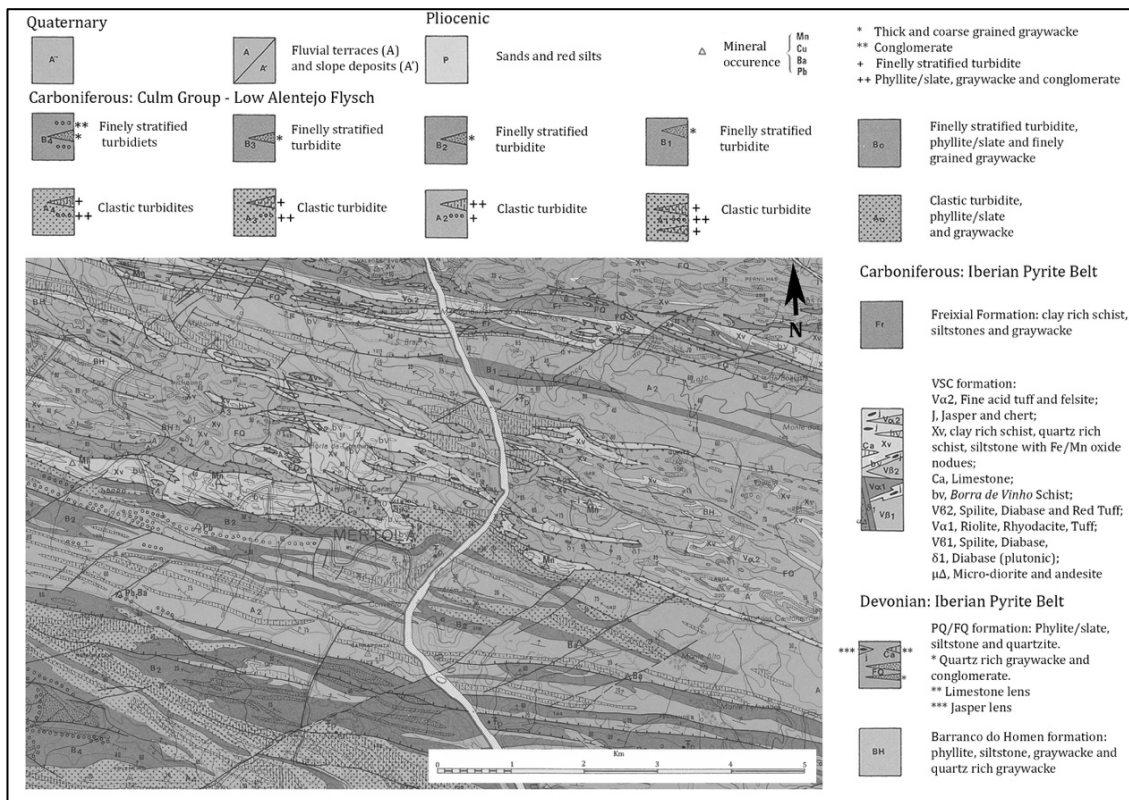


Figure 4: Simplified Mértola region geology (adapted by Beltrame M. from Oliveira & Silva, 1990, Sh. 46D Mértola, SGP).

2.2.3 Silves

The city of Silves (Figure 5) is located in the Algarve basin, very close to the South Portuguese Zone (SPZ). The territory is characterized by three different zones. The Brejeira Formation (Upper Carboniferous) outcrop at northwest of Arade river, it is included in the Baixo Alentejo Flysch geological unit (SPZ). It is mainly composed of a turbiditic succession which includes pelitic rocks (i.e. slates), quartzite and greywackes (1 in the figure). Between the Brejeira Formation and the alluvial plain of the Arade river, the rocks are mainly sandstones (Silves sandstones) of the Upper Triassic (2 in the figure), followed by Upper Triassic to Lower Jurassic limestones and evaporites (2a in the figure), the Volcano Sedimentary complex (2b in the figure) (i.e. dolerite and basalt) and dolomites and red-clay of the Lower Jurassic. The more recent geologic formations are identified in the southern part of the valley of the river Arade, and it is mainly composed of dolomites and limestones of the Lower Jurassic (3 in the figure) (Trindade et al., 2013; Trindade et al., 2018).

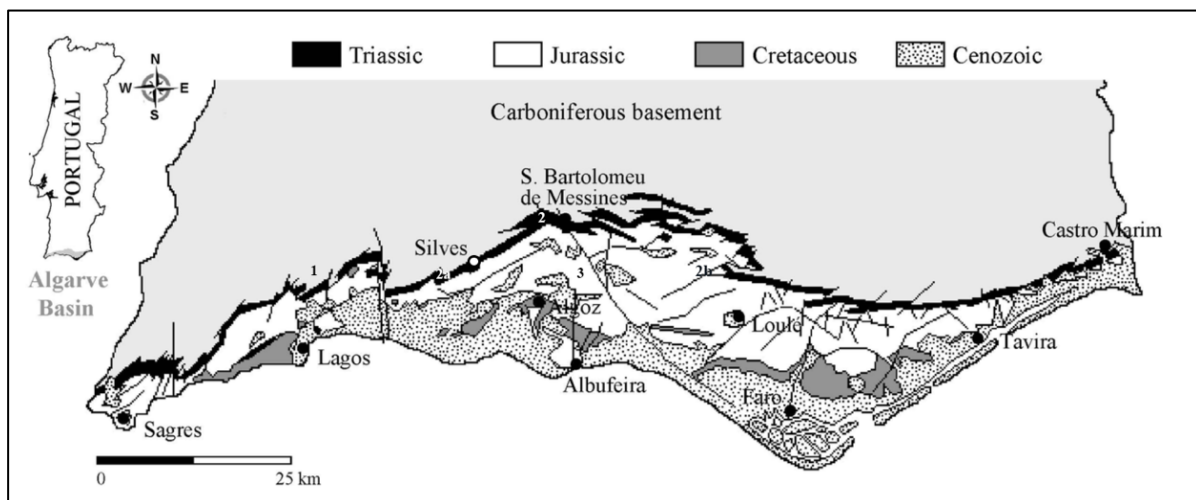


Figure 5: Geological map of the Algarve basin with the location of Silves and the above-mentioned three zones (adapted from Trindade et al., 2013, p. 61).

2. 3 GLAZED POTTERY PRODUCTION DURING ISLAMIC PERIOD

2.3.1 Ceramic Technology

In *al-Andalus*, and more generally in the Islamic world, pottery production was linked to the exploitation of two different types of clayish raw materials, namely, calcareous and non-calcareous. These materials could be chosen and modified according to the raw material's physical properties during firing and the ceramic piece's function (Tite et al., 1998; Pradell & Molera, 2020). Glazed ceramic could also be produced using stone paste ceramic bodies (Mason & Tite, 1994; Tite et al., 2011), but this technology has never been identified with certainty in the Iberian Peninsula (Molera et al., 2017).

Calcareous clay

The preferent use of calcareous clay to produce glazed ceramics has been widely documented since the Emiral period in the *al-Andalus* for two different reasons. The first one, is a similar thermal contraction coefficient¹ between the ceramic paste and the glaze, which improved glaze adhesion. The second one, points to the colour because calcareous clays normally become buffy after firing.

Besides, during firing (i.e. above 900 °C) specific mineralogical phases such as pyroxenes, plagioclase and akermanite or gehlenite could crystallize in the ceramic paste during firing. In particular, pyroxene crystallization prevents hematite formation as the iron oxide eventually present in the raw material is normally included inside this mineral during crystallization, and the ceramic paste does not become red (Molera et al., 1997a, 1997b; Molera et al., 2007, Trindade et al., 2009; Molera et al., 2017; Salinas & Pradell, 2018; Salina et al., 2019; Heiman & Maggetti, 2019). When a proper calcareous clay was not available, limestones could be added to the ceramic paste (Molera et al., 1996).

The Islamic glazed pottery production normally involved glaze application over a biscuit-fired ceramic bodies, which underwent a previous firing process. The purpose was to favour the complete oxidation of the ceramic paste, and to avoid a strong reaction with the glaze during firing² (i.e. glaze application). Besides, during glaze application and firing, the glaze and the

¹ The thermal contraction coefficient is the tendency of shrinkage of a clay ceramic body and the overlying glaze during the cooling process. The thermal contraction coefficient of the glaze is the same or slightly less than the calcareous ceramic body. It means, that the shrinkage of a glaze surface did not exceed that of the body in which a tensile stress situation of the glaze would provoke cracking and crawling. Contrary, when the body shrinkage is greater than of the glaze, was less a problem since glazes are capable to bear with compression than in tension (Tite et al., 1998).

² When the clay body underwent to a previous firing, the processes is defined as “double firing”. On one hand, the advantages of having a biscuit-fired body was thank to its porous structure which allowed readily to absorb

ceramic body interact, chemical oxides diffusion take place in both directions, and new crystallites form at the glaze-ceramic body interface. The interdiffusion of different oxides could also influence the final glaze chemical composition and colour (Molera et al., 1997b; Molera et al., 2017). Contrary, the interaction is normally stronger when the glaze is applied over an unfired ceramic body (Molera et al., 2001), and the resulting interface is much thicker. The final colour of calcareous clay may range from buffy-red to grey, depending on the firing condition. Thus, when transparent high-lead glazes were applied on a biscuit-fired support the final glaze colour, since early Islamic times, could be yellow, honey, or brown in oxidizing condition. Green glazes could appear when the ceramic body was fired under reducing conditions or the ceramic support was not fully oxidized (Molera et al., 1997b). Evenly, in the case of tin-opacified glazes, it was preferable the use of buffy than red body colours, in order to ease glaze opacification³ using less cassiterite (i.e. SnO₂) (Molera et al., 1997a). Thereby, the final glaze appearance could be a superimposition of colours from the body and the glaze (Molera et al., 1997b).

Non-calcareous clay

Unglazed cooking pots, kitchen wares and kiln tools were normally manufactured using non-calcareous raw materials (Beltrame et al., 2020). The firing temperature could vary, but in these cases, hematite and magnetite can crystallize freely, and for higher firing temperature (i.e. higher than 1000°C), mullite could also appear at the expense of clay minerals (Heiman & Maggetti, 2019). The colour of the ceramic paste could range between red and grey depending on the firing condition (Molera et al., 1997a, 1997b).

Cooking pots could be elaborated with several coarse inclusions (i.e. quartz sand and rock fragments) for improving the thermal shock resistance⁴ and heating effectiveness⁵ (Molera et al., 1996). This technology is generally attested in every workshop (Molera et al., 1997a, 1997b; Molera et al., 2007, Molera et al., 2017; Salinas & Pradell, 2018; Salina et al., 2019).

water from the glaze suspension. On the other hand, due to the full oxidation of the clay body, unoxidized and/or dark areas beneath the glaze in a second firing were avoided. A disadvantage was related to the cost of production which implied more fuel and time (Tite et al., 1998).

³ In the case of white tin-opacified glazes the use of calcareous clays were preferred. It was easier for ceramists the employment of buff-coloured ceramic bodies upon which lower quantities of tin minerals (i.e. cassiterite-SnO₂) was needed for obtaining the desired white glaze colour (Tite et al., 1998).

⁴ Thermal shock resistance is the ability of ceramic object to bear sudden temperature changes (i.e. heating and cooling), causing stress and the resulting fracture. This can improve during the tempering process, adding to the clay paste inclusions with different rate and degree of thermal expansion (Quinn, 2013).

⁵ Heating effectiveness is the rate in which a ceramic vessel transfers heat to its content, from an external heating source. It is a benefit to consider in the production of cooking pots (Quinn, 2013).

Nevertheless, cooking pots and kitchen wares could have also been glazed. In the Iberian Peninsula cooking pots started to be glazed just by the end of the Islamic domination (Molera et al., 1997b). The glaze was normally brown in colour due to the high concentration of iron oxide.

Another option, it is represented by the exploitation of kaolinite rich clays to produce glazed kitchen wares (Beltrame et al., 2021). As calcium-rich clays, they also become buffy after firing, so when a high-lead transparent glaze is applied, it become generally yellow or honey.

2.3.2 Glazed Ceramic Technology

The first glaze technology to appear in the *al-Andalus* was first documented at Pechina (second half of the 9th century AD – Spain) (Salinas et al., 2019). It involved the production and application of a transparent high-lead glaze on the ceramic surface. In this specific case, lead oxide (i.e. PbO) is the main flux. The contribution of alkali earth metals (i.e. Na₂O and K₂O), as fluxes, was generally low. Later, by the end of the 9th century AD and the beginning of the 10th century AD, another glazing tradition developed for the production of white tin-opacified lead-alkali glazes. In this case, cassiterite minerals (SnO₂) were utilized to opacify the glaze (Molera et al., 2017). These two kinds of glaze technology have been identified in the ceramic assemblage under analysis.

*Transparent high-lead glaze*⁶

On transparent high-lead glaze, lead oxide (PbO) and silicon oxide (SiO₂), are the unique main components. The procurance of lead ore could be diverse⁷ but, preferentially, galena ore (PbS) was largely exploited as it is/was a naturally occurring ore in the south east of the Iberian Peninsula (Almodóvar et al., 2019). The raw galena was first subjected to a previous roasting process to obtain lead oxide (PbO)⁸. In the case of silicon oxide (silica, SiO₂), quartz sand, ground quartzite and/or chert pebbles could be possible raw material sources (Tite et al., 1998; Molera et al., 2007; Schibille et al., 2020).

⁶ The preferentially use of lead oxide (PbO) as a main flux in the production of high transparent glazes was as a result of the benefits in both the glaze production (e.g. ease of preparation, low firing temperature and reduction cost) and the resulting glaze properties (e.g. high optical brilliance and glaze-body fit) (Tite et al., 1998).

⁷ Other lead ores could be used to produce high-lead glaze such as litharge (PbO), red lead (Pb₃O₄) and white lead (2PbCO₃.Pb(OH)₂) (Tite et al., 1998).

⁸ The usage of lead through galena (PbS) implied first its oxidation to form lead oxide (PbO) and then mixed with silica (SiO₂) for making glaze. Although sometimes galena was used directly (PbS-SiO₂ system) in the process of glaze production, it required higher temperature and oxidizing condition for becoming to oxide (Di Febo et al., 2017c).

As a part of the glaze recipe, once obtained lead oxide (PbO), it was mixed with silica and subjected to additional firing called fritting process⁹. This procedure consisted of the preparation of a lead-silica mixture close to the eutectic composition¹⁰. Then, the resulting frit was ground and fired again to obtain a more homogeneous mixture. More silica could be eventually added. In this manner, a high-lead glass was obtained, and it was ready to be ground and mixed with water. Other components such as gum or clay could be added to the suspension to improve the binding properties of the glaze. The final step was the application of the glaze suspension onto a biscuit-fired ceramic body, and they were jointly subjected to a second and ultimate firing as the glaze adhered onto the object surface (Molera et al., 1997a; Molera et al., 2007; Salina et al., 2019).

Thereby, by using frits, the ceramist was able to reduce the firing temperature and time, to get a homogeneous melt and, thus, a more uniform glaze¹¹. The firing temperature was reported to be about 717°C (Tite et al., 1998; Molera et al., 2007; Di Febo et al., 2017c; Salinas et al., 2019; Pradell & Molera, 2020). The application of raw glaze materials over the ceramic body could also be possible, consisting of the raw mixture of lead oxides (PbO) and silica directly applied on the object surface with the addition, eventually, of a colourant such as copper oxide (CuO) or iron oxide (FeO) for example (Molera et al., 2007).

The preferent use of frits has been reported from the beginning of high-lead glazed ceramic production (i.e. Pechina) (Salinas et al., 2019), with the exclusive use of biscuit-fired ceramic bodies. This glazing technique implied the use of special kilns, vessels and kiln tools specialized for the fritting process (Molera et al., 1997a; Molera et al., 2007; Salinas & Pradell, 2018). With the use of frits and of biscuit-fired ceramic bodies the obtained glaze layer is generally more homogeneous and the formation glaze-ceramic body interface is limited (Tite et al., 1998; Pradell & Molera, 2020)

Powdered lead ore could also be applied by itself on the object surface without silica. Nevertheless, this technological option is rarely employed in the Islamic world (Tite et al., 1998; Walton & Tite, 2010), but it was largely utilized by Romans. Moreover, this technological option was mainly used in combination with non-calcareous raw materials. Thus,

⁹ Frit is a glassy material obtained when a mixture of silica (i.e. quartz sand) and flux materials (lead oxide and/or alkaline earth metal oxides) were submitted to a previous firing process (Di Febo et al., 2017c). Frits were widely used in the Medieval period and from early Islamic times, and it was documented in Persian Abul's Qasim's "Treatise on Ceramics" (1301 AD) (Molera et al., 2007).

¹⁰ Eutectic point (70wt% PbO and 30wt% SiO₂) (Tite et al., 1998).

¹¹ The homogeneous amorphous phase is a result of the production of a glaze mixture with chemical composition close to the eutectic point (70wt% PbO and 30wt% SiO₂). Thus, fusion began earlier in lower firing temperature, extending the maturing range if was required (Tite et al., 1998; Molera et al., 2007; Pradell & Molera, 2020).

to determine whether lead ore by itself or lead-silica mixture (i.e. frits or silica plus lead oxide) were used, a specific evaluation model is normally employed. In this case, the glaze chemical composition is compared with that of the ceramic paste after the removal of lead oxide (i.e. PbO, from ceramic paste and glaze) and colourant (i.e. eventually present in the glaze). The obtained results are then normalized to 100%. If the obtained chemical composition from the ceramic paste and the glaze are very similar or the same, this means that lead ore by itself was applied on the object surface and fired, and chemical oxides such as SiO₂, Al₂O₃, FeO, CaO and MgO were digested from the ceramic paste and included in the glaze. Otherwise, a frit or mixture of lead and silica were utilized.

Regarding coloured or transparent glazes, the colour was obtained by the addition of transition metals to the glaze mixture (e.g. to obtain green glazes). MnO and/or FeO could be normally utilized to develop black decorations (Molera et al., 2013; Di Febo et al., 2017a), and it will be discussed in the next section.

In the case of transparent glazes, the final glaze colour was generally influenced by the ceramic support. This could make the final glaze appearance challenging for Islamic potters. Thus, ancient Islamic ceramists considered not only the nature of the ceramic bodies¹² but also the firing condition (i.e. oxidizing or reducing atmosphere), and the firing steps applied (i.e. single or double firing) (Molera et al., 1997a).

Single or double firing techniques could also influence the final glaze colour of the glaze. Thereby, the resulting glaze appearance was often a colour superimposition¹³ between glazes and clay bodies (Molera et al., 1997a; Tite et al., 1998; Pradell & Molera, 2020). In this case, iron was the most important transition metal chemical element that could contribute to the glaze colour, and it could have either been yellow to honey/brown (i.e. if the object was previously fired under oxidizing condition) or green (i.e. if the object previously was fired under reducing condition) (Molera et al., 1997b; Molera et al., 2017).

Tin-opacified lead-alkali glazes

Tin-opacified lead-alkali glazes were utilized in the Islamic world to obtain white glazes. In this manner, differently from transparent high-lead glazes, the colour of the ceramic paste could

¹² Calcareous or non-calcareous clay paste for pottery forming were employed. Thus, ancient ceramist preferentially used calcareous clay bodies for controlling the glaze colour, (Pradell & Molera, 2020). In this case, the ceramic body become generally creamy or buffy, and the glaze is generally honey colour. This is because iron, generally do not contribute to the final colour of the ceramic paste, being generally included in pyroxenes minerals who crystallized during the firing process. In this case, hematite crystallization is prevented (Molera et al., 1997b).

¹³ The resulting glaze colour is caused by the absorption of light at specific wavelength by metal ions and/or crystallites when opacity is desirable (Tite et al., 1998).

not be seen. The technique took advantage of the precipitation of small cassiterite crystals (Vendrell et al., 2000) into the glaze to make it opaque, and it was utilized for the decoration of different glazed ceramics like green and brown and lustre ceramics (Molera et al., 2013; Di Febo et al., 2017a, 2017b; Salinas & Pradell, 2018; Matin, 2019).

Different works have been published regarding the origin of this technique and the technology applied (Tite et al., 1998; Molera et al., 1997a; Molera et al., 1999; Molera et al., 2007; Molera et al., 2013), and the bibliography has also been recently revised (Salinas & Pradell, 2018; Matin, 2019; Matin et al. 2018; Pradell & Molera, 2020).

Glaze opacification was successfully accomplished when the glaze totally covered the ceramic body colour, and a significant amount of cassiterite crystallites were homogeneously concentrated and distributed¹⁴ all over the glaze surface (Vendrell et al., 2000). Moreover, to fulfil the desired opacification, calcareous clay bodies previously fired under slightly reducing condition¹⁵ were chosen, giving rise soft colours easier to opacify and, therefore, minimizing the utilization of tin minerals (Molera et al., 1997a; Tite et al., 1998).

The traditional method was called calx¹⁶, in which lead and tin ores were first roasted together (i.e. roughly at 600°C) to obtain oxides. Depending on the PbO/SnO₂ ratio, the glaze preparation procedure was different, but the resulting calx powder continued a procedure similar to the fritting process, and silica (SiO₂)¹⁷ and alkaline earth metals were generally added. Subsequently, the frit was ground down and put into water suspension for being applied onto the clay body. A final stage was the jointly firing to obtain a white tin-opacified glaze¹⁸, caused by the precipitation of small crystallites (i.e. cassiterite-SnO₂) (Tite et al., 1998; Molera et al., 1999; Vendrell et al., 2000; Molera et al., 2007; Matin, 2019).

¹⁴ The physical reason of the opacification is the similar SnO₂ particle diameter to the light visible wavelength, resulting in the reflection and scattering of light (Vendrell et al., 2000).

¹⁵ Poor reducing firing condition make the calcareous clay become into buff or cream colours due to the incorporation of iron in calcium and aluminum silicates structures reducing the formation of iron oxides responsible for red and black colours (Pradell & Molera, 2020).

¹⁶ Persian Abul' Qasim's Treatise dated from 1301 AD describe the frit production in Islamic world in which some terms are useful in order to understand the process. One of them is "sirinj", that means the resulting lead-tin roasted powder which could be related to the calx (Molera et al., 2007).

¹⁷ The presence of alkaline earth metals (i.e. Na₂O and K₂O) promoted the precipitation of tin oxide (SnO₂) at lower temperature, enhancing the white opacity. Also, the reduction of lead oxide to lead metal avoiding blackening and blistering of the glaze was hindered (Tite et al., 1998; Pradell & Molera, 2020).

¹⁸ Opacification in the Islamic world was performed using tin oxide. According the Pb/SnO₂ ratio the resulting calx powder varied from whitish yellow to deep yellow in colour. The ratio of the mixture was controlled in order to obtain the desire colour (Matin, 2018).

2.3.3 Black Decoration

In Islamic honey-glazed ceramic, the black decoration was generally obtained using a mixture of manganese oxide (MnO)¹⁹ and/or iron oxide (FeO)²⁰. Nevertheless, the first option was more common (Molera et al., 1997a, 1997b; Molera et al., 2013; Molera et al., 2017). Pigments could be applied over or under the glaze, and the glaze could have appeared either completely homogeneous (i.e. the pigment was completely dissolved into the glaze) or heterogeneous, in which different crystallites could be present inside the glaze (Tite et al., 1998; Pradell & Molera, 2020).

The characteristics of new crystallites are directly correlated to the original pigment and/or the mixture employed for the decoration. Thus, when crystallites are identified in Mn-bearing black decoration areas, braunite ($\text{Mn}_7\text{SiO}_{12}$) and kentrolite ($\text{Pb}_2\text{Mn}_2\text{Si}_2\text{O}_9$) could appear by the reaction of silica- and lead-rich areas, respectively. Evenly, by the reaction of calcium-rich areas, Mn-containing pyroxene could show up, such as bustamite ($\text{CaMnSi}_2\text{O}_6$). In addition, bixbyite (Mn_2O_3) precipitate at low temperature when pyrolusite (MnO_2) is fired, whilst the transformation to hausmannite (Mn_3O_4) requires about 1000°C, but the use of glaze frits helped the formation of the latter at lower temperature (Molera et al., 2013; Pradell & Molera, 2020). On the other hand, and according to the recipe, iron (Fe) in the form of hematite (Fe_2O_3) was also present in Mn-bearing black decorations, and could have formed melanotekite ($\text{Pb}_2\text{Fe}_2\text{Si}_2\text{O}_9$).

Therefore, the chemical and structural examination of recurrent crystallite formations into black decoration areas may shed light on the environment and the firing temperature in what they could have grown, using them as technological markers in glaze pottery production (Molera et al., 2013; Di Febo et al., 2017a, 2017b; Molera et al., 2017).

2.3.4 Archaeological Evidences

The present description is a summary of the most highlighted archaeological evidences concerning glaze pottery production in the *al-Andalus*, especially the findings related to high-lead monochromatic, and honey- and black-glazed ceramics found in the southernmost part of the Iberian Peninsula.

¹⁹ The most common natural pigment from ancient time is manganese oxide (MnO_2) which is mostly present as pyrolusite mineral (Molera et al., 2013).

²⁰ Iron (Fe) is mostly present as hematite (Fe_2O_3) (Di Febo et al., 2017b).

Pechina

During the first years of the Islamic conquest (i.e. 711 AD) there are not registered evidence of glaze production, although new unglazed pottery types were introduced to the Iberian Peninsula. Nevertheless, glaze technology was already developing in the late 7th and the beginning of the 8th centuries AD in Egypt and Syria (i.e. Fustat and Raqqa workshops, respectively). These places were already experimenting with lead and tin for making glazes. Glaze technology reached the western end of the Islamic world in the mid-9th century AD when Pechina, southeast of *al-Andalus*, started producing advanced high lead-glazed ceramics. A set of new tablewares and kiln furniture (i.e. tripods and kiln rods), associated with wasters and slags, particular fritting vessels, crucibles and two sizes of kilns were unearthed. Thereby, the material and methods of lead glaze production were able to reconstruct.

The analyses carried out on the retrieved materials revealed important information on the material and production methods such as the previous roasted of galena into lead oxide, application of two-stage fritting process for making glaze mixtures, and the application of high-lead glaze and metallic pigments to obtain copper-green and iron-amber colours. Additionally, it was possible to reconstruct the entire fritting procedure, which had the benefit to reduce the firing temperature and time of the lead glaze once it was adhered to the ceramic body which, in turn, was calcareous and previously fired (Salina et al., 2019).

San Nicolás

Remains of an Islamic workshop was revealed in Murcia-Spain dated at the end of the 9th century AD, and working during the 10th century AD during the Caliphal period. The findings consist of ceramic fragments, kiln furniture and wasters, from a production workshop of tablewares, cookwares and utilitarian pots. Also, two types of fritting vessels (i.e. pot and crucible) were found, similar to other workshops, for the production of yellow- and brown-coloured transparent lead, brown- and yellow-decorated transparent lead, and green ‘*cuerda seca*’ glazes.

The analyses showed the use of two types of clay material, calcareous and non-calcareous, related to the vessel function to be elaborated, which those intended for glazing underwent to a pre-firing, prior to the glaze application. In addition, although it was corroborated the employment of frits for making high-lead glazes, the retrieving and analysis of brown- and green-decorated tin glazes shown a negative evidence for the use of fritting processes for white tin-glaze production. Additionally, manganese contents were found into the brown decoration.

Thereby, the evidence of lead glaze production's fritting process demonstrated the persistence of the same glazing technique afterwards, at least for the initial Caliphal period. The production of white tin-opacified glazes, and the onset of this glazing technique, is attested by the retrieved materials (Molera et al., 1997a; Molera et al., 2007).

Vega of Granada

In the archaeological site Vega of Granada has been documented well-contextualized monochrome green and honey glazes, in addition to the production of green and black glazed ceramics, since the early mid-9th century AD. During the 10th century AD onward, the glaze production of black-painted decoration over honey-glazed vessels became popular. Afterwards, by the 11th century AD cooking wares started being glaze by a monochrome high-lead glaze (Molera et al., 2017).

The analyses applied over the decorated shards demonstrated the lead-rich glazes and the application of iron-honey, copper-green and manganese-brown as metallic colourants. Additionally, based on the chemical composition of glazes and the glaze-body interface, were determined the application of either raw glaze materials or pre-fritted glaze mixture over biscuit-fired ceramic bodies. Also, it was identified cassiterite crystallites precipitated into the tin-glazed areas, coloured by brown and green. A high-lead oxide content was identified into the green decoration which, in turn, depicts the previous lead-colourant mixture. As well as, manganese-containing pyroxene and lead manganese silicates for the new mineral phases such as bustamite and kentrolite, respectively, were observed within the black decoration.

The analysis carried out in the glaze layer identified high lead-silica mixture, but without the evidence of either they were previously fritted or raw glaze materials were applied instead. Evenly, the same concern was addressed to the case of tin glazes. Additionally, the use of biscuit-fired ceramic bodies is presumed by limited interaction layers (Molera et al., 2017).

Medinat Qurtuba

It was identified a period, during the second half of the 9th and the first half of the 10th centuries AD (i.e. Emiral and Caliphal periods, respectively), in which the production of monochrome and bichrome transparent high-lead glazes (i.e. green and honey) and polychrome tin glazes (i.e. green and black decoration) coexisted.

Emiral and Caliphal glaze pottery productions have been identified in the archaeological site of Medinat Qurtuba, in which the manufacture of polychrome tin glazes began at the end of the independent Emiral period. A multi-elemental analyses were carried out over well-

contextualized two assemblages of glazed ceramics, which depict the above-mentioned productions.

The analyses determined the use of biscuit-fired calcareous clay bodies, for the application of transparent high-lead glazes. It was observed, as well, the limited glaze-body interaction layer and the use of buff colour bodies for tin-opacified glazes. Evenly, the glaze colours of monochrome and bichrome transparent high-lead glazes were based on the use of copper-green and iron-honey metallic pigments. Copper and manganese metallic colourants applied overglaze were identified in polychrome transparent lead glazes. Thus, it was notified of the novelty use of manganese as a metallic pigment by this period. Tin-opacified glazes are lead-alkali type with crystallites of cassiterite precipitated.

A new technological innovation is identified in Medinat Qurtuba in which plane monochrome and bichrome transparent lead glaze continued from the previous glaze production, and coexist with the polychrome transparent lead and polychrome white-tin glazes (Salinas & Pradell, 2018).

Balaguer

Traces of an ancient workshop were unearthed, dating from the 11th century AD. A set of kiln tools and furniture and unglazed vessels were found. The ceramic pieces, in process of production, revealed the use of calcareous and non-calcareous clay pastes for the distinctive manufacture of vessels according to their functionality, namely, tableware and cookwares, respectively (Molera et al., 1997a).

Denia

A glaze pottery production was identified by the excavation of a workshop dated from the 13th century AD. Materials such as kiln furniture and tools, vessels and wasters were retrieved from the workshop production. Also, it was corroborated the common use of calcareous and non-calcareous clay pastes, identifying the mixture of different types of clayey materials. The use of frits for lead-tin glaze mixture was corroborated, as well as the presence of MnO into the black-painted decoration in honey glaze (Molera et al., 1997a).

Paterna

The excavation of a workshop (i.e. “Olleries Majors”, in Paterna-Valencia) shows the importance of this place as a main production centre during the 13th and 16th centuries AD, with a likely beginning in the 12th century AD.

The data from this site is essential to see the development and transition from the Islamic pottery tradition and the subsequent Hispano-moresque one.

A set of findings were retrieved such as fritting vessels (i.e. only crucibles), biscuit-fired vessels associated with white-tin glazes, and transparent lead glazes (i.e. yellow, honey, brown and green).

The compositional analyses of crucible' drops and trickles, glazes and ceramics determined the use of frits for the production of white-tin glaze, which once prepared were applied over biscuit-fired ceramic bodies. In addition, essential information on transparent lead glaze was obtained, such as the use of raw glaze materials over unfired ceramic bodies, without the employment of fritted mixtures, and the resulting range colour of the glaze by simple iron diffusion of cations from the ceramic paste, in the form of Fe^{2+} and Fe^{3+} (Molera et al., 1997a, 1997b; Molera et al., 2007).

CHAPTER 3: TYPOLOGY AND CHRONOLOGY

3.1 ARCHAEOLOGICAL CONTEXTS AND MATERIALS

Évora, Mértola and Silves were important cities within the Islamic trading network which took part of a inland, river and maritime commerce, respectively.

A short description of the archaeological sites and contexts from where each specimen was retrieved and the typological characteristics of all of them are given in the following section. At the end, a summarised information about this regard is found in table 1. Archaeological drawings of each ceramic piece can be found in Appendix I.

Évora

Colegio dos Meninos do Coro

The pottery assemblage was found during the monitoring archaeological works inside the building called Colegio dos Meninos do Coro da Sé de Évora, which is located in the most ancient part of the city. A limited number of sherds of different forms and styles were unearthed from a pit with a presumed past food storage function which, eventually, was reused as a rubbish pit intended for leveling in a subsequent occupation. Thus, according to a preliminary analysis of the sherds, which keep a temporal and typological homogeneity, were assigned to a date between the beginning of the 10th century AD and the end of the first half of 11th century AD, corresponding to the Emirate and Caliphal periods, and the Taifas kingdoms. The entire pottery assembly consists of cookwares, tablewares and storage vessels, but the analysed pieces from this archaeological context belong to the first two functional groups (Santos, 2015; Santos, 2016).

Description of the ceramic pieces

EVR 1 – *cooking pot, panela, marmita*²¹

Closed ceramic vessel composes of a seemingly globular shape and a circular opening mouth, showing a vertical everted rim with an outer triangular lip, and a reduced concave neck (*curved inverted bitronchoconic*²²). As well as two opposed handles remnants emerging from the rim, one lost and another partially broken with an oval, wide form and vertically projecting. The

²¹ Morpho-functional names are given in English, Portuguese and Spanish, for further references.

²² Some references written in cursive are the direct morphological translation of Islamic ceramics retrieved in the Gharb al-Andalus (Bugalhão et al., 2010).

ceramic body displays a coarse manufacture, with a simple decoration remains of shallow grooves and a partially covered brown-coloured finishing by some soot remains, evidence of the vessel function as a cooking pot (Figure 6).



Figure 6: Ceramic fragments corresponding to a cooking pot.

EVR 4 – *cooking pot, panela, marmita*

Closed ceramic vessel composes of a globular shape and a circular opening mouth, showing a vertical everted rim with an outer triangular lip, and a concave neck (*curved inverted bitronchoconic*). Likewise, the ceramic body has been made of a coarse manufacture, displaying a finishing of shallow grooves onto a dark brown-coloured surface partially covered by soot remains, evidence of the vessel function as a cooking pot (Figure 7).



Figure 7: Ceramic fragments corresponding to a cooking pot.

EVR 5 – *cooking pot, panela, marmita*

Closed ceramic vessel composes of a globular shape and a circular opening mouth, showing a vertical everted rim with an outer triangular lip, and a concave neck (*curved inverted bitronchoconic*). Likewise, the ceramic body has been made of a coarse manufacture, displaying a finishing of shallow grooves onto a brownish-coloured surface partially covered by soot remains, evidence of the vessel function as a cooking pot (Figure 8).



Figure 8: Ceramic fragment corresponding to a cooking pot.

EVR 6 – *casserole, caçoila, cazuela*

Open ceramic vessel composes of an inverted rim with a flat lip, and a semi-spherical body (*inverted tronchoconic*) showing a soft central carinated. The ceramic body is made of a coarse manufacture, showing a careful inner polished surface and a simple outer design in the uppermost part, consisting of a shallow line around the rim. The body colour have been blackening by the reduction condition effects but was coated by dark brown slip found scattered over both sides, as well as soot remains which shed light on the vessel function as a casserole (Figure 9).



Figure 9: Ceramic fragment corresponding to a casserole.

EVR 7 – *small jug, jarrinha, jarrita*

Closed ceramic vessel made up of an everted curved cylindrical neck (*inverted tronchoconic*) with a slightly inverted rim and a rounded lip showing, moreover, a high-carinated globular body with a vertical oval handle, emerging from the rim to the body, and a flat base. Likewise, the ceramic piece presents a light brown-coloured coarse manufacture, with some brownish slip remnants over both sides. Additionally, the estimated small size, plus the distinguishable

body-neck separation and the likely existence of an opposite handle, suggest the vessel function as a small jug (Figure 10).



Figure 10: Ceramic fragment corresponding to a small jug.

EVR 8 – *small jug, jarrinha, jarrita*

Closed ceramic vessel composes of a vertical cylindrical neck (*straight cylindrical*) with a slightly inverted rim and a rounded lip displaying, moreover, a globular body with a vertical oval-shaped handle, joining rim and body, and a flat base. Likewise, the ceramic sherd presents a brownish-coloured coarse manufacture, showing a white-paint remnants and a shallow groove pattern over the body. Additionally, the estimated small size with a clear body-neck division and a supposed opposite handle, suggest the vessel function as a small jug (Figure 11).



Figure 11: Ceramic fragment corresponding to a small jug.

Da Natatio das Termas Romanas

The Roman thermal baths were found in what is now the Paços do Concelho de Évora, which was excavated by the scholar Panagiotis Sarantopoulos during the 1990's decade. The Islamic pottery assemblages are diverse and numerous, becoming into a unique archaeological context that encompasses a diachronic period characteristic of the Islamic presence in Évora from the Emirate and Caliphal period (10th century AD) to the beginning of the Almoravid period (first

half of 12th century AD). Despite the great alteration of the archaeological deposit used as a rubbish dump for a long time-lapse, it was possible to retrieve chronologically reliable Islamic material from a sealed pit found on the very *Natatio*, and relatively dating between the end of 11th century AD and the first half of 12th century AD (Santos, 2015; Lopes & Santos, 2015).

Description of the ceramic pieces

EVR 3 – *bowl, tigela, ataifor*

Open, seemingly spherical body with a everted rim (*extroverted*) and a semi-circular lip, coated both sides by a honey glaze and displaying black colour designs on the inner one. The body shape and the special treatment given to the vessel is a reflect of its function as a bowl into which the meal was served (Figure 12).



Figure 12: Ceramic fragment corresponding to a bowl.

Pousada dos Loios

In the place where was located an ancient alcáçova or palace during the Islamic period, some archaeological excavations were carried out in 1987. A Muslim housing area was found adjacent to a wall portion, where the retrieved ceramic materials were relatively dated between 10th and 11th century AD (Santos, 2015).

Description of the ceramic pieces

EVR 2 – *small jug, jarrinha, jarrita*

Closed ceramic vessel composes of a part of a globular body with a divergent small neck as a remnant. The ceramic piece presents a honey-glazed decoration over both sides and displays a black decoration pattern on the outer one. The body shape, the fully-glazed coating and the short preserved neck shed light on the vessel function as a small jug (Figure 13).



Figure 13: Ceramic fragment corresponding to a small jug.

EVR 12 – *small jug, jarrinha, jarrita*

The small ceramic fragment with honey-glazed coating over both sides display a black decoration on the outer one. The fully-glazed coating and the external black decoration give some clues on its function as a small jug (Figure 14).



Figure 14: Ceramic fragment corresponding to a small jug.

Roman temple

As a part of a research about Roman temples in the Iberian peninsula, the scholar Theodor Hauschild and the German Archaeological Institute in Lisbon carried out a series of archaeological excavations around Diana's Temple (Évora). Several pottery assemblages from Roman era, passing by Visigothic and Islamic periods, until up to the Christian post-reconquest were retrieved. It was during an excavation season in 1992 when was opened an excavation area to the southwest of the Diana's temple, where a series of stratigraphical layers were recorded, belonging to the occupation stages of the Islamic period and further to the Christian period (Teichner, 1995; Santos, 2015).

Description of the ceramic piece

EVR 10 – *casserole, caçoila, cazuela*

Open ceramic vessel made up of a strongly central-carinated body (*straight inverted tronchoconic*) with a seemingly oval opening mouth, showing a straight everted rim and a triangular lip. Also, a vertical oval-shaped handle and part of a flat base, are preserved. The ceramic body is made of a coarse manufacture, without any superficial treatment, displaying a brown-coloured body. The vessel function as a casserole was determined according to the morphological features (Figure 15).



Figure 15: Ceramic fragments corresponding to a casserole.

Casa de Burgos

Excavations carried out in the zone called casa Burgos²³ in 1989 identified three occupation periods. Associated with the Roman structures was unearthed a series of household structures and strata related to the Medieval period, where was retrieved materials from the Islamic period in Évora. Preliminary typological analysis dated those finds roughly between Caliphal and Taifas periods, that is, at the end of 10th century AD and the first half of 11th century AD (Santos, 2015).

Description of the ceramic pieces

EVR 9 – *tripod stand-stilt, trempe, tripode*

Small ceramic piece made up of three equidistant helices with a shallow hollow in the intersection, and resting on slightly pointed supports. Likewise, the ceramic body is made of a coarse manufacture displaying a brownish-coloured rough surface. Additionally, the stilt or

²³ Additional information was found in the webpage: Direção Geral de Cultura e Património <https://arqueologia.patrimoniocultural.pt>

tripod stand function given to the piece is confirmed by some glaze remains present both coating the supporting feet and bathing certain protuberances on top, wherein are supposed to have been the vessel during firing (figure 16).



Figure 16: Partially completed ceramic object corresponding to a tripod stand – stilt.

EVR 14 – bowl, tigela, ataifor

Ceramic sherd corresponding to the bottom part of a honey glaze-decorated vessel with a convex inner surface, displaying a black-colored designs, and low annular foot on the opposite side. The vessel function as a bowl was determined, following the body shape and decoration characteristics (Figure 17).



Figure 17: Ceramic fragments corresponding to a bowl.

Paço dos Lobo da Gama

In 2008 was performed some archaeological interventions in the area of the seventeenth-century manor house called Paço dos Lobo da Gama (Coradeschi et al., 2017). Over the field works was found eight pits, one well and one fossa, wherein in some of them were retrieved important Islamic ceramic materials. The find of a gold Dinar coin was possible to make a *terminus post quem* correlation, dating the evidence to the end of 11th century AD. Also, the

previous date was supported by the oil lamp (*candil*) typology forms recorded during the excavations (Santos, 2015).

Description of the ceramic pieces

EVR 11 – *bowl, tigela, ataifor*

Ceramic fragment with some particular features such as a slightly convex-shaped body, an internal black-coloured decorations and a small carinated part preserved, for determining the vessel function as a bowl (Figure 18).



Figure 18: Ceramic fragment corresponding to a bowl.

EVR 13 – *bowl, tigela, ataifor*

Ceramic fragment consisting of a strongly highly-carinated honey-glazed body (*inverted tronchoconic*), with a straight rim, a triangular-shape lip and a seemingly oval opening mouth. The vessel function as a bowl was determined according to the morphological features (Figure 19).



Figure 19: Ceramic fragments corresponding to a bowl.

EVR 15 – oil lamp, *candil*

Oil lamp composed of a closed repository, for the fuel source and a spout, where was placed the fabric wick. The former consists of a strong central-carinated body (*bitronchoconic*), with a relatively long concave cylindrical neck, from where a handle trace emerges towards the body bottom, and a circular opening mouth. The latter, moreover, is a long three-faceted body, extending clearly from the repository, and jointly forming a flat base. Additionally, the piece is coated by a honey glaze, concealing a reddish-colored core (Figure 20).



Figure 20: Partially completed ceramic object corresponding to an oil lamp.

EVR 16 – oil lamp, *candil*

Oil lamp made up of a closed repository, with a strong central carinated (*bitronchoconic*), linking in a clear transition to an extended four-faceted spout. Likewise, the former shows a concave cylindrical neck, opening to a circular mouth, with an everted rim and a rounded lip, besides to display a flat base that runs at the bottom of the entire body. Additionally, the piece is coated by a honey glaze disguising a buffy-colored core (Figure 21).



Figure 21: Partially completed ceramic object corresponding to an oil lamp.

EVR 17 – bowl, tigela, ataifor

Ceramic fragment consisting of a honey-glazed spherical body (*spherical cap*) with black decoration remnants, an everted, rounded rim and oval-shaped opening mouth. The vessel function as a bowl was determined according to the morphological features (Figure 22).



Figure 22: Ceramic fragments corresponding to a bowl.

EVR 18 – bowl, tigela, ataifor

Ceramic fragment consisting of a honey-glazed spherical body (*spherical cap*), an everted, rounded rim and oval-shaped opening mouth. Also, a part of a low diagonal foot was registered. The vessel function as a bowl was determined according to the morphological features (Figure 23).



Figure 23: Ceramic fragments corresponding to a bowl.

Mértola

Encosta do Castelo de Mértola

Archaeological excavations to the north of the castle, within the area called Alcáçova do Castelo, have been carried out from 1978. In this place, an ancient suburb of the city was unearthed, dating from the first three-quarters of the 12th century (until 1175 AD) during the late Almohad period prior to the Christian conquest of Mértola in 1238 AD. The Almohad

neighbourhood was built for people who were running away from the Christian forces, and wherein was found a series of household structures and a set of pottery assemblage associated. The material samples under study were documented as a part of the rubbish pit filling (Gómez et al., 2012; Gómez, 2014; Macias, 2014).

Description of the ceramic pieces

MER 19 – *bowl, tigela, ataifor*

Ceramic sherd corresponding to the bottom part of a vessel with inner flat surface and outer vertical low annular foot, covered completely by honey glaze, over a orangish-colored core, and internal black-colored decoration remains. The piece was identified as a bowl (Figure 24).



Figure 24: Ceramic fragment corresponding to a bowl.

MER 20 – *small bottle, bilha, redoma*

Fragment of a ceramic piece that consists of a closed, cylindrical body with a part of a circular handle, forming a section of a bottle which have been define as a *bilha*. Additionally, the outer surface of the piece has been coated by a brownish-colored glaze, without any inner side treatment, and displaying a buff-colored ceramic paste (Figure 25).



Figure 25: Ceramic fragment corresponding to a small bottle.

MER 21 – *bowl, tigela, ataifor*

Small ceramic fragment corresponding to the part of a strongly carinated body, coated totally by honey glaze over a reddish-colored core. The piece was identified as a bowl (Figure 26).



Figure 26: Ceramic fragment corresponding to a bowl.

MER 22 – *bowl, tigela, ataifor*

Small ceramic fragment that consists of the part of a strongly carinated body, coated totally by honey glaze over a brownish-colored core. The piece was identified as a bowl (Figure 27).



Figure 27: Ceramic fragment corresponding to a bowl.

MER 23 – *small jug, jarrinha, jarrita*

Ceramic sherd corresponding to a honey-glazed body part from where is observed a trace of a handle. The absence of any treatment in the inner surface suggests the closed characteristics of a seemingly small jug (Figure 28).



Figure 28: Ceramic fragment corresponding to a small jug.

MER 24 – oil lamp, candil

Pointed-form ceramic sherd consisting to one of the side of an oil lamp spout, displaying a three-faceted body and thoroughly coated by a honey glaze, over a buff-colored core (Figure 29).



Figure 29: Ceramic fragment corresponding to an oil lamp.

Silves

Arrabalde Islâmico de Silves

During the years 2001 and 2004 were undertaken a series of archaeological excavations in the southeast of the castle or *alcáçova*, prior to the construction of a new town library. The fieldwork unearthed a continuous occupation that would be later identified as a part of the suburb (*arrabalde*) of the ancient Islamic city of Silves, dating between the 10th and 13th centuries AD. The ceramic materials under analysis come from different deposits in this area, such as a rubbish pit, a leveling and an important rubbish dump, which were formed over the Almohad period (second half of 12th century AD) (Gonçalves, 2008; Gonçalves et al., 2009).

Description of the ceramic pieces

SIL 25 – *tureen, terrina, sopera*

Small ceramic sherd with a central carinated, coated totally by a honey glaze, over a reddish-coloured core, and displaying an internal black-coloured decoration. It has been determined as a bowl into which a special meal was served (Figure 30).



Figure 30: Ceramic fragment corresponding to a tureen.

SIL 26 – *small bowl, taça, jofaina*

Ceramic sherd corresponding to the bottom part of a vessel which displays a relatively flat inner surface, with a diagonal low annular foot in the outer one. Also, the ceramic body has been totally coated by a honey glaze, over a reddish-colored core, and showing internal black-colored designs. Thereby, the vessel function as a small bowl was determined according to its morphological characteristics, such as the estimated foot size of the piece (Figure 31).



Figure 31: Ceramic fragment corresponding to a small bowl.

SIL 27 – *small bowl, taça, jofaina*

Ceramic sherd with a flat internal surface and an external diagonal low annular foot, coated totally by a honey glaze, over a buff-coloured core, and displaying inner black-colored designs. The vessel function was determined to be a small bowl (Figure 32).



Figure 32: Ceramic fragment corresponding to a small bowl.

SIL 28 – *small bowl, taça, jofaina*

Ceramic sherd with a flat internal surface and an external diagonal high annular foot, covered totally by a honey glaze, over a reddish-coloured core, and showing inner black-colored designs. The vessel function was determined to be a small bowl (Figure 33).



Figure 33: Ceramic fragment corresponding to a small bowl.

SIL 29 – *small bowl, taça, jofaina*

Ceramic sherd made up of the bottom part of a vessel displaying in the inner and outer parts, a slightly spherical surface and a diagonal low annular foot, respectively. Likewise, the ceramic body have been coated totally by a honey glaze, over a reddish-coloured core, displaying an internal black-colored design. The vessel function was determined to be a small bowl (Figure 34).



Figure 34: Ceramic fragment corresponding to a small bowl.

Table 1: Provenance, morphology, decoration and relative chronology of the specimen collection.

Reference	Code	Glaze decoration	Type	Function	Chronology	Context	Location
CMCS.48/53	EVR-1	Unglazed	Cookware	Cooking pot	X - XI	Colegio dos Meninos do Coro	Évora
EVR.LOIOS.23	EVR-2	Honey and black	Tableware	Small jug	X - XI	Pousada dos Loios	Évora
EVR.LOG.243/XII/90	EVR-3	Honey and black	Tableware	Bowl	XI - XII	Da Natatio das Termas Romanas	Évora
CMCS.5/44	EVR-4	Unglazed	Cookware	Cooking pot	X - XI	Colegio dos Meninos do Coro	Évora
CMCS.25/6	EVR-5	Unglazed	Cookware	Cooking pot	X - XI	Colegio dos Meninos do Coro	Évora
CMCS.455	EVR-6	Unglazed	Cookware	Casserole	X - XI	Colegio dos Meninos do Coro	Évora
CMCS.830	EVR-7	Unglazed	Tableware	Small jug	X - XI	Colegio dos Meninos do Coro	Évora
CMCS.49	EVR-8	Unglazed	Tableware	Small jug	X - XI	Colegio dos Meninos do Coro	Évora
EVR-GOU.142	EVR-9	Glaze drop	Kiln tool	Tripod stand	X - XI	Casa de Burgos	Évora
EVT-92-12	EVR-10	Unglazed	Cookware	Casserole	XI - XII	Roman Temple	Évora
PLG.S2.Si8 [2] 1136	EVR-11	Honey and black	Tableware	Bowl	XI - XII	Paço dos Lobo da Gama	Évora
EVR.LOIOS.149	EVR-12	Honey and black	Tableware	Small jug	XI - XII	Pousada dos Loios	Évora
PLG.S2.Si8 [2] 1119	EVR-13	Monochrome	Tableware	Bowl	XI - XII	Paço dos Lobo da Gama	Évora
EVR3-IV-F-1	EVR-14	Honey and black	Tableware	Bowl	X - XI	Casa de Burgos	Évora
PLG.S2.Si2 [1] 785	EVR-15	Monochrome	Lighting	Oil lamp	XI - XII	Paço dos Lobo da Gama	Évora
SEM.REF.PLG	EVR-16	Monochrome	Lighting	Oil lamp	XI - XII	Paço dos Lobo da Gama	Évora
PLG.S2.Si8 [2] 1129	EVR-17	Honey and black	Tableware	Bowl	XI - XII	Paço dos Lobo da Gama	Évora
PLG.S2.Si8 [2] 1118	EVR-18	Monochrome	Tableware	Bowl	XI - XII	Paço dos Lobo da Gama	Évora
M [20.110] 24	MER-19	Honey and black	Tableware	Bowl	mid-XII - mid-XIII	Encosta do Castelo de Mértola	Mértola
M [20.110] 59	MER-20	White glaze	Tableware	Small bottle	mid-XII - mid-XIII	Encosta do Castelo de Mértola	Mértola
M [20.110] 67	MER-21	Monochrome	Tableware	Bowl	mid-XII - mid-XIII	Encosta do Castelo de Mértola	Mértola
M [20.110] 68	MER-22	Monochrome	Tableware	Bowl	mid-XII - mid-XIII	Encosta do Castelo de Mértola	Mértola
M [20.110] 54	MER-23	Monochrome	Tableware	Small jug	mid-XII - mid-XIII	Encosta do Castelo de Mértola	Mértola
M [20.110] 43	MER-24	Monochrome	Lighting	Oil lamp	mid-XII - mid-XIII	Encosta do Castelo de Mértola	Mértola
BIB.03 M7 E10 1020	SIL-25	Honey and black	Tableware	Tureen	mid-XII - mid-XIII	Arrabalde Islâmico de Silves	Silves
BIB.03 K7 E6	SIL-26	Honey and black	Tableware	Small bowl	mid-XII - mid-XIII	Arrabalde Islâmico de Silves	Silves
BIB.02 J2/E6 66	SIL-27	Honey and black	Tableware	Small bowl	mid-XII - mid-XIII	Arrabalde Islâmico de Silves	Silves
BIB.04 J7 E2 4A 60	SIL-28	Honey and black	Tableware	Small bowl	mid-XII - mid-XIII	Arrabalde Islâmico de Silves	Silves
BIB.03 Sap6 Est2A	SIL-29	Honey and black	Tableware	Small bowl	mid-XII - mid-XIII	Arrabalde Islâmico de Silves	Silves

CHAPTER 4: INSTRUMENTATION

4.1 OPTICAL MICROSCOPY (OM)

Petrography is an optical microscopy technique initially employed in geology to study minerals and rocks using a polarised light²⁴ microscope. The main components of the microscope are summarised in figure 35.

A 30 µm thick thin-section²⁵ has to be prepared. In this manner, the sample is transparent, the optical properties of anisotropic²⁶ minerals can be evaluated, mineral can be identified, and the characteristics of different rock types (magmatic, metamorphic, sedimentary) can be established (Quinn, 2013; Braekmans & Degryse, 2017; Whitbread, 2017).

Thin-section is positioned in the rotating stage, between the polariser and the analyser, normally positioned at 90 degrees (i.e. with orientation N-S/E-W). Thus, the light emitted by a light source is first polarised by the lower polariser, interact²⁷ with the crystal, and afterwards is polarised (or not) a second time by the analyser (Price & Burton, 2011; Whitbread, 2017).

Two modes of observation can be employed for mineral identification in OM: plane polarised light (PPL) and crossed polarised light (XPL). In the first case, just the polariser is used, and specific optical characteristics are observed such as colour, pleochroism, habit, cleavage and relief. In the second case, the polariser and the analyser are inserted, and other properties such as isotropism, birefringence, extinction angle, twinning and zoning can be evaluated. In addition, in XPL, it is also possible to determine the interference figures (i.e. using the amicro Bertrand lens) and the optical sign of minerals (using a gypsum plate) (Gribble & Hall, 1985; Raith et al, 2014; Barker, 2014). Resolution and magnification are also extremely important in a polarised light microscope in which very fine particles are distinguished and enlarged,

²⁴ Optical microscopy use the directional properties of polarized light, that is, the orientation of all the light waves into the same direction by the employment of one polarizer filter (PPL) and/or the addition of another one called analyzer (XPL) (Price & Burton, 2011; Whitbread, 2017).

²⁵ Thin section preparation involves a mounted sample on a transparent glass slide which, in turns, is ground into a thickness of 30 µm.

²⁶ A mineral is called optically anisotropic when the light rays pass through the crystalline substance in different directions and velocities as a function of the crystal system and the specific mineral property, besides the crystal orientation disposed onto the thin section, so these minerals show birefringence. Contrary, the identical atomic arrangement of isotropic minerals make the light rays do not be transmitted, bringing about that the light travels inside the crystal with the same velocity in all direction (i.e. cubic system minerals) (Gribble & Hall, 1985; Raith et al, 2014; Barker, 2014).

²⁷ Minerals have different optical properties according to their particular crystal systems (i.e. triclinic, monoclinic, etc.). That is, a plane polarized light will be transmitted in a certain velocity and direction depending on the distinctive ordered, three-dimensionally periodic spatial atomic structure of crystalline substances, observing different optical characteristics for each mineral (Vainsthein, 1994; Raith et al, 2014; Barker, 2014).

respectively, in a magnification range from 40x to 1000x (Price & Burton, 2011; Whitbread, 2017).

Thus, optical microscopy has demonstrated its usefulness in archaeology by the determination of provenances and production technologies of ceramic objects. The former, by the identification of non-plastic inclusions in ceramic matrices, characterising the mineralogical composition and thus, approaching the likely geological settings from where the raw materials were procured (i.e. local or non-local ceramics). And the latter, by the joint analysis of the clay paste and the porosity (voids), shedding light on the different manufacturing techniques (e.g. coiling, wheel throwing, slab building) with which those objects were manufactured (i.e. production centres) (Shepard, 1985; Orton et al., 1993; Rice 2005; Quinn, 2013; Hunt, 2017). Additionally, the qualitative examination of non-plastic inclusions, clay paste and voids in thin section is complemented by the quantification methods such as image analysis (i.e. clay, temper and porosity percentage) and grain-size distribution (i.e. modal and unimodal method), giving additional insight regarding the manufacturing technology, raw material processing (Quinn, 2013; Braekmans & Degryse, 2017; Whitbread, 2017).

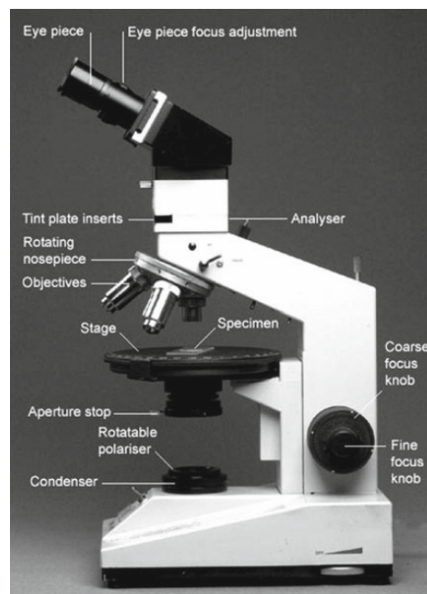


Figure 35. A typical petrographic microscope and its component parts (Price & Burton, 2011, p. 117).

4.2 X-RAY DIFFRACTION (XRD)

Pottery is a polycrystalline material made up of different mineralogical phases (i.e. clay and non-plastic inclusions). Minerals can be defined as a geometric arrangement of atoms bound together by strong chemical bonds and organized in a unit cell, periodically repeated in the

three dimensions. The distance between different planes is called interplanar space (Jenkins, 1999; Price & Burton, 2011; Heimann, 2017).

Powder XRD is the most common analytical technique for structural identification of inorganic materials, including minerals (Pollard et al., 2007). It works by means of a known-wavelength monochromatic X-ray beam addressed upon the sample. As a result, a series of re-emitted X-rays, in specific directions and angles, give rise to specific diffraction patterns or maxima²⁸, which are the fingerprint of distinct mineralogical phases. The relative amount of each mineralogical species can also be evaluated (Janssens, 2004; Pollard et al., 2007; Price & Burton, 2011; Heimann, 2017; Skoog et al., 2017).

Fundamental Bragg's law [$n\lambda=2d \sin\theta$] gives the theoretical conditions for the diffraction (Figure 36). When a crystal is irradiated with a beam of X-rays of known wavelength λ and this beam is diffracted²⁹ by a crystalline material over an angle θ , it is possible to determine the interplanar spacing d of a set of atomic planes inside the crystal that caused the diffraction (Janssens, 2004, pp. 142-143). The X-ray scattering from a set of atomic planes within a solid specimen (Heimann, 2017) displays unique patterns as a series of diffracted lines in a plot of intensity versus diffraction angle (i.e. 2θ) or interplanar spacing (Jenkins, 1999; Skoog et al., 2017). Additionally, a full database as Powder Diffraction File (PDF)³⁰ can be checked as a means of phase mineral identification (*Ibid.*).

Therefore, minerals in ceramic artifacts, can be unambiguously identified using the X-ray diffraction method. The samples can be powdered (i.e. in the case of powder X-ray diffraction–pXRD) or not (i.e. in the case of micro X-ray diffraction – μ XRD), but the instrumental setting must change.

After the mineral identification, this technique can also shed light on the thermal treatments in ceramic production (Pollard et al., 2007), estimate firing temperature range and give some information regarding the provenance of certain samples (Heimann, 2017).

²⁸ XRD method use the short-wavelength/high-energy X-ray radiation capability for going deeper through the crystalline materials, being scattered by the electrons in constructive and destructive interferences. In other words, constructive interference describes scattered X-ray wavelengths in phase with the atomic spacing layers, and destructive interference does not, being an incoherent phase (Jenkins, 1999; Janssens, 2004; Pollard et al., 2007; Skoog et al., 2017).

²⁹ Diffraction of X-rays take place when a constructive interference of X-rays is scattered from a regularly spaced series of atoms, bringing information on the crystallographic structure of the specimen under analysis (Janssens, 2004).

³⁰ Powder Diffraction File (PDF) by the International Centre for Diffraction Data, Newtown Square, Pennsylvania, U. S. A., maintains a collection of powder diffraction patterns for more than 800 000 materials (Jenkins, 1999; Heimann, 2017; Skoog et al., 2017).

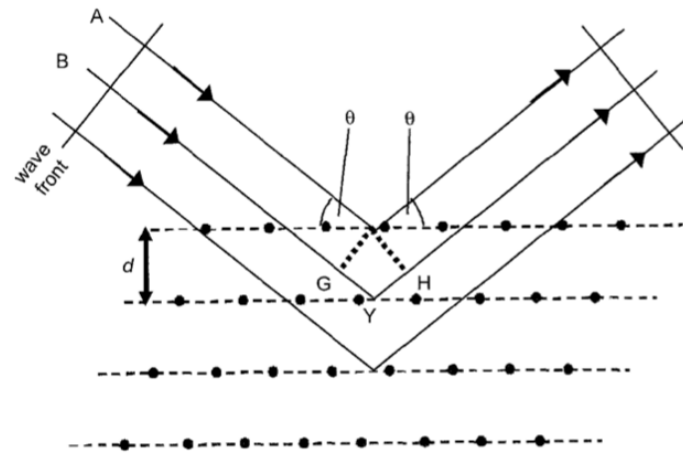


Figure 36: Fundamental Bragg's condition depicted by X-ray incident radiations (A-B), impinging the spaced plane of atoms (d) at an angle θ , resulting in a constructive interference ($GY = YH = d \sin\theta$)

(Janssens, 2004, p. 142).

4.3 X-RAY FLUORESCENCE SPECTROSCOPY (XRF)

X-rays or Röntgen rays are electromagnetic radiations of very short/high energy wavelengths included in the region between gamma and ultraviolet rays (Figure 37). The XRF method involves the interaction between X-rays and atoms, bringing about the ionization³¹ of the latter. The successful X-ray/matter interaction yields energy absorption by electrons positioned in different orbitals (e.g. K, L, M), resulting in the dislodgement of tightly bonded electrons. As a result, a series of simultaneous holes³² are created, which, in turn, will be filled by outer shell electrons giving rise to the emission of characteristic photons. In the end, an unstable atom (i.e. excited, ionized) returns to a more stable state (i.e. ground-state electron configuration) (Pollard & Heron, 1996; Markowicz, 2002; Janssens, 2004; Langhoff & Simionovici, 2006; Pollard et al., 2007; Shackley, 2011).

The emission of characteristic photons (i.e. photoelectric effect), which is distinctive of a specific chemical element, is then collected by a detector. In a multielement material, a series of de-excitation processes take normally place depending on the energy applied (Figure 38) (Pollard & Heron, 1996; Jenkins, 1999; Janssens, 2004; Shackley, 2011). Consequently, the X-rays capacity of exciting inner tightly-held electrons (Langhoff & Simionovici, 2006) makes

³¹ A series of electrons become unstable by the absorption of energy when an incident photon (i.e. X-ray beam) impinges the inner atomic shells (Janssens, 2004).

³² Vacancies occur in the atom as a result of energy absorption (*photoelectric absorption*) from the primary beam, and when the *absorption edge* of the element was overcome and an inner orbital electron was ejected (*photoelectron*) (Markowicz, 2002; Langhoff & Simionovici, 2006; Arkadiev et al., 2006; Skoog et al., 2017).

them unique in the identification and quantification of major and trace elements³³ (Janssens, 2004; Hall, 2017).

The mechanism of production of X-rays (Figure 39) is well-known and works through a sealed X-ray tube, composed of a target material (*anode*) and high-voltage electrons (*cathode*), generating a continuum (*bremstrahlung*) and characteristic X-rays, supposedly being able to reach certain element's excitation threshold. Then, a detector (*silicon drift detector*) measures the energy and intensity of secondary X-ray from the specimen, converting each photon into an electric signal. At the end, data is collected and distributed in a quasi-Gaussian fashion spectrum with bell-shaped X-ray peaks over several adjacent channels using a software routine (Jenkins, 1999; Markowicz, 2002; Janssens, 2004; Pollard et al., 2007; Shackley, 2011).

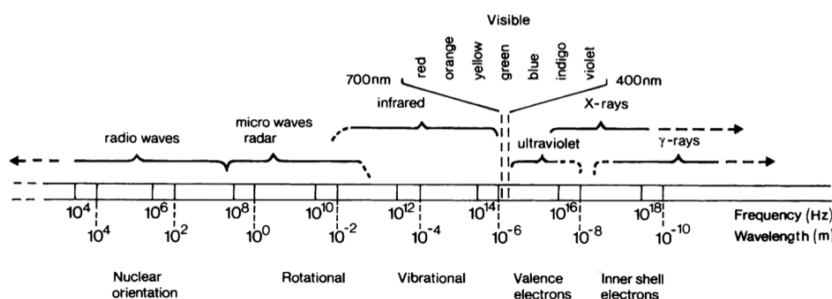


Figure 37: The electromagnetic spectrum, showing the X-ray area overlapping the ultraviolet and gamma regions (Pollard & Heron, 1996, p. 353).

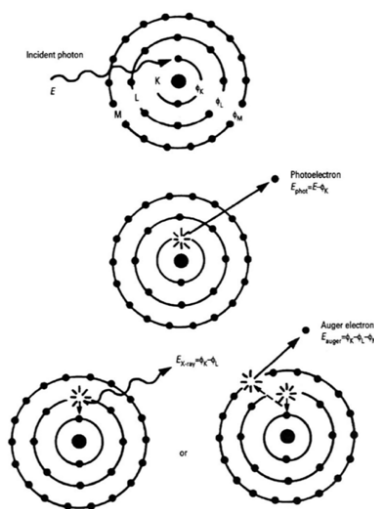


Figure 38: Photoelectric ionization (A) produced different de-excitation processes (B): the emission of either a characteristic X-ray fluorescence (radiative relaxation) (C) or a Auger electron (non-radiative relaxation) (D). The released energy is depicted by the binding energy difference of an electron from each atomic shell (ϕ_K , ϕ_L and ϕ_M) (Janssens, 2004, p. 134).

³³ Basically, qualitative and quantitative elemental analyses for elements greater than that of sodium (^{11}Na) are possible depending on the equipment. Using a portable XRF spectrometer Na cannot be detected (or accurately detected) because of the low energy of the photons emitted (Janssens, 2004).

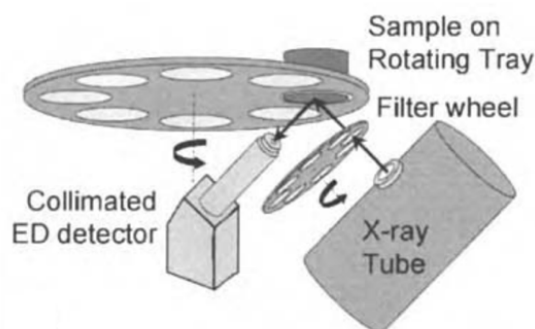


Figure 39: Schematic drawing showing the X-ray source and other components of a common benchtop XRF spectrometer (Janssens, 2004, p. 169).

4.4 SCANNING ELECTRON MICROSCOPE COUPLED TO AN ENERGY DISPERSIVE SPECTROMETER (SEM-EDS)

Further microstructural-chemical analysis can be achieved by the extremely high magnification (250 000x) and resolution properties³⁴ of a scanning electron microscope coupled to an energy dispersive spectrometer, SEM-EDS (Figure 40A). Thus, SEM-EDS once the specimen³⁵ is bombarded with an electron³⁶ beam, a depth-of-field examination of very small areas and compositional data can be obtained (Pollard et al., 2007; Price & Burton, 2011; Skoog et al., 2017; Ionescu & Hoeck, 2017).

Thereby, the interaction of the primary electron with the shallow surface of the specimen causes several phenomena that will be the basis of SEM-EDS (Figure 40B). The most important are the emission of secondary electrons, extremely useful to evaluate sample topography; the emission of backscattered electrons, which show high sensitivity to differences in atomic number (the higher the atomic number, the brighter the material appears in the image); the chemical identification and concentration via X-ray emission³⁷ normally presented in counts versus energy plot (Skoog et al., 2017; Ionescu & Hoeck, 2017).

³⁴ High-resolution imaging in SEM is characterized by sharp, shadowed, and three-dimensional images (Price & Burton, 2011).

³⁵ All the surface specimen under SEM analysis must be flat, polished and shiny, and normally electrically conducting. Thus the sample is generally coated with a thin carbon or gold layer for avoiding the primary electron beam to be deflected (Pollard & Heron, 1996; Price & Burton, 2011).

³⁶ A primary electron beam is produced by a conventional electron gun in a positive potential (about 30 kV) and addressed to specimen surface using different magnetic lenses. Also, the specimen chamber must be evacuated to counteract electron attenuation and scatter (Pollard & Heron, 1996; Pollard et al., 2007; Skoog et al., 2017).

³⁷ Instead of using X-ray radiation, SEM method employed high-energy electron beam for creating inner shell vacancies in specimen atoms, and the de-excited via the *Auger electron* ejection or the characteristic X-ray fluorescence. This process is the basis of the analytical operation of SEM coupled with EDS (Pollard & Heron, 1996).

In the field of ceramic studies, SEM-EDS allows the user to collect essential information, in this case, regarding ceramic paste and glaze characteristics. It is possible to evaluate the microstructure of specific inclusion and to understand the distribution of different chemical elements via elemental mapping. Also, a further examination can be carried out through the application of point and area analysis to analyse very small inclusions (Molera et al., 2007; Molera et al., 2013; Coentro, 2017; Molera et al., 2017; Salinas et al., 2018; Salinas & Pradell, 2018; Schurr et al., 2018; Costa et al., 2021).

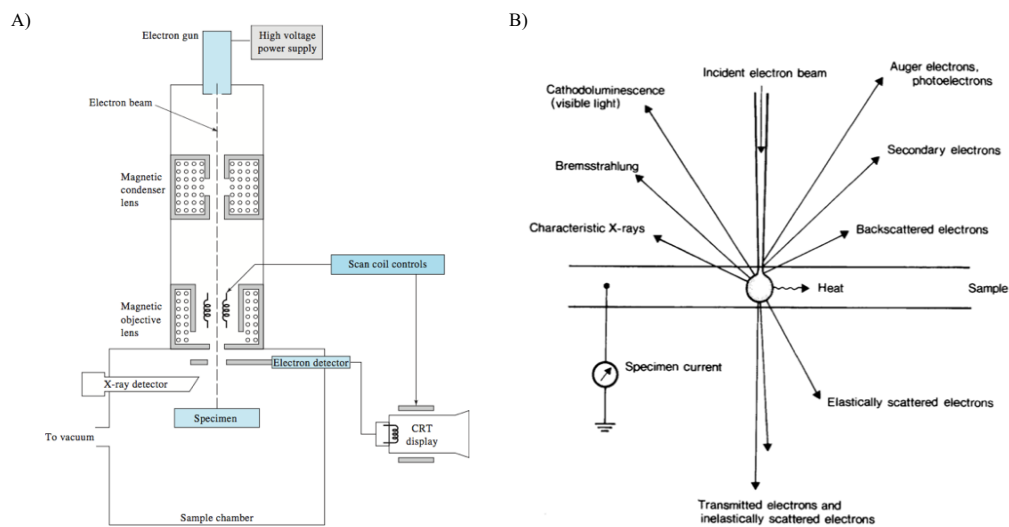


Figure 40: A) Schematic diagram of SEM with both electron and X-ray detection (EDS) (Skoog et al., 2017, p. 555). B) the result of the interaction between a primary electron beam and a solid sample (Pollard & Heron, 1996, p. 51).

CHAPTER 5: METHODS

5.1 SPECIMEN³⁸ PREPARATION PROCESS

The present specimen preparation description explains the steps carried out during the specimen preparation process in Hercules Laboratory (Évora-Portugal). The pottery assemblage was essentially composed of glazed and non-glazed ceramic fragments from Évora, Mértola and Silves. Due to their original sizes and the analytical instrumentations to be applied, a specific and different procedure was applied in specimen preparation.

Besides, pottery is a heterogeneous material and must be pre-treated to become a specimen appropriate for analysis. The samples were cut off, and the glazed decoration was removed using a straight grinder in the case of glazed coated specimens. Afterwards, one fragment of each sample was washed, dried and converted into a fine powder to perform XRD, XRF analyses and to evaluate the loss on ignition (LOI) in each case. A second fragment was utilized to prepare thin sections, and a third fragment was utilized to prepare polished blocks to develop the SEM-EDS analysis.

Sectioning Process

The starting point was the sectioning in several pieces (at least 3) from the bulk samples (Figure 41), taking into account a representative part of each ceramic fragment or chip³⁹. Thus, the body part of cooking and tablewares were cut perpendicularly to the ceramic walls, and an essential section of candles and handles was selected (Figure 42) (Cullum & Vo-Dinh, 2003; Injuk et al., 2006; Quinn, 2013; Whitbread, 2017).

It is noteworthy that the criteria for selecting the width and length of the ceramic chips were arbitrary⁴⁰, although some parameters should be followed. For instance, in the case of bichrome glazed ceramic, the black designs were included as a part of the chip (i.e. for polished blocks subjected to SEM-EDS). In addition, three slices with a rough weight of 2.5g were cut off for the incoming processes (Injuk et al., 2006; Whitbread, 2017).

³⁸ Most of the literature uses the term ‘sample’ and/or ‘specimen’ indistinctively, but some of them make a clear division between both concepts. For instance, any bulk sample can be used directly for analysis, but it is called a specimen as long as a pre-treatment is performed for a particular instrument (Jenkins, 1999; Janssens, 2003; Injuk et al., 2006).

³⁹ A cut ceramic fragment is often called chip in the related literature (Quinn, 2013; Whitbread, 2017).

⁴⁰ However, for thin section specimen part of the body, the base or the rim were chosen rather than other parts. Also, it was preferably performed vertical sections across the thickness of the ceramic wall which, according to Quinn (2013), contain more information about manufacturing process.

The sectioning process was performed with a cutting-grinding machine⁴¹, choosing end spots in regular-sized shards for preserving as much as possible the physical integrity of the specimen. Due to the usage of water for cutting off each fragment into slices, all the sub-samples were kept in a drying chamber (Figure 43) at a temperature around 40°C before being used again.



Figure 41. Process of cutting off the bulk samples (upper left). 42. Displaying of the sectioned ceramic pieces (lower left). 43. Drying chamber where were kept the chips after the sectioning procedure (right).

XRD and XRF Specimens

The glazed ceramic assembly underwent an additional practice, in which the glazed surface was removed from both inner and outer sides by a drilling machine. As a result, a chip was ready for making the fine powder and glass bead specimens for the incoming XRD and XRF analyses, respectively.

Fine powder⁴²

The whole batch of chips from whose glazed surface was removed were first subjected to a hand crushing using an agate mortar (Figure 44) and then ground into tiny particles using an automatic mill machine⁴³ (Figure 45 and 46) (Gauglitz & Vo-Dinh, 2003; Injuk et al., 2006).

⁴¹ The sectioning process was performed in a Discoplan-TS Struers®, with a rotary tile cutter with a circular, diamond-tipped blade lubricated with water.

⁴² In fine powder specimens some criteria must be taken into account for avoiding particle size effect in XRD and XRF analyses. Fine powder specimens must be ground to a particular grain size and have an uniform grain size distribution. Commonly, the grain size average for XRF is about 60 µm and for XRD is about 10 to 30 µm (Cullum & Vo-Dinh, 2003; Janssens, 2004; Injuk et al., 2006; Heimann, 2017).

⁴³ A Planetary ball mill – Retsch® with a ceramic drum and solid ceramic balls inside, performed in 500 rpm during 15 min, was used for becoming the samples into tiniest particles size.

Lastly, the resulting fine powder specimens were put in small plastic containers (Figure 47), labelled and preserved until being used for the XRD analysis. However, for XRF analysis, this stage was a necessary procedure to prepare glass beads.



Figure 44. Use of an agate mortar for the first hand-crushing (upper left). 45. A full ground using an automatic mill machine (lower left). 46. Solid ceramic balls inside a drum are involved in the ground process (upper right). 47. Fine powder specimens were preserved in small plastic containers and labelled (lower right).

Glass bead

A limited amount of fine powder was (1.2 gr) was used to prepare glass beads using a fusion machine⁴⁴. This procedure includes a flux addition (i.e. 12g of lithium tetraborate) mixed with the specimen in a standard proportion (1:10) (Figure 48).

The mixture of lithium tetraborate and fine powder took place inside a platinum-based crucible (Schmeling & Grieken, 2002; Injuk et al., 2006). Afterwards, the crucible with the mixture is inserted into the fusion machine⁴⁵ and fired at 1065 °C, for 24 min (Figure 49). At the end of the firing process, the molten liquid is casted into a smooth, circular mould for cooling down, resulting in a formation of a homogeneous solid glass disk with a mirror-like, flat surface (Cullum & Vo-Dinh, 2003; Hall, 2017). Subsequently, the glass beads were kept in hard-plastic containers, labelled and stored under a moisture-free environment desiccator (Schmeling & Grieken, 2002) until being used for analysis by XRF.

⁴⁴ In 1956, Claisse proposed preparing fused samples for XRF analysis in order to overcome the problems with powder and pellets. Thereby, this technique has become one of the most successful methods for XRF analysis, especially for making a homogeneous specimen with a given glass disk-like shape ideal for direct placement in a spectrometer (Jenkins, 1999; Schmeling & Grieken, 2002; Injuk et al., 2006).

⁴⁵ Claisse LeNeo® fusion furnace.



Figure 48. A certain amount of lithium tetraborate-metaborate-iodide and fine powder specimen is mixed for making glass beads (left). 49. Claiss LeNeo® fusion furnace and crucible inside (right).

Additionally, for the analysis of glass beads by XRF, LOI (loss on ignition) was carried out. It consisted of the calcination of ceramic crucibles (Figure 50) in a furnace at a temperature of 1100°C for 2 hours (Figure 51). After that, the crucibles were removed and placed into a desiccator with silica gel and closed until they got cool down (Figure 52). Subsequently, the crucible was weighted and around 1g of specimen powder was placed inside and weighted once again. The next step is the calcination of specimens and crucibles with the same above-mentioned temperature-time setting, then placed into the desiccator, cooled and weighed. The loss of weight was calculated with the differential weight of the calcinated crucible, crucible and specimen, and the final weight of the calcinated crucible plus sample (Figure 53) (Heiri et al., 2001).



Figure 50. Ceramic crucibles inside the furnace for the calcination (upper left). 51. A furnace where the calcination of fine powder specimens was carried out (upper right). 52. Desiccator with silica gel and crucibles getting cold inside in a dry environment. 53. Measuring the respective weights of crucibles and specimens (lower right).

SEM-EDS Specimens

Polish block

In this case, glazed ceramics was only considered in polish block specimens. Thus, all the chips intended to be used for the SEM-EDS analysis went through a different treatment, which consisted of putting them into a small plastic circular cast and englobed in an epoxy resin (i.e. 2 components: resin plus hardener) (Figure 54). The resulting resin block⁴⁶ will be used as a polish block specimen.

The filling was made up of a certain resin and hardener in the ratio of 3:1⁴⁷, poured into small cups with a chip inside, displaying the clay matrix (core) and decoration once the resin hardened (Figure 55). Additionally, the opposite side was polished and then labelled with a new and brief code.

A manual polishing for clearly displaying the core and decoration sections was practised on each resin block being, then coated with a thin film of epoxy resin⁴⁸. Afterwards, a thorough by-hand polishing was done just after the resin film got dried, making use of different emery paper⁴⁹ for getting a very clean, exposed chip, without any resin remnants (Figure 56).

The resin blocks, almost ready for becoming an appropriate specimen for the SEM-EDS analysis, were subjected to a soft finishing polishing carried out by a semi-automatically polishing-lapping machine with a coupled rotary platform upon which was placed a velvet-coated magnetic foil⁵⁰ (Figure 57). Additionally, deep scratches overglazed surface areas were removed by the application of different types of polishing suspensions⁵¹. In the end, an ultrasonic cleaning bath was considered for removing any fine grain contamination (Quinn, 2013; Hall, 2017; Ionescu & Hoeck, 2017).

⁴⁶ According to Quinn (2013), cross section will be called resin block.

⁴⁷ In a proportion of resin 25 gr per hardener 3 gr.

⁴⁸ Resin blocks are often impregnated with epoxy resin to fill the clay body pores and improving the mineral quantification and classification in thin section petrography (Braekmans & Degryse, 2017).

⁴⁹ Those were waterproof silicon carbide paper of certain roughness numbers in a progressive order of #320, #600, #220, #2400 and #4000.

⁵⁰ A couple of velvet-coated magnetic foils were used in a progressive order of 15 µm and 6 µm.

⁵¹ Diamond pastes in a progressive order of 15 µm, 6 µm and 1 µm were used.



Figures 54. A particular resin and hardener mixed together for making the epoxy resin (upper left). 55. Epoxy resin was poured into a small cups with the chips inside (upper right). 56. Process of hand-polishing for removing resin remnants (lower left). 57. A semi-automatically polishing-lapping machine with a coupled rotary platform for the finishing polishing onto a velvet-coated magnetic foil (lower right).

OM Specimens

Thin section

Another set of resin blocks, intended for OM (petrography) analysis, were subjected to another polishing process, employing silicon carbide (SiC) grit⁵² and water onto a thick-flat glass (Figure 58). The resin remnants over the resin block surface were removed and a thoroughly smooth and uniform, flat surface was obtained.

In order to keep the resin block surfaces in suitable condition for the next practice, additional finishing was performed using SiC, whether by hand and/or semi-automatically polishing-lapping device⁵³. In the former, was employed 800 grain-size SiC grit mixed with water over a flat, thick glass. For the latter, a rotating plate for the simultaneous polishing of eight resin blocks was used, employing a 1000 grain-size SiC grit, water and glycerine (Figure 59) (Quinn, 2013; Hall, 2017).

The next practice involved glueing the resin blocks against the polished glass slide surfaces through an epoxy resin coating⁵⁴, avoiding the appearance of bubbles. A drying period of 24 hours took place before a section of the resin blocks were removed by a saw (Figure 60). Then,

⁵² The first usage of silicon carbide grit with a grain size of 800 or 1000 were employed for getting a smooth resin block surface to easily bond to a glass slide (Schmeling & Grieken, 2002; Quinn, 2013).

⁵³ Automatic polishing of the resin block surfaces was performed in an RotoPol-35 Struers® abrasive rotary-type tool, coupled with a PdM-Force-20 Struers® lapping device.

⁵⁴ Glass slides should be previously polished down to a thickness about 1.16 mm by means of a diamond-covered rotating wheel, in this case a Discoplan-TS Struers® cutting-grinding semi-automatic machine.

the glass slide thickness was polished down into about 1.30 mm by a mechanical polishing⁵⁵ (Figure 61) (Quinn, 2013; Whitbread, 2017; Braekmans & Degryse, 2017). Finally, a time-consuming by-hand polishing was performed using 800 and 1000 grain-size SiC grits, water and a thick, flat glass plate. The uniform thickness and levelling was checked on by the interference colour pattern of mineral inclusions by a microscope⁵⁶ (Figure 62). Carborundum particles were taken away by smooth rubbing on an emery paper (Quinn, 2013; Braekmans & Degryse, 2017).



Figure 58. Hand polishing of polish blocks using a SiC grit, water and a flat, thick glass (upper left). 59. A semi-automatically polishing-lapping device was used in the process (middle up). 60. Glass slides attached to the resin blocks ready for polishing (lower left). 61. Mechanical polishing of glass slides by means of a diamond-covered rotating wheel (middle down). 62. Leveling of the glass slides were checked out through the interference colour pattern using and microscope (right).

⁵⁵ Once the resin block was totally attached over the glass slide was held in a jig under vacuum, and swept back and forth across a diamond-covered rotating wheel.

⁵⁶ A desired thin section thickness is achieved by-hand polishing until most mineral are translucent and the optical properties are visible (Braekmans & Degryse, 2017). Thus, by observing the interference colours of a key mineral like quartz, which displays pale yellow to grey and white colour about 30 μm (0.03 mm), is possible to determine the thickness of a specimen (Quinn, 2013).

5.2 INSTRUMENTAL CONDITIONS AND METHODS

A total of twenty-nine (29) ceramic fragments were selected from three important Portuguese cities during the Islamic rule of *al-Andalus* in the Iberian Peninsula: Évora, Mértola and Silves. They were analysed by OM (i.e. optical microscopy), X-Ray mineralogy (XRD), X-Ray fluorescence (XRF). In addition, in the case of glazed samples, microchemical and microstructural analyses were performed using a Scanning electron microscope coupled to an energy dispersive spectrometer (SEM-EDS).

Optical Microscopy (OM)

Thin sections were examined using a Leica DM2500P transmitted light microscope equipped with a Leica MC 170HD digital camera for image capture.

The clay matrix, particulate inclusion and voids in pottery fabric groups were described following the scheme proposed by P. S. Quinn (2013) and Adams et al. (1984) for the degree of sphericity and grain size description. Likewise, textural analysis (e.g. clay, temper and porosity percentage) and modal grain distribution were performed using the image processing package FIJI 1.0 software onto PPL and XPL images converted into a binary.

Additionally, high-quality pictures for each pottery group were collected using a different microscope, namely Hirox HR 5000E (140x magnification).

X-ray Diffraction (XRD)

Mineralogical analysis of each specimen was performed using fine powders (≈ 1 g). Analyses were performed using a BrukerTM AXS D8 Discovery diffractometer with Da Vinci design, equipped with Cu K α radiation source, operating at 40kV and 40mA, and a LynxEye 1-dimensional detector. The patterns were collected from 3°-75° 2θ , at a step size of 0.05° 2θ and 1s/step measuring time. Afterwards, identification of minerals was done using Diffract.EVA 5.0 software with PDF-2 mineralogical database (International Centre for Diffraction Data – ICDD). The semi-quantitative determination of the mineral abundance in the specimen was done following the Reference International Ratio (RIR) method, resulting in a percentage relative to a presumed 100% matrix of crystalline minerals (Hubbard et al. 1976; Hillier 2000).

X-ray Fluorescence Spectroscopy (XRF)

Major and minor chemical element concentrations were determined using a BrukerTM S2 Puma energy-dispersive XRF spectrometer (ED-XRF), equipped with a silver anode X-ray tube, and running after a careful calibration routine by siliceous commercial standards.

Spectra Elements 2.0 software was utilised for acquisition and data processing, giving rise to a resulting table with the oxides/elements concentration and the instrumental statistical error associated. Loss of ignition (LOI) data was taken into account for the final specimen weight. The data interpretation was done by means of the correlation between chemical elements using binary and ternary plots. Thus, in order to evaluate the interrelationship between glaze and clay bodies as a result of manufacturing processes (i.e. procurement, firing temperature), some chemical constituents such as CaO, MgO, Al₂O₃, SiO₂, Na₂O and K₂O were especially important.

Scanning Electron Microscope – Electron Dispersive Spectrometer (SEM-EDS)

A scanning electron microscope coupled to an energy dispersive X-ray spectrometer (SEM-EDS) was used for the micro-chemical and structural examination of glazed specimens, as well as the chemical composition of their clay bodies. Thereby, for the former, undecorated and black-decorated glazed areas over the inner and outer surfaces were selected for the analyses and for the latter, were chosen preferentially clay matrix areas avoiding mineral inclusions.

The equipment was a variable pressure Hitachi™ S-3700N SEM, operated with an accelerating voltage of 20 kV, in a pressurised chamber at 40Pa and a 10-13mm working distance. The coupled QUANTAX EDS microanalysis system equipped with Bruker™ XFlash 5010 Silicon Drift EDS Detector® (SDD), with a spectral resolution of 129 eV at FWHM/Mn K α .

The chemical composition of glazed and ceramic bodies was an average result of three (3) different analytical spots, considering the natural spatial and compositional heterogeneity and avoiding any inclusion interferences. Additionally, punctual microanalyses were performed in bubbles, mineral phases and glaze/body interface. Thus, elemental concentrations were subsequently converted to oxides by stoichiometry and normalised to 100%.

The EDS data were acquired by point microanalyses and in elemental distribution maps, processed with Esprit 1.9 software. The SEM images were acquired in backscattered (BSE) and secondary electron (SE) modes.

CHAPTER 6: RESULTS AND DISCUSSION

6.1 CHRONOLOGY AND TYPOLOGY – RESULTS AND DISCUSSION

The following typological and chronological description will be a way to put in order the ceramic material acquired in the present study, and to notice some temporal patterns based on the morphofunctional analysis.

A first distinction was confirmed by archaeological studies in which two sets of wares were identified as a preliminary classification approach: tableware and cookware (Gomez, 2004; Gonçalves et al., 2009; Santos, 2015).

All the ceramic objects intended to be used in a kitchen are grouped into the cookware assembly, whether or not for being directly exposed to the fire. According to their morphological characteristics and physical attributes and referential literature were identified two kinds of vessels: cooking pots and casseroles (Gomez, 2004)

In the set of vessels, suitable for displaying and serving food, called tablewares, were possible to identify bowls and small bowls, small jugs and only one small bottle and a tureen. Most of them display either monochrome or black-decorated honey glazes. However, in those with unglazed treatment (EVR 7 and 8), remnants of additional superficial finishing, namely slip covering, were identified.

Additionally, other ceramic objects are present in the analysed assembly, such as three oil lamps, totally covered by a monochromatic glaze, and only one kiln tool called tripod stand or stilt, without any special superficial treatment.

Relative Chronology

Évora

The following explanation about the relationship between formal ceramic characteristics and chronology will consider the contextual circumstances (i.e. archaeological context) in which, the ceramic objects were retrieved to give a temporal sense to the given typological assembly. Évora ceramic assemblage comes from different archaeological contexts, most of them with a reliable relative chronology and preliminary typological analyses carried out by their respective researchers (Teichner, 1995; Gomez, 2004; Gonçalves et al., 2009; Santos, 2015; Lopez & Santos, 2015; Santos, 2016). Thus, the time-lapse established as a working framework goes from the 10th to mid-13th centuries AD, considering the Christian conquest of Évora (1165 AD),

Silves (1189 AD) and Mértola (1238 AD). Thereby, the period of time is corroborated by the formal typological analysis of each ceramic piece, following explained.

Regarding the collection of cooking pots was documented a remnant 'S' profile from the Emiral period, but with some additional modification such as the overall globular body, relatively short, concave neck (*curved inverted bitronchoconic*) and especially triangular lips, which placed the cookwares in a range of time between the second half of the 10th and 11th centuries AD (Gómez et al., 2015; Lopez & Santos, 2015; Santos, 2016). Additionally, the common usage of a rapid wheel throwing in the ceramic production, attesting by the stretch marks over the surface, support the above-mentioned relative chronology (Acien et al., 1995; Gómez, 2018).

It is noteworthy that the documented reduced neck and the triangular form of rims are traces that will develop later about the 11th century AD, jointly with shorter bodies (Gómez et al., 2012; Lopez & Santos, 2015).

A morphological development is seen in the group of casseroles (EVR 6 and 10). In EVR 6 were documented traces from Emiral period such as a soft carination, an inverted rim and a semi-spherical body (Gómez, 2018); on the other hand, attributes that belong to a later formal change such as a strong carination, an everted rim and two potential handles, were reported in EVR 10 (Santos, 2016). Thereby, the chronology for these ceramic specimens goes from the second half of the 11th century AD (Taifa kingdoms) to the subsequently 12th century AD (Almohad period) (Gómez et al., 2012; Lopez & Santos, 2015).

A set of ceramic vessels are small jugs. Two of them (EVR 7 and 8) are undecorated and display the common simplified shape evidenced from the 10th to 11th centuries AD, besides other characteristics such as everted cylindrical neck and carinated body, and potential handles and slip coatings (Lopez & Santos, 2015; Santos, 2016; Gómez, 2018). Evenly, the other ones (EVR 2 and 12), as a part of a small jug totally covered by honey glaze with some black-decorated designs, belong to around the 11th century AD, when the honey-glazed black-decorated ceramic production are more frequent in all the Gharb *al-Andalus* until the 12th century AD⁵⁷ (Acien et al., 1995; Gómez et al., 2012).

A temporal grouping was noticed in two sets of vessels consisting of black-decorated honey-glazed and monochrome bowls. One group (EVR 11 and 13) with a characteristic broken profile (strong carination) are temporally related to others (EVR 3, 14 and 18) with attributes

⁵⁷ Although, honey brown glazes with black decoration were reported from the 10th century and become more abundant onwards, regarding the entirely al-Andalus (Molera et al., 2017)

such as low annular feet, everted rims and thick walls. These formal correlations establish a period of time around the 11th century AD and onwards (Acien et al., 1995; Gómez et al., 2012; Lopez & Santos, 2015; Santos, 2016; Gómez, 2018).

By means of the formal characterisation of the oil lamps, a range of relative time could be established firmly. Thus, the relatively small repository with long, faceted spout are highlighted attributes that set the collection of oil lamps into a chronological time around the 10th and 11th centuries AD (Gómez et al., 2012; Lopez & Santos, 2015).

In addition, kiln tools such as tripod stand or stilt have been reported from early Islamic time (second half of 9th century AD) into the kiln furniture of the first workshops (i.e. Pechina), so the presence of one of them in the ceramic collection does not mean any important temporal information (Salinas et al., 2009).

Mértola

The ceramic sherd assemblage was retrieved from a reliable archaeological context dating about the second half of the 12th century AD and the first half of the 13th century AD, during the Almohad occupation. The material attributes shed important light on the glazing and pottery production at that time. The collection consists of a black-decorated honey-glazed and monochrome bowls displaying low annular foot and strong carination, a monochrome-glazed faceted-body oil lamp⁵⁸, and a opacified glaze coating over a part of a small jug.

Silves

The ceramic materials were unearthed from a secure deposit formed over the Almohad period (second half of 12th and the first half of 13th centuries AD). The collection consists of tablewares covered by a honey glaze with black decorations. Additionally, it is noteworthy that some morphological attributes such as thick walls and diagonal high annular foot could belong to the last part of the Almohad occupation.

6.2 OPTICAL MICROSCOPY (OM) – RESULTS AND DISCUSSION

In the present section, the individual characteristics of each specimen are reported in ceramic paste analysis (Table 2) and temper material description (Table 3). The data allowed to group the specimens in 6 different fabrics.

⁵⁸ The morphological characteristic of oil lamps with faceted sides started to appearing from the late 11th century AD to the half of 12th century AD (Gomez, 2004).

Pottery Fabric 1 (PF1)

Pottery included in PF1 comprised five cookware (EVR 1, 4, 5, 6 and 10), two tableware (EVR 7 and 8) and the tripod (EVR 9). Cookware and tableware are not glazed and show a coarse manufacture. On the tripod, some glaze drops have been observed attached to the surface.

The PF1 group (Figure 63) has a brown-coloured, highly homogeneous and iron-rich clay paste (74% - 85%). The only exception is sample EVR 9, that has a slightly red-buffy-coloured ceramic matrix. Porosity is mainly composed of meso-vughs and meso-elongate voids (4% - 11%), while non-plastic inclusions (11% - 17%) are close-spaced, weakly aligned, very poorly sorted and very angular to subangular in shape. In addition, most of them show a unimodal grain size distribution. The only two exceptions are EVR 1 and 9, which shows bimodal grain size distribution.

Mineralogically, PF1 is characterized by non-plastic inclusions of amphiboles (probably hornblende and/or cummingtonite), plagioclases, biotite, quartz, opaque minerals, potassium-rich feldspars (rare), and muscovite (rare). In addition, pyroxene (rare) were also identified in EVR 5, 6, 7, 8 and 9 specimens. Regarding rock fragments, inclusions of plutonic acid (i.e. granite and tonalite) were identified.

The mineralogy and rock fragments identified during the petrographic analysis of the specimens included in fabric PF1 indicate that they are compatible with the regional geology of the area of Évora (Moita et al., 2009) described in section 2.2. Consequently, they were undoubtedly locally produced. The raw material was not accurately treated and decanted, and this was related to the final object function. Actually, PF1 was indistinctively employed in the fabrication of cooking pots and tablewares (i.e. jugs). Additionally, the employment of temper-rich materials was probably intended to improve the thermal shock resistance and heating effectiveness of cooking pots or the refractoriness of kiln tools (Quinn, 2013).

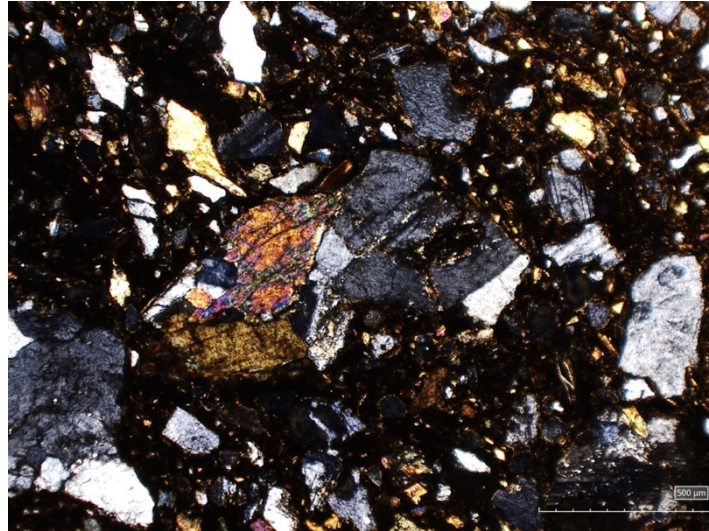


Figure 63: A representative microphotograph (XPL) of the Pottery Fabric 1 belonging to the specimen EVR 6.
A tonalite rock fragment can be seen in the picture.

Pottery Fabric 2 (PF2)

The pottery assemblage of PF2 comprised six tableware (EVR 3, 14, 18, MER 21, 22, 23 and SIL 27) and one oil lamp (EVR 15), characterized by displaying a honey-glazed coating with black-coloured designs only in EVR 3, 14 and SIL 27 specimens.

The PF2 has a heterogeneous brown/red-buff coloured ceramic paste (84% - 94%). Lime nodules and unmixed red clay pellets could be frequently observed (Figure 64 and 65). It seems that two different components were equally included in the ceramic past (calcium-rich and iron-rich). Porosity is composed of micro-to-macro-sized vughs, vesicles and elongate voids (1% - 4%). Non-plastic inclusions (5% - 14%) are generally very angular to subrounded, moderately sorted, weakly aligned, and with a close-to-single-spaced packing. Likewise, all of them show a unimodal grain size distribution.

Mineralogically, PF2 is characterized by the recurrent presence of quartz, potassium-rich feldspar, muscovite (rare) and plagioclase. Amphiboles (rare) were also detected in specimens EVR 3, MER 21 and 23. Regarding rock fragments, most specimens present are quartzite, sandstone (Figure 66) and granite inclusions.

The mineralogy and rock fragments identified during the petrographic analysis of the specimens included in fabric PF2 suggest that they are compatible with the regional geology of Silves area described in section 2.2. Besides, the identification of sandstone fragments is extremely diagnostic in this sense, considering the presence of the Silves sandstone formation close to the city. It is important to notice the specimen origin heterogeneity, and fragments

recovered in the city of Mértola and Évora that have been included in this group, suggests an active trade among these three localities.

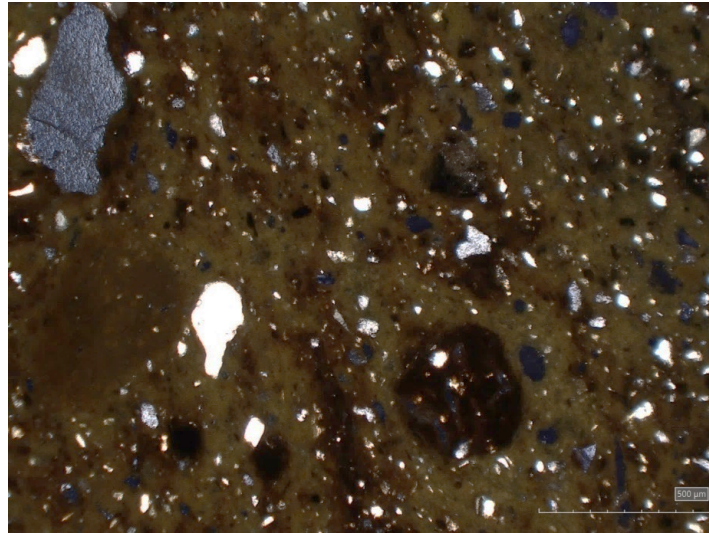


Figure 64: A representative microphotograph (XPL) of the Pottery Fabric 2 belonging to the specimen EVR 18.
Lime nodules and clay pellets can be clearly distinguished

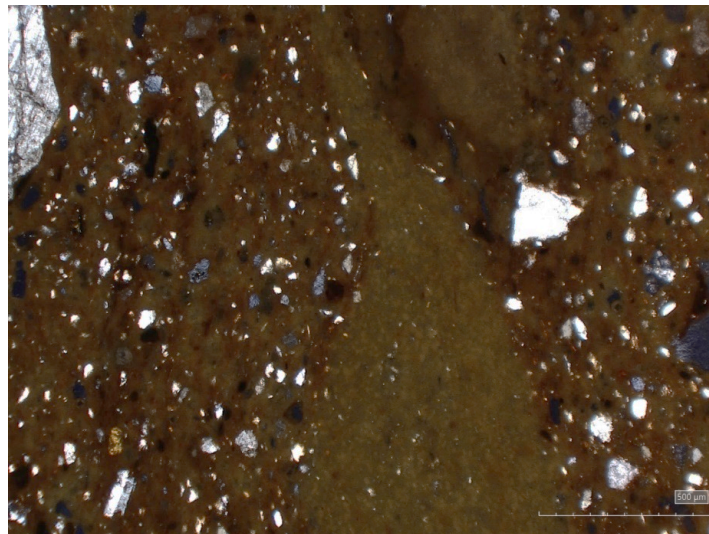


Figure 65: A representative microphotograph (XPL) of the Pottery Fabric 2 belonging to the specimen SIL 27.
An unmixed lime nodule can be clearly distinguished.

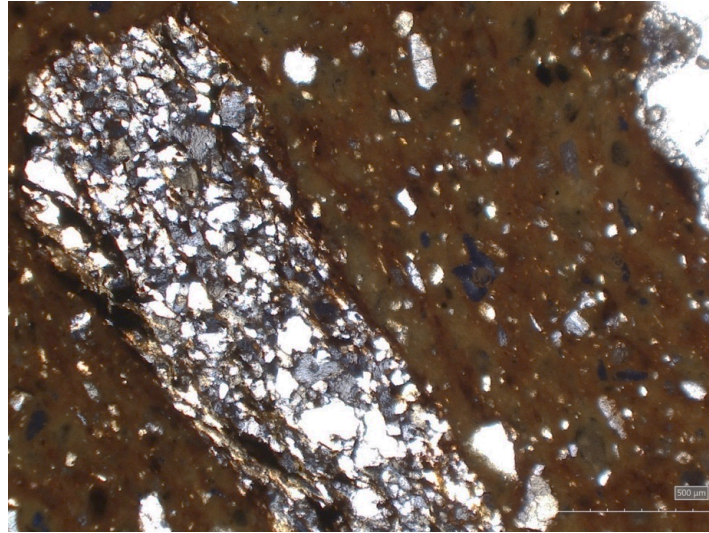


Figure 66: A representative microphotograph (XPL) of the Pottery Fabric 2 belonging to the specimen SIL 27. A fragment of sandstone can be clearly observed.

Pottery Fabric 3 (PF3)

The pottery assemblage of PF3 comprised five tableware (EVR 11, 13, 17, SIL 25 and 26), displaying honey glaze with black decoration in most of them, excepting EVR 13 with just honey glaze.

The PF3 has a red-buffy coloured and slight to moderate homogeneous ceramic paste (88% - 93%). Unmixed red clay pellets were observed in the whole batch (Figure 67 and 68). Lime nodules were observed just in EVR 13 and SIL 26 specimens. Thus, two different components (iron rich and lime rich), similarly to PF2, were included in the ceramic paste, but the contribute of the lime component is stronger if compared to PF2. So, similar raw materials were probably employed. Porosity is composed of meso-to-macro-sized vughs, vesicles and elongate voids (1% - 2%). Non-plastic inclusions are subangular to subrounded in shape (5% - 10%), moderately sorted, weakly aligned, and whit a close-to-single-spaced packing. Grain size distribution is unimodal in most cases, except in specimens EVR 17 and SIL 25 (weakly bimodal) and SIL 26 (bimodal).

Mineralogically, PF3 is characterized by the presence of quartz, potassium-rich feldspars, plagioclase feldspars (rare), and muscovite (rare). Amphiboles (rare) were also identified in specimens EVR 17, SIL 25 and 26. Regarding rock fragments, most specimens present quartzite, sandstone and granite inclusions. In addition, thermally altered limestone, bioclast, and secondary calcite were observed in SIL 25.

The mineralogy and rock fragments identified during the petrographic analysis of the specimens suggest that fabric PF3 is very similar/compatible with fabric PF2, and the same observation regarding specimen's provenance are valid.

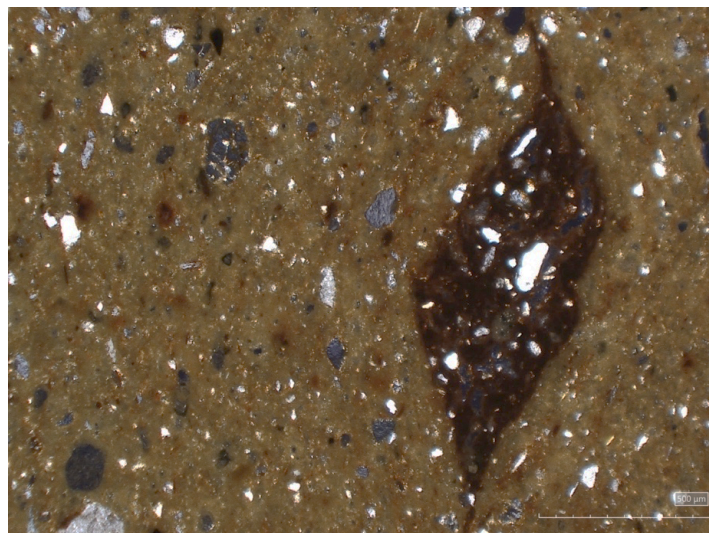


Figure 67: A representative microphotograph (XPL) of the Pottery Fabric 3 belonging to the specimen SIL 26.
A clay pellet can be clearly observed.

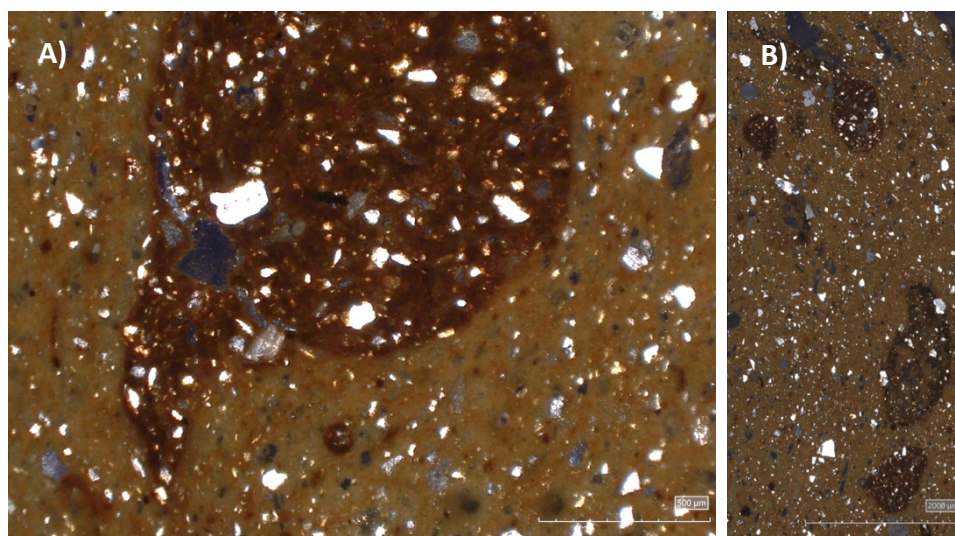


Figure 68: A representative microphotograph (XPL) of the Pottery Fabric 3 belonging to the specimen EVR 13.
A unmixed clay pellet (A) and lime nodules (B) can be clearly identified.

Pottery Fabric 4 (PF4)

The PF4 includes only one specimen (EVR 12) (Figure 69), a honey-glazed with black decoration tableware. The specimen has a buffy-coloured, highly homogeneous and calcium-rich ceramic paste (95%), displaying a porosity composed of meso-vughs and meso-elongate

voids (1%). Non-plastic inclusions are angular to subangular (4%), moderately sorted, weakly aligned, and with a single-to-double-spaced packing. Grain size distribution is unimodal.

Mineralogically, PF4 contains quartz, potassium-rich feldspar, plagioclase feldspars, muscovite (rare) and biotite. Regarding rock fragments, thermally altered limestone and schist fragments were identified in addition to some bioclast.

From the mineralogy and rock fragments identified in specimen EVR 12, at present, it is not possible to indicate its provenance. It is supposed that it was probably imported to Évora from an unidentified workshop located in southern Iberia.

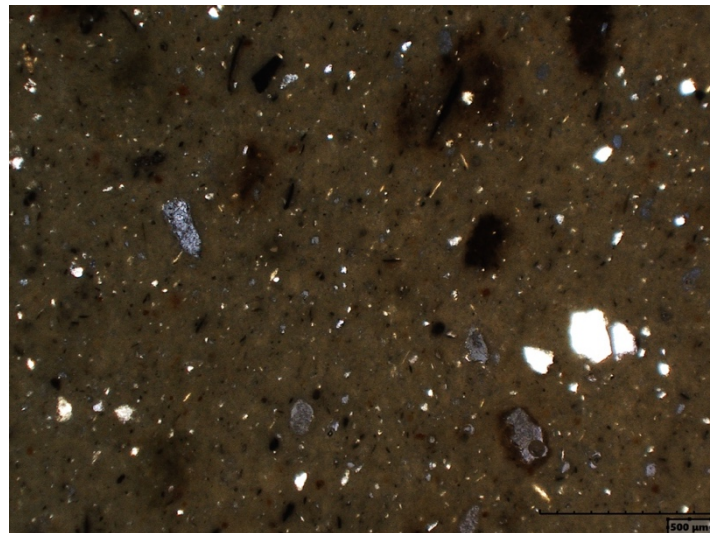


Figure 69: A representative microphotograph (XPL) of the Pottery Fabric 4 belonging to the specimen EVR 12.

Pottery Fabric 5 (PF5)

The PF5 comprised two specimens (EVR 16 and MER 24) with a honey glaze. The ceramics have a buffy-coloured, moderately homogeneous and calcium-rich ceramic paste (88% - 96%), displaying a porosity composed by meso-to-macro-sized vughs and elongate voids (2%). Non-plastic inclusions are angular to subangular (2% - 10%), moderately sorted, weakly aligned, and with a close-to-single-spaced packing. Grain size distribution is unimodal.

Mineralogically, PF5 is made up of quartz, potassium-rich feldspar, muscovite, biotite (rare) and calcite (some crystals thermally altered, figure 70). Pyroxene and amphibole were also identified in EVR 16. Regarding rock fragments, thermally altered limestone and gneiss were detected, with the additional presence of quartzite and schist in EVR 16. Additionally, secondary calcite could also be observed in the porosity system.

Considering ceramic paste characteristics, the mineralogy and rock fragments identified in specimens EVR 16 and MER 24, it is not possible to indicate with certainty their provenance.

Nevertheless, it is supposed that they were probably imported to Mértola and Évora from an unidentified workshop located in southern Iberia.

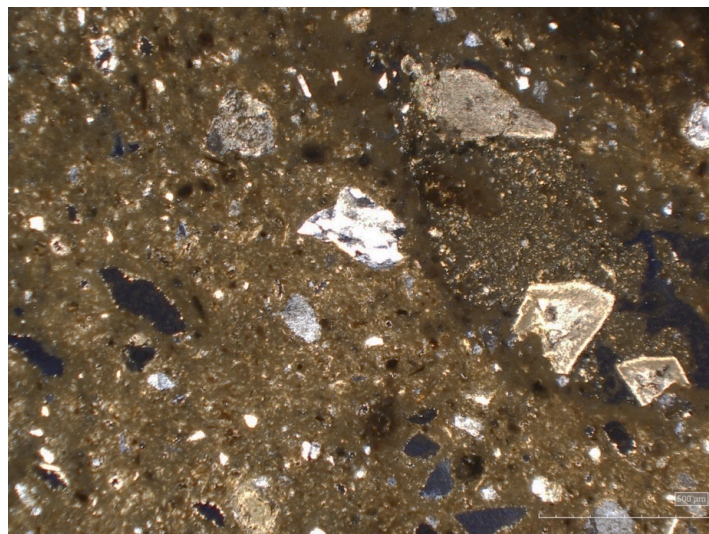


Figure 70: A representative microphotograph (XPL) of the Pottery Fabric 5 belonging to the specimen EVR 16. Thermally altered crystals of calcite can be observed on the right side of the picture.

Pottery Fabric 6 (PF6)

The pottery assemblage of PF6 comprised five tableware (EVR 2, MER 19, 20, SIL 28 and 29), displaying honey glaze with black decoration, except MER 20 that has a whitish glaze.

The PF6 has a red-buff coloured, moderately homogeneous and iron-rich ceramic paste (90% - 94%), displaying a porosity made up of meso-to-macro-sized vughs and elongate voids (2% - 4%). Non-plastic inclusions are very angular to subangular (3% - 7%), moderately sorted, weakly aligned and with a close-to-single-spaced packing. Grain size distributions are both unimodal (EVR 2 and MER 20) (Figure 71) and bimodal (MER 19, SIL 28 and 29).

Mineralogically, PF6 is characterized by the presence of muscovite (very abundant, especially mixed in the ceramic matrix, figure 72), quartz and potassium-rich feldspar and plagioclase feldspar (rare). Amphiboles (brown) could be observed in EVR 2, MER 19 and 20 only. Regarding rock fragments, quartzite, greywacke and chert were identified (Figure 9). Additionally, glass fragments were observed within the ceramic paste of specimen MER 20.

The mineralogy and rock fragments identified on ceramic specimens included in PF6 are compatible with the local geological setting of Mértola area, described in section 2.2. It is interesting to notice that the same tempering materials have been identified within the ceramic matrix of some ceramic pieces from Mértola itself, Évora and Silves, which correspond to the PF 6 (EVR 2, MER 19, 20, SIL 28 and 29). So, Mértola ceramics were traded to different cities.

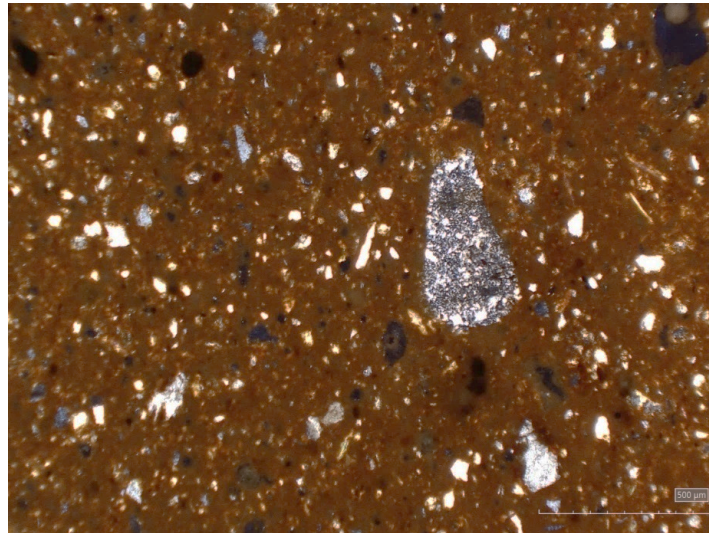


Figure 71: A representative microphotograph (XPL) of the Pottery Fabric 6 belonging to the specimen EVR 2.
A fragment of chert can be clearly observed in the picture.

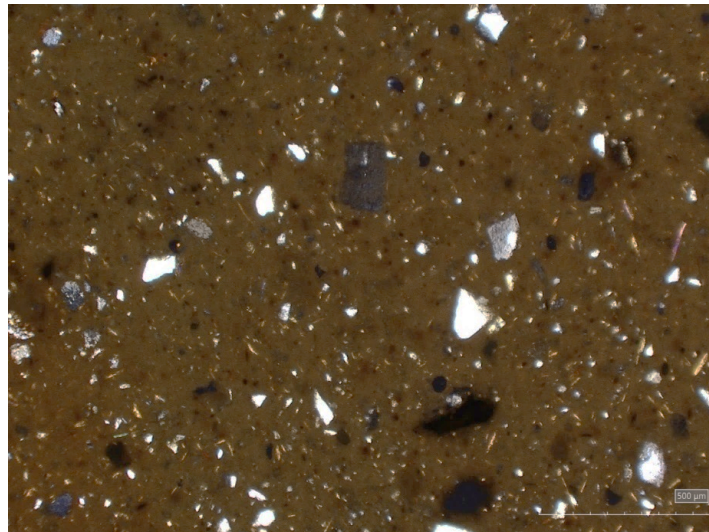


Figure 72: A representative microphotograph (XPL) of the Pottery Fabric 6 belonging to the specimen MER 20.
The ceramic paste is extremely rich in small muscovite crystals.

Table 2: Ceramic paste analysis (Decoration: unglaze ware, U; glazed ware, G; black-decorated glazed ware, BG – Pottery fabric, PF – Matrix homogeneity/heterogeneity: highly homogeneous, H. Hom.; moderately homogeneous, M. Hom.; slightly homogeneous, S. Hom.; highly heterogeneous, H. Het.; moderately heterogeneous, M. Het.; slightly heterogeneous, S. Het. – Fe-Ca rich matrix: Iron-rich matrix, Fe; moderately iron, m. Fe; slightly iron, s. Fe; calcium-rich matrix, Ca; slightly calcitic, s. Ca; moderately calcitic, m. Ca; highly calcitic, h. Ca – Matrix activity: slightly active, S; moderately active, M; highly active, H; isotropic, I – Alignment: weak, W; moderate, M; strong, S – Main grain shape: mainly equal (rounded) and elongated grains, Eq & El; mainly elongated and equal grains, El & Eq – Roundness: very angular, Va; angular, A; subangular, Sa; subrounded, Sr; rounded, R; well rounded, Wr – Packing: close-spaced, CS; single-spaced, CS; double spaced, DS; open spaced, OS – Sorting: very poor, VP; poor, P; moderate, M; well, W - Grain size distribution (G.S.D.): unimodal, U; bimodal, B; polymodal, P).

SAMPLE	Typology	Decoration	Fabric	Ceramic paste description					Porosity			Temper description							
				Colour	Hom. – Het.	Fe- Ca rich matrix	Activity (S-I)	%	Description	%	Shape	Description	Roundness	Packing	Max size μm	Alignment	Sorting	G.S.D.(BM-U)	%
EVR-1	Pot	U	PF1	Brown	H. Hom.	Fe	S	81.81	Meso-macro vughs and el voids	6.65	Eq&El	Very ang-subrounded eq/ang-subang el	Va-Sr	Cs	754	W	VP	B	11.54
EVR-2	Small Jug	BG	PF6	Red-Buffy	M. Hom.	Fe-s.Ca	I	91.75	Meso-mega vughs and meso el voids	1.56	Eq&El	Very and-subang eq and el	Sa-Sr	Cs-Ss	1160	W	M	U	6.68
EVR-3	Bowl	BG	PF2	Brown-buffy-black	M. Het.	Fe-s.Ca	I	83.79	Meso-mega vughs/ meso vesicles	4.34	Eq&El	Angular-subrounded eq/el ang-subrounded	Sa-Sr	Cs	1082	W	M	U	11.87
EVR-4	Pot	U	PF1	Brown	H. Hom.	Fe	I	77.93	Meso-macro vughs and meso el voids	5.16	Eq&El	Very ang-subang eq and el	Va-Sa	Cs	1582	W	VP	U	16.91
EVR-5	Pot	U	PF1	Brown	H. Hom.	Fe	I	80.14	Meso-macro vughs/meso el voids	5.85	Eq&El	Very ang-subang eq/very-ang-subang el	Va-Sa	Cs	1107	W	VP	U	14.02
EVR-6	Casserole	U	PF1	Brown	M. Hom.	Fe	I	74.79	Meso and mega vughs and meso and micro el voids (channel)	9.56	Eq&El	Very ang-subang eq/very ang-subang el	Va-Sa	Cs	1113	W	VP	U	15.65
EVR-7	Small Jug	U	PF1	Brown	H. Hom.	Fe	S	79.90	Meso-macro vughs and el voids	8.10	Eq&El	Very ang-subang eq/very ang-subang el	Va-Sa	Cs	1825	W	VP	U	12
EVR-8	Small Jug	U	PF1	Brown	H. Hom.	Fe	S	77.95	meso vughs/meso el voids	7.24	Eq&El	Very ang-subang eq/very ang-subang el	Va-Sa	Cs	1435	W	VP	U	14.81
EVR-9	Tripod	G	PF1	Red-Buffy	M. Het.	Fe-s.Ca	I	85.10	Meso-mega vughs and el voids	4.05	Eq&El	Ang-subang eq and el	A-Sa	Cs-Ss	1204	W	VP	B	10.85
EVR-10	Casserole	U	PF1	Brown	H. Hom.	h. Fe	S	73.86	Meso mega vughs and el voids	10.84	Eq&El	Very yang-subang eq/very ang-subang el	Va-Sa	Cs	896	W	VP	U	15.30
EVR-11	Bowl	BG	PF3	Buffy	M. Hom.	Ca-s.Fe	I	93.08	Meso-macro vughs/meso-el. voids	0.97	Eq&El	Subang-subround eq and el	Sa-Sr	Cs-Ss	912	W	M	U	5.95
EVR-12	Small Jug	BG	PF4	Buffy	H. Hom.	h.Ca	I	95.42	Meso el. voids and vughs	1.13	Eq&El	Angular-subang eq/ang-subang el	A-Sa	Ss-Ds	954	W	M	U	3.5
EVR-13	Bowl	G	PF3	Buffy-Red	M. Hom.	Ca-s.Fe	S	90.56	Meso-macro vughs/meso vesicles	1.33	Eq&El	Subang-subround eq and el	Sa-Sr	Cs-Ss	1899	W	M	U	8.11
EVR-14	Bowl	BG	PF2	Red-buffy	S. Het.	Fe-m.Ca	I	93.50	Meso-micro vughs and el voids	1.35	Eq&El	Very ang-subang eq and el	Va-Sa	Ss-Ds	117	W	M	U	5.16
EVR-15	Oil Lamp	G	PF2	Red-buffy	M. Het.	Fe-s.Ca	I	83.50	meso-macro vesicles/macro-el. voids	2.17	Eq&El	Angular-subang eq/ang- subang el	Sa-Sr	Cs-Ss	1321	W	M	U	14.33
EVR-16	Oil Lamp	G	PF5	Buffy	M. Hom.	h.Ca	S	88.14	Micro-meso vughs/meso el. voids	1.95	Eq&El	Ang-subang eq/ang-subang el	As-Sr	Cs-Ss	470	W	M	U	9.91

EVR-17	Bowl	BG	PF3	Buffy	M. Hom.	Ca-s.Fe	I	92.26	Meso-macro vughs/micro-meso vesicles	0.61	Eq&El	Subang-subround eq and el	Sa-Sr	Cs-Ss	939	W	M	B	7.12
EVR-18	Bowl	G	PF2	Buffy-Brown	H. Het.	Ca-m.Fe	S	89.70	Micro-meso vughs/micro-meso el. voids	1.01	Eq&El	Subang-subround eq and el	Sa-Sr	Cs-Ss	798	W	M	U	9.30
MER-19	Bowl	BG	PF6	Red-Buffer	M. Hom.	Fe-m.Ca	I	90.47	Meso-macro vughs/meso vesicles/meso-macro el. voids	4.16	Eq&El	Very ang-subang eq/el ang-subang el	Sa-Sr	Cs-Ss	770	W	M	B	5.37
MER-20	Small Bottle	G	PF6	Buffy-Red	S. Hom.	Fe-m.Ca	I	94.02	Meso vesicles, vughs and el. voids	2.60	Eq&El	Subang-subround eq and el	Sa-Sr	Cs-Ss	275	W	M	U	3.38
MER-21	Bowl	G	PF2	Red-Buffer	M. Het.	Fe-s.Ca	I	90.37	Meso-micro vughs/meso vesicles/meso-macro el. voids	2.63	Eq&El	Ang-subang eq/ang-subang el	A-Sa	Cs-Ss	373	W	M	U	6
MER-22	Bowl	G	PF2	Red-Buffer	H. Het.	Fe-m.Ca	I	87.53	Meso vughs, vesicles and el. voids	0.92	Eq&El	Very ang-subround eq and el	Va-Sr	Cs-Ss	1091	W	M	U	11.54
MER-23	Small Jug	G	PF2	Red-Buffer	M. Het.	Fe-s.Ca	S	86.16	Micro-mega vughs and el voids.	1.50	Eq&El	Very ang-subang eq/very ang-subang el	Va-Sa	Cs	958	W	M	U	12.35
MER-24	Oil Lamp	G	PF5	Buffy	M. Hom.	h.Ca	I	95.92	Meso-macro vughs/meso vesicles and el. voids	2.03	Eq&El	Ang-subang eq and el	A-Sa	Ss	243	W	M	U	2.04
SIL-25	Tureen	BG	PF3	Red-Buffer	M. Hom.	Ca-s.Fe	I	87.84	Meso vesicles and meso-mega vughs and el. voids	2.00	Eq&El	Subang-subround eq and el	A-Sa	Cs-Ss	346	W	M	U	10.17
SIL-26	Small Bowl	BG	PF3	Buffy-Red	M. Hom.	Ca-s.Fe	I	92.82	Meso vesicles and meso-macro vughs and el. voids	2.27	Eq&El	Subang-subround eq and el	A-Sa	Ss	494	W	M	B	4.91
SIL-27	Small Bowl	BG	PF2	Red-Buffer	H. Het.	Fe-m.Ca	I	88.44	Meso vesicles and meso-macro vughs and el. voids	1.43	Eq&El	Very ang-subang eq and el	A-Sa	Cs-Ss	1718	W	VP	U	10.13
SIL-28	Small Bowl	BG	PF6	Red-Buffer	M. Hom.	Fe-m.Ca	I	94.44	Meso-mega vughs and el voids	1.86	Eq&El	Subang-subrounded eq/very ang-subang el	Sa-Sr	Cs-Ss	1892	W	M	B	3.71
SIL-29	Small Bowl	BG	PF6	Red	S. Hom.	Fe-s.Ca	S	93.70	Meso vesicles, vughs and el. voids	0.84	Eq&El	Subang-rounded eq/ang-subang el	Sa-Sr	Cs-Ss	725	W	M	B	5.46

Table 3: Temper material description of the mineral, rock fragments and distinctive inclusion particulates identified by Optical Microscopy.

Sample	Typology	Dec	Fabric	Mineralogy	Rock fragments	Observations
EVR1	POT	U	PF1	Plagioclase, amphiboles (hornblende), opaque minerals, quartz, biotite	Rock frag. of plutonic mafic (tonalite) and acid rock (granite)	
EVR2	SMALL JUG	BG	PF6	Muscovite, quartz, amphibole (brown), feldspar, plagioclase (rare)	Quartzite, greywacke, chert	Very small crystals mixed in ceramic matrix muscovite – VERY ABUNDANT
EVR3	BOWL	BG	PF2	Quartz, feldspar, plagioclase, muscovite (rare), amphibole (rare)	Frag. of granitic rock (felsic), quartzites, sandstone	Big lime inclusion. Highly het. ceramic matrix
EVR4	POT	U	PF1	Plagioclase, amphiboles (hornblende), opaque minerals, quartz, biotite	Rock frag. of plutonic mafic (tonalite) and acid rock (granite)	
EVR5	POT	U	PF1	Plagioclase, amphiboles (hornblende), opaque minerals, quartz, biotite, pyroxene (rare)	Rock frag. of plutonic mafic (tonalite) and acid rock (granite)	
EVR6	CASSEROLE	U	PF1	Plagioclase, amphiboles (hornblende), opaque minerals, quartz, biotite, pyroxene (rare)	Rock frag. of plutonic mafic (tonalite) and acid rock (granite)	
EVR7	SMALL JUG	U	PF1	Plagioclase, amphiboles (hornblende), opaque minerals, quartz, biotite, pyroxene (rare)	Rock frag. of plutonic mafic (tonalite) and acid rock (granite)	
EVR8	SMALL JUG	U	PF1	Plagioclase, amphiboles (hornblende), opaque minerals, quartz, biotite, pyroxene (rare)	Rock frag. of plutonic mafic (tonalite) and acid rock (granite)	
EVR9	TRIPOP	G	PF1	Plagioclase, amphiboles (hornblende), opaque minerals, quartz, biotite (rare), muscovite (rare), pyroxene (rare)	Rock frag. of plutonic mafic (tonalite) and acid rock (granite)	Different amphiboles

EVR10	CASSEROLE	U	PF1	Plagioclase, amphiboles (hornblende), opaque minerals, quartz, biotite	Rock frag. of plutonic mafic (tonalite) and acid rock (granite)	Much more less amphibole
EVR11	BOWL	BG	PF3	Quartz, plagioclase (rare), feldspar, muscovite (rare)	Frag. of sandstone, quartzite, frag. of granitic rock	Clay pellet, lime nodules. More homog. ceramic matrix
EVR12	SMALL JUG	BG	PF4	Biotite, muscovite (rare), quartz, feldspar, plagioclase	Limestone, schist	Bioclast (bivalves)
EVR13	BOWL	G	PF3	Quartz, plagioclase (rare), feldspar, muscovite (rare)	Frag. of sandstone, quartzite, frag. of granitic rock	Clay pellet, lime nodules. More homog. Ceramic matrix
EVR14	BOWL	BG	PF2	Quartz, plagioclase (rare), feldspar, muscovite	Frag. of granitic rock (felsic), quartzites, sandstone	Big lime inclusion. Highly het. ceramic matrix
EVR15	OIL LAMP	G	PF2	Quartz, plagioclase, feldspar, muscovite (rare)	Quartzite, sandstone	Highly het. ceramic matrix
EVR16	OIL LAMP	G	PF5	Feldspar, biotite (rare), quartz, muscovite (rare), plagioclase (rare), amphibole (rare), calcite (thermally altered), pyroxene (rare)	Quartzite, micritic limestone (thermally altered), schist, gneiss	Sec calcite in porosity
EVR17	BOWL	BG	PF3	Amphibole, muscovite (rare), plagioclase (rare), quartz	Frag. of granitic rock (felsic), quartzites, sandstone	Clay pellet
EVR18	BOWL	G	PF2	Muscovite (rare), quartz, feldspar, plagioclase (rare)	Frag. of granitic rock (felsic), quartzites, sandstone	Clay pellet, big lime inclusions
MER19	BOWL	BG	PF6	Quartz, muscovite, feldspar, plagioclase (rare), amphibole (brown)	Quartzite, greywacke, chert	Very small crystals mixed in ceramic matrix muscovite – VERY ABOUNDANT
MER20	SMALL BOTTLE	G	PF6	Muscovite, quartz, feldspar, plagioclase (rare), amphibole (brown)	Quartzite, greywacke	Very small crystals mixed in ceramic matrix muscovite – VERY ABOUNDANT vitreous inclusions. Glassy incl.
MER21	BOWL	G	PF2	Plagioclase (rare), feldspar, quartz, amphibole (rare), muscovite (rare)	Quartzite	Big lime inclusions. Highly het. ceramic matrix
MER22	BOWL	G	PF2	Quartz, feldspar, plagioclase, muscovite (rare)	Frag. of sandstone, quartzite and granitic rock (felsic)	Highly het. ceramic matrix
MER23	SMALL JUG	G	PF2	Quartz, feldspar, plagioclase (rare), amphibole (rare)	Frag. of sandstone, quartzite and granitic rock (felsic)	Highly het. ceramic matrix
MER24	OIL LAMP	G	PF5	Quartz, muscovite, feldspar, plagioclase (rare), biotite (rare), calcite (thermally altered)	Limestone (thermally altered), gneiss,	Sec calcite in porosity
SIL25	TUREEN	BG	PF3	Quartz, feldspar, plagioclase (rare), muscovite, amphibole (brown-rare)	Frag. of sandstone, quartzite, granitic rock, thermally altered limestone	Sec calcite in porosity, bioclast (bivalves), clay pellet. More homog. Ceramic matrix
SIL26	SMALL BOWL	BG	PF3	Quartz, muscovite, amphibole (rare), plagioclase (rare), feldspar	Frag. of sandstone, quartzite, frag. of granitic rock	Clay pellet, lime nodules. More homog. Ceramic matrix
SIL27	SMALL BOWL	BG	PF2	Quartz, feldspar, muscovite (rare), plagioclase (rare)	Frag. of sandstone, quartzite, frag. of granitic rock	Clay pellet, lime nodules. Highly het. ceramic matrix
SIL28	SMALL BOWL	BG	PF6	Quartz, feldspar, plagioclase (rare), muscovite	Greywacke, chert	Very small crystals mixed in ceramic matrix muscovite – VERY ABOUNDANT, vitreous incl.
SIL29	SMALL BOWL	BG	PF6	Quartz, feldspar, plagioclase, muscovite	Quartzite, greywacke, chert	Very small crystals mixed in ceramic matrix muscovite – VERY ABOUNDANT, vitreous incl.

6.3 XRD – RESULTS AND DISCUSSION

The XRD results mostly confirmed the observations carried out during OM analysis. In addition, considering specimen characteristics, two main groups (i.e. 1 and 2 / coarse ware – glazed ware) of wares were isolated once the XRD results were tabulated. Group 2 was afterwards divided into two sub-groups (A and B).

Group number 1 includes all specimens of fabric *PF 1*, the coarse wares and the tripod from the city of Évora. The main mineralogical phases identified are plagioclase (frequent), amphiboles (moderate), pyroxene (scarce) and biotite (scarce) in addition to K-feldspar (moderate), quartz (abundant) and illite/muscovite (moderate). In particular, the relative abundance of plagioclase and amphiboles completely reflects the observations carried out during OM observations. Mineralogical phases such as smectite (EVR 8), hematite and calcite were also identified (scarce) (see Table 4).

Regarding the firing temperature of this group, the identification of illite/muscovite, hematite on XRD pattern can give some clues on ceramic firing temperature. Illite/muscovite signals normally disappear for firing temperatures higher than 950 °C (Riccardi et al., 1999; Cultrone et al., 2001; El Ouahabi et al., 2015). However, hematite generally starts to nucleate at 750°C (Duminuco et al., 1998; Riccardi et al., 1999; Nodari et al., 2007). Thus, diffractograms interpretation suggests that ceramics were probably fired in a temperature range between 750°C and 950°C. The only exception is represented by specimen EVR 8 (see Figure 73). In this case, a smectite clay mineral (i.e. probably montmorillonite) was identified, suggesting a lower firing temperature, probably below 600 °C (Malek et al., 1997) or the weathering of the ceramic in the soil. The identification of calcite (i.e. not observed during OM examination) can be explained as the recrystallization of some lime after the firing (Fabbri et al., 2014).

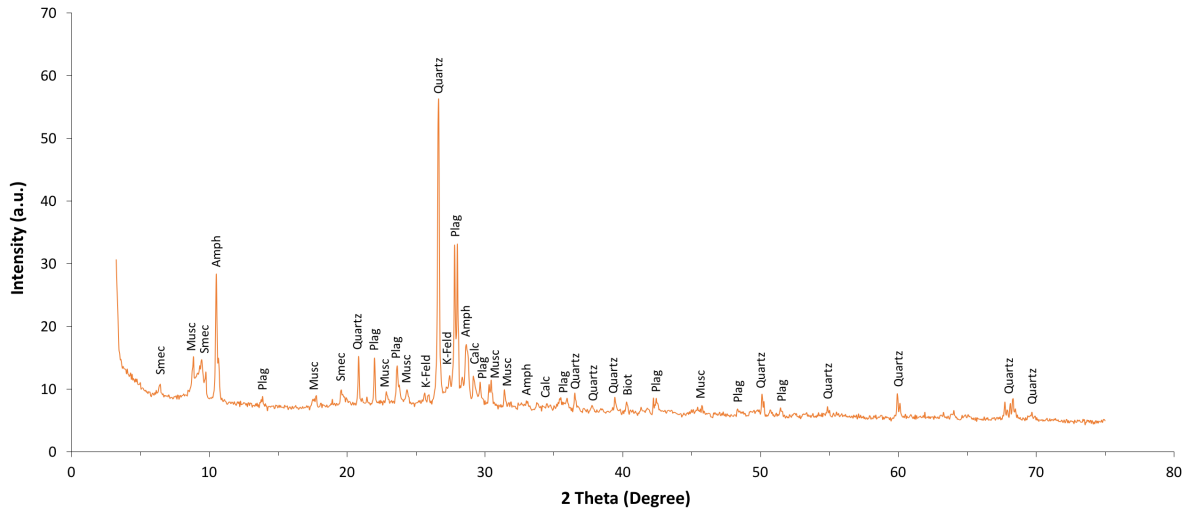


Figure 73. Representative XRD pattern from EVR 8 specimen depicting the mineralogical composition of the Subgroup 1 coarse wares. Assigned peaks: muscovite (Musc), smectite (Smec), amphibole (Amph), plagioclase (Plag), quartz, K-feldspar (K-feld), calcite (Calcite) and biotite (Biot).

Group number 2 is made up of the glaze-bearing ceramic specimens included in fabrics *PF 2, 3, 4, 5 and 6*. Nevertheless, after the interpretation of XRD patterns, two different sub-groups were formed.

On specimens included in sub-group 2A (i.e. samples EVR 3, 14, 15 and MER 23), the mineralogy identified is coherent with the exploitation of calcium poor raw material (see Figure 74), and mineralogical phases such as quartz (abundant), plagioclase (scarce), potassium-rich feldspars (moderate) and hematite (scarce) were generally identified. Illite/muscovite and calcite peaks (scarce) could also be present in some specimens. The overall interpretation is coherent with OM observations. Thus, ceramics were probably fired at 950-1000°C considering the total lack of mullite (i.e. it normally develops for firing temperature higher than 1000°C) and the identification of illite/muscovite in some specimens (Riccardi et al., 1999; El Ouahabi et al., 2015).

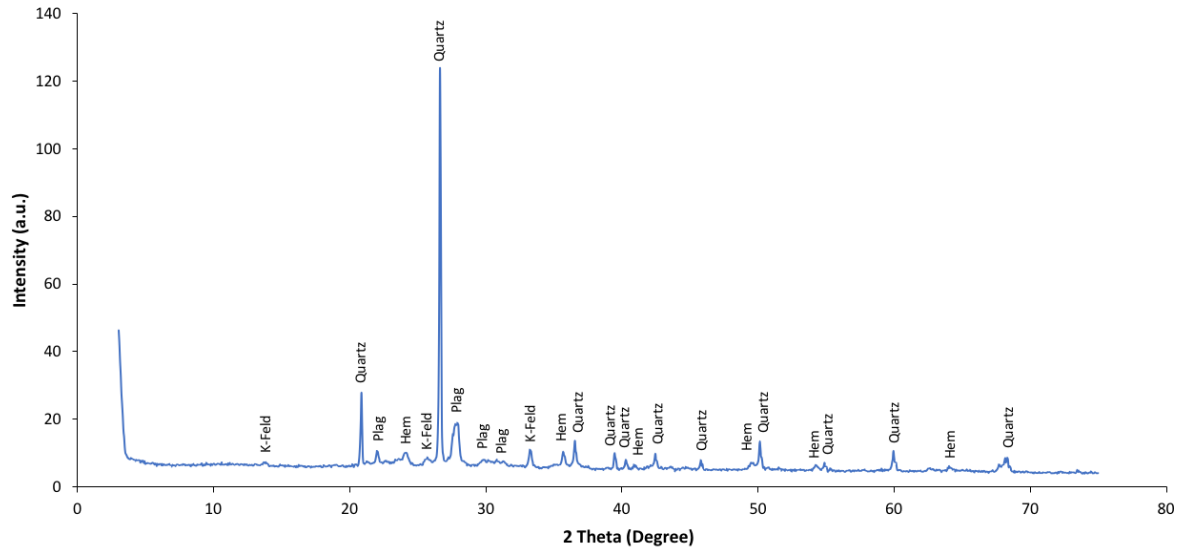


Figure 74. Representative XRD pattern from MER 23 specimen depicting the mineralogical composition of the Subgroup 2A glazed wares. Assigned peaks: K-feldspar (K-feld), quartz, plagioclase (Plag) and hematite (Hem).

Specimens included in sub-group 2B are characterized by calcium rich-bearing raw clay materials (see Figure 75). As seen in table 4, the presence of mineral phases such as quartz (abundant), plagioclase and K-feldspars (frequent and moderate, respectively) corroborate the particulate inclusions identified by OM. Moreover, the identification of mineralogical phases such as pyroxene (i.e. just identified on sample EVR 16 by OM), plagioclase (i.e. identified in most sample in low quantity), and akermanite (i.e. never identified during OM) suggests they developed during firing. Thus, they are included in ceramic matrices.

The distinctive pyroxene presence (i.e. generally diopside) in most of the specimens (see Figure 75) demonstrates its association with carbonate-rich raw materials and a firing temperature starting at about 800°C, while the decomposition of carbonates between 750°C to 850°C is in progress. Subsequently, a new mineral phase such akermanite appears (i.e. roughly at 900 °C) as evidence of the decarbonation reaction at high firing temperature (Trindade et al., 2009; Heimann & Maggetti, 2019). Plagioclases (i.e. rarely identified during OM) also crystallized in most specimens indicating that the firing temperature could be higher than 1050°C (Heimann & Maggetti, 2019).

Additionally, the scarce representativity of illite/muscovite in some specimens confirm that a high temperature was attained (higher than 950-1000°C) for its decomposition which, in turn, explain the scarce presence of calcite. (Fabbri et al., 2014). The appearance of moderate analcime amounts is due to the weathering conditions that the shards were subjected (Schwedt et al., 2006).

Consequently, specimens included in sub-group 2B were probably fired in a temperature range comprised between 850°C and 1050°C.

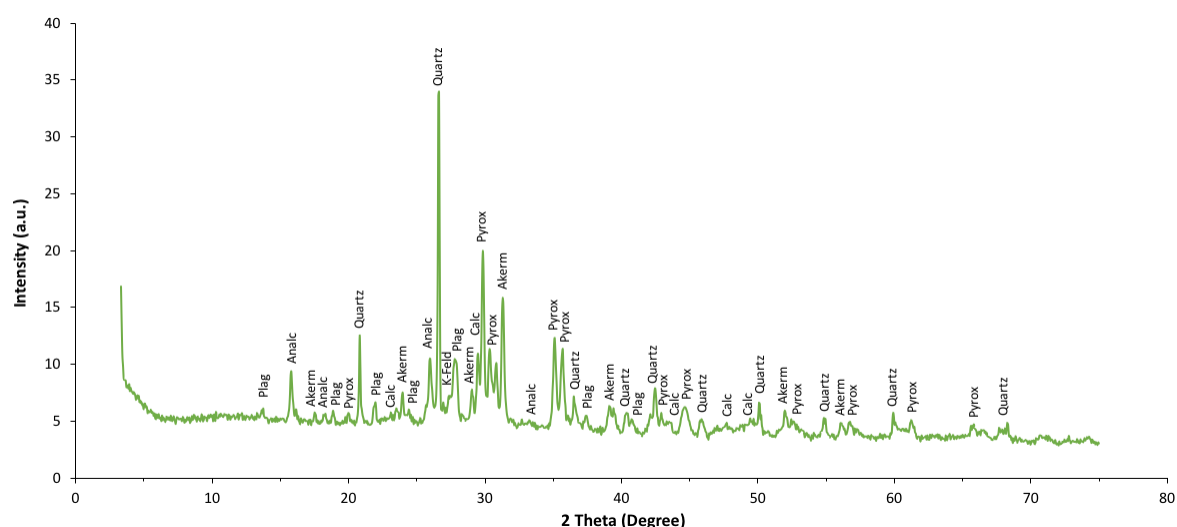


Figure 75. Representative XRD pattern from EVR 12 specimen depicting the mineralogical composition of the Subgroup 2B glazed wares. Assigned peaks: plagioclase (Plag), analcime (Analc), akermanite (Akerm), pyroxene (Pyrox), quartz, calcite (Calc) and K-feldspar (K-feld).

Table 4. Semi-quantitative determination of the mineralogical phase's abundance identified by XRD.
(Legend: TR, traces; X, scarce; XX, moderate; XXX, frequent; XXXX, abundant).

Item	Samples	PF	XRD-groups	Quartz	Plagioclase	K-Feldspar	Pyroxene	Biotite	Illite/Muscovite	Amphibole	Calcite	Hematite	Analcime	Akermanite	Smectite
1	EVR-1	PF1	1	xxx	xxxx	xx		x	x	xx					
2	EVR-2	PF6	2B	xxxx	xx	xx	xx		x		x	x		x	
3	EVR-3	PF2	2A	xxxx	xx	xx						x			
4	EVR-4	PF1	1	xxx	xx	xx		xx	xxx	xx	x				
5	EVR-5	PF1	1	xxx	xxx	xx	TR	x	xx	xx	TR	x			
6	EVR-6	PF1	1	xxxx	xx	xx		x	x	xx	TR	x			
7	EVR-7	PF1	1	xxxx	xxx	xxx	TR	x	xx	xx	xx	x			
8	EVR-8	PF1	1	xxxx	xxx	xx	TR	xx	xx	xxx	x				x
9	EVR-9	PF1	1	xxxx	xx	xx	x			x		x			
10	EVR-10	PF1	1	xxx	xxx	xxx		x	xx	x					
11	EVR-11	PF3	2B	xxxx	xx	xx	xxx				TR		xx		
12	EVR-12	PF4	2B	xxxx	xx	x	xxxx				xxx		xx	xxx	
13	EVR-13	PF3	2B	xxxx	xxx	xx	xxx				TR	x			
14	EVR-14	PF2	2A	xxxx	x	x			x		TR	x			
15	EVR-15	PF2	2A	xxxx	x	x						x			
16	EVR-16	PF5	2B	xxxx	x	x	xx				xx			xx	
17	EVR-17	PF3	2B	xxxx	xxx	xx	xxx		x			x	xx	xxx	
18	EVR-18	PF2	2B	xxxx	xxx	xx	xx				x				
19	MER-19	PF6	2B	xxxx	x	xx	xx		x			x		xx	
20	MER-20	PF6	2B	xxxx	x	x	xx		x					xx	
21	MER-21	PF2	2B	xxxx	xx	x	x				x	x		x	
22	MER-22	PF2	2B	xxxx	xxx	xx	x					x			
23	MER-23	PF2	2A	xxxx	xxx	x						x			
24	MER-24	PF5	2B	xxxx	x	xx	xxx		x		x		xx	xxx	
25	SIL-25	PF3	2B	xxxx	xx	x	x			xxxx	x	x	x		
26	SIL-26	PF3	2B	xxxx	xx	xx	xxx				xx	x	xx		
27	SIL-27	PF2	2B	xxxx	xxx	xx	xx		x			x			
28	SIL-28	PF6	2B	xxxx	x	x	x		x			x	x		
29	SIL-29	PF6	2B	xxxx	xx	xx	x				x	x		x	

6.4 XRF – RESULTS AND DISCUSSION

The results of the major chemical elements obtained by XRF analyses were plotted in the ternary (CaO+MgO)–Al₂O₃–SiO₂ (CAS) phase diagram (Duminuco et al., 1998; Riccardi et al., 1999; Heiman & Maggetti, 2019). The specimens are distributed as a function of their chemical variabilities, farther or closer to the mineralogical phases forming during pottery firing above 1000°C. The following description is coherent with the results obtained by XRD analysis.

Évora assembly (Figure 76) show two distribution patterns which, according to the XRD analysis, depict those specimens poor and rich in CaO+MgO (i.e. carbonate component). A CaO-MgO poor group includes specimens from XRD group 1 and sub-group 2A (i.e. coarsewares and some glazed ceramics), and they are generally enriched in Al₂O₃ and SiO₂. These shards clustered in the triangle quartz [Qz]- anorthite [An]- mullite [Mu].

Specimens included in the XRD sub-group 2B (i.e. only glazed ceramics) are displayed in the triangle delimited by quartz [Qz]- anorthite [An]- diopside [Di]. This zone is described as enriched in CaO+MgO, and tendentially depleted in SiO₂ and Al₂O₃. Thereby, most of the specimens, as seen in the XRD results, developed high-temperature CaO- and MgO-rich mineralogical phases such as diopside, akermanite and plagioclase.

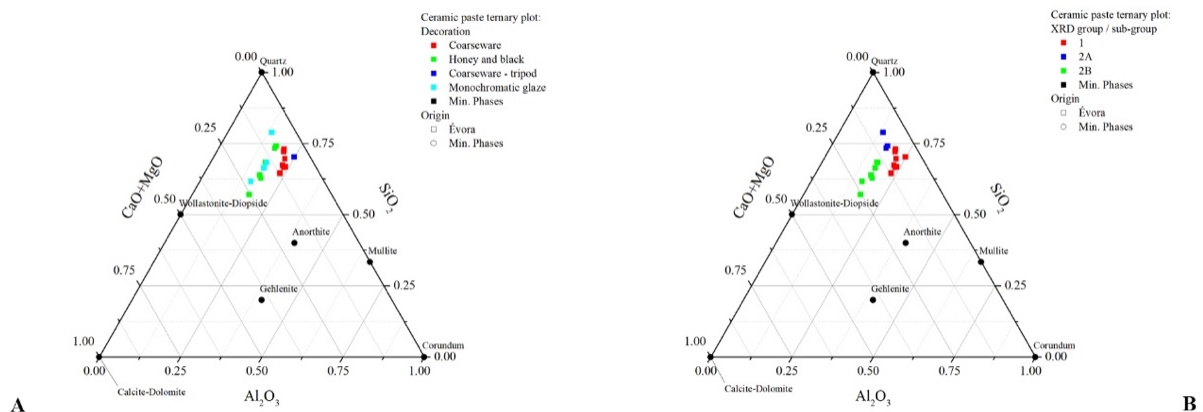


Figure 76: Évora specimens plotted on the ternary (CaO+MgO)–Al₂O₃–SiO₂. Considering glazed decoration types (A) and XRD groups (B).

Mértola assembly (Figure 77) is composed only by glazed ceramics. In this group, most specimens, as attested by XRD data, have developed whether diopside and/or akermanite and plagioclase during the firing process according to the attained firing temperature and they plot in the quartz [Qz]- anorthite [An]- diopside [Di] field. The only exception is the specimen

MER 23, which sit over the quartz [Qz]- anorthite [An]- mullite [Mu] phase triangle, being characterized by its higher alumina and silica content.

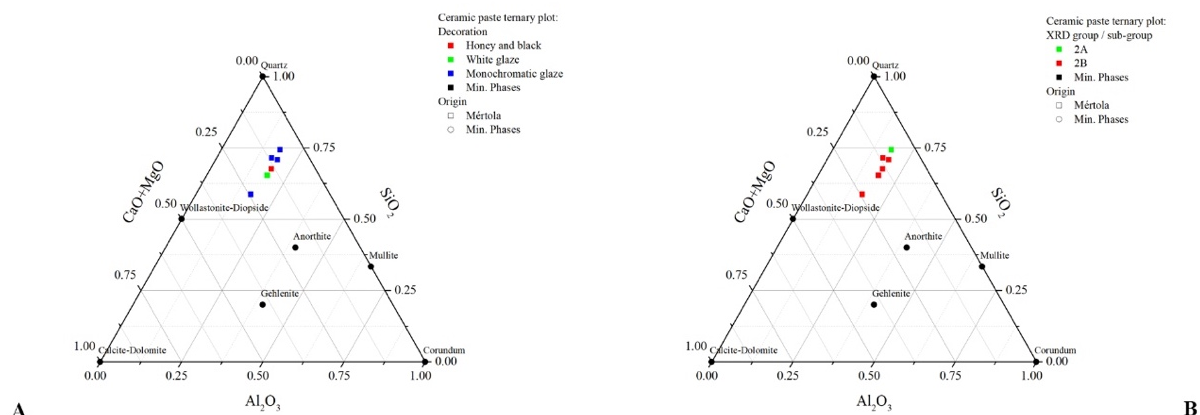


Figure 77: Mértola specimens plotted on the ternary (CaO+MgO)–Al₂O₃–SiO₂. Considering glazed decoration types (A) and XRD groups (B).

Silves assembly (Figure 78) plots over the calcareous-rich zone into the [Qz]- anorthite [An]- diopside [Di] field compositional phase triangle. Therefore, high-temperature calcium-rich mineralogical phases developed during firing, as evidenced on XRD pattern.

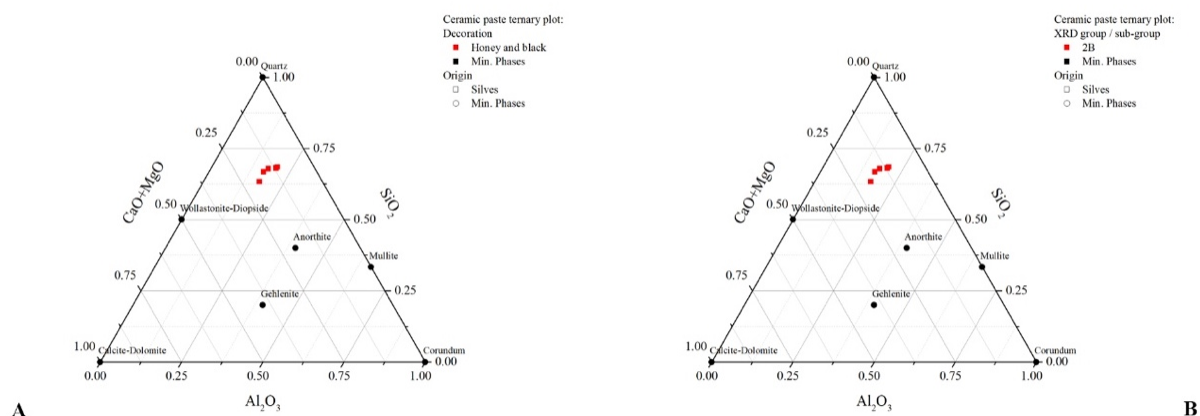


Figure 78: Silves specimens plotted on the ternary (CaO+MgO)–Al₂O₃–SiO₂. Considering glazed decoration types (A) and XRD groups (B).

Regarding samples provenance, chemical analysis results evidenced that none of the glazed ceramics recovered in Évora is compatible with the coarseware (i.e. specimens included in fabric PF1). This is testified by the binary plot Na₂O/K₂O vs CaO (Figure 79 A, B). PF1 specimens are characterized by a relatively low concentration of CaO, as explained above, and high Na₂O/K₂O ratio. Thus, K₂O concentration is tendentially lower in this group. On the contrary, Na₂O is linearly correlated whit CaO, and they are probably included in plagioclase crystals (i.e. PF1 fabric is extremely rich in plagioclase crystals as observed during OM

analysis). PF1 specimens also show a higher concentration of Al_2O_3 , being mainly the result of the higher biotite and muscovite content as evidenced by OM.

In the case of specimens included in fabric PF2, 3, 4, 5 and 6 alkaline earth metal concentration is quite stable, but the CaO concentration is significantly different, and it is possible to clearly distinguish most fabrics (Figure 79 A, B).

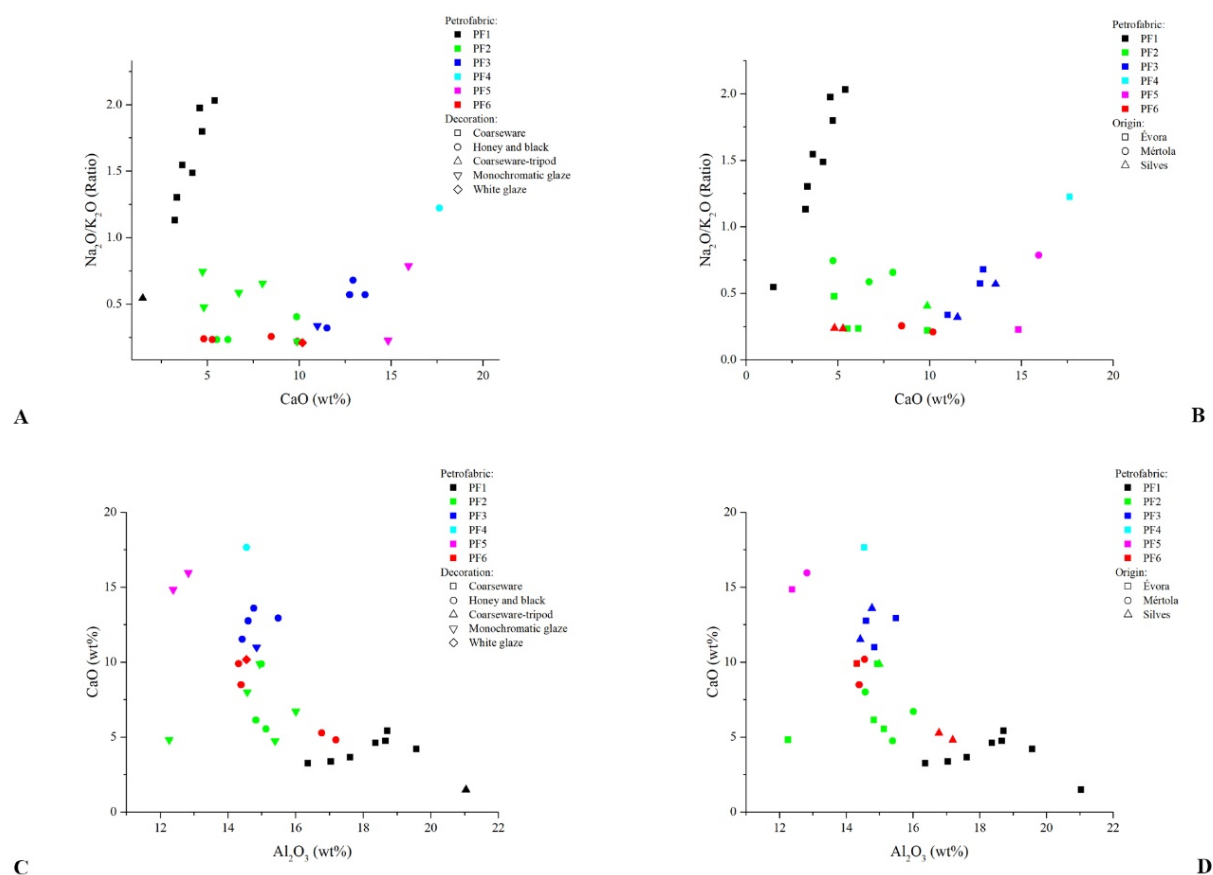


Figure 79: Provenance analysis depicted by the binary plots $\text{Na}_2\text{O}/\text{K}_2\text{O}$ vs CaO (A-B) and Al_2O_3 vs CaO (C-D).

In any case, based on the CaO content, specimens included in fabrics PF2 and PF6 partly overlap, while fabrics PF3, 4 and 5 are completely differentiated (Figure 79 C, D). As an internal reference measure, Sr also show a linear correlation with CaO. Thus, Sr is included in calcium-rich mineralogical phases, and it confirms the previously observed trends.

Nevertheless, the SiO_2 vs CaO binary plot (Figure 80 A, B) clearly shows that fabrics PF2 and PF6 are sensitive to the SiO_2 content, in which they can be distinguished. A similar trend is also observed in the Zr vs CaO binary plot, measured internally as a reference. So, SiO_2 and Zr concentrations were probably influenced by the ceramist/s and/or by raw material characteristics. To conclude, the chemical analysis by XRF spectroscopy evidenced that the

mineralogy observed is compatible with specimens' chemical composition, and it is also possible to confirm the OM observations (i.e. the identification of different petrofabrics).

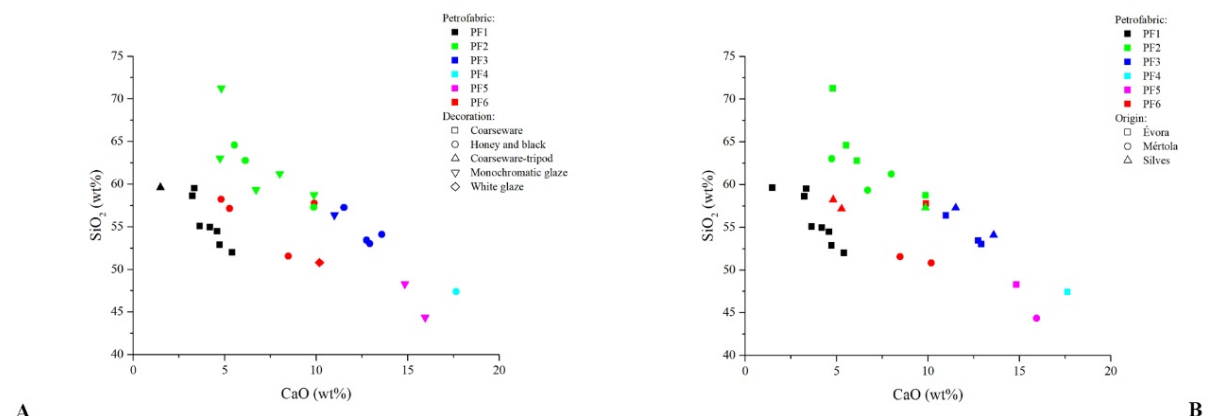


Figure 80: Provenance analysis depicted by the binary plot SiO₂ vs CaO in which all the specimen collection are differentiated owing to the SiO₂ content.

6.5 SEM-EDS – RESULTS AND DISCUSSION

Thanks to the micro-structural/chemical analysis by SEM-EDS, it was possible to determine specimens' glaze technology (i.e. glaze application technique and firing technology), morphological characteristics and major oxides chemical composition. In addition, the chemical composition of the ceramic paste was also evaluated to fully determine the glaze application technique. Backscattered electron images (BSE images), secondary electron (SE) images, elemental mapping distribution analysis and punctual and areal chemical examination were used for these purposes.

Table 5. Pottery fabrics and XRD groups related to the inner/outer glazed-colour decoration of the collection.

Item	Code	Provenance	Chronology	Typology	Decoration	Glaze C. Inner/Outer	Black Dec.	Pottery Fabric	XRD Group
1	EVR-1	Évora	X - XI	Cooking pot	Unglazed			1	1
2	EVR-2	Évora	X - XI	Small jug	Honey and black	Honey / Honey	Outer	6	2B
3	EVR-3	Évora	XI - XII	Bowl	Honey and black	Honey / Honey	Inner	2	2A
4	EVR-4	Évora	X - XI	Cooking pot	Unglazed			1	1
5	EVR-5	Évora	X - XI	Cooking pot	Unglazed			1	1
6	EVR-6	Évora	X - XI	Casserole	Unglazed			1	1
7	EVR-7	Évora	X - XI	Small jug	Unglazed			1	1
8	EVR-8	Évora	X - XI	Small jug	Unglazed			1	1
9	EVR-9	Évora	X - XI	Tripod stand	Glaze drop	Green - Outer		1	1
10	EVR-10	Évora	XI - XII	Casserole	Unglazed			1	1
11	EVR-11	Évora	XI - XII	Bowl	Honey and black	Honey / Honey	Inner	3	2B
12	EVR-12	Évora	XI - XII	Small jug	Honey and black	Honey / Honey	Outer	4	2B
13	EVR-13	Évora	XI - XII	Bowl	Monochrome	Honey / Honey		3	2B
14	EVR-14	Évora	X - XI	Bowl	Honey and black	Honey / Honey	Inner	2	2A
15	EVR-15	Évora	XI - XII	Oil lamp	Monochrome	Honey / Honey		2	2A
16	EVR-16	Évora	XI - XII	Oil lamp	Monochrome	Honey / Honey		5	2B
17	EVR-17	Évora	XI - XII	Bowl	Honey and black	Honey / Honey	Inner	3	2B
18	EVR-18	Évora	XI - XII	Bowl	Monochrome	Honey / Honey		2	2B
19	MER-19	Mértola	mid-XII - mid-XIII	Bowl	Honey and black	Honey / Honey	Inner	6	2B
20	MER-20	Mértola	mid-XII - mid-XIII	Small bottle	White glaze	Whitish - Outer		6	2B
21	MER-21	Mértola	mid-XII - mid-XIII	Bowl	Monochrome	Honey / Honey		2	2B
22	MER-22	Mértola	mid-XII - mid-XIII	Bowl	Monochrome	Honey / Honey		2	2B
23	MER-23	Mértola	mid-XII - mid-XIII	Small jug	Monochrome	Honey - Outer		2	2A
24	MER-24	Mértola	mid-XII - mid-XIII	Oil lamp	Monochrome	Honey / Honey		5	2B
25	SIL-25	Silves	mid-XII - mid-XIII	Tureen	Honey and black	Honey / Honey	Outer	3	2B
26	SIL-26	Silves	mid-XII - mid-XIII	Small bowl	Honey and black	Honey / Honey	Inner	3	2B
27	SIL-27	Silves	mid-XII - mid-XIII	Small bowl	Honey and black	Honey / Honey	Inner	2	2B
28	SIL-28	Silves	mid-XII - mid-XIII	Small bowl	Honey and black	Honey / Honey	Inner	6	2B
29	SIL-29	Silves	mid-XII - mid-XIII	Small bowl	Honey and black	Honey / Honey	Inner	6	2B

The following section is divided into two parts: the glaze (on both sides of the specimens, inner and outer glaze) and the black decoration when present. Table 5 shows the characteristic of each specimen, such as glaze colour and location of the black de decoration.

The glaze chemical composition of the ceramic collection is given in table 6 and 7, with the average values and standard deviations of each oxide in weight percentage (wt%). Additionally, the glaze application technique was evaluated following the scheme proposed by Walton and Tite (2010). In this case, the chemical composition of the ceramic paste, after the removal of PbO when present, was compared with that of the glaze after the removal of PbO, CuO and MnO (i.e. colourant), and SnO₂ (i.e. opacifier) when present. These “renormalised values” of the ceramic paste and the glaze of each specimen are presented in the tables 8 and 9 (A-B), respectively. A comparative register for inner and outer glaze is shown in table 10. Lastly, chemical data concern to the black decoration is displayed in tables 11 and 12.

Glazes Appearance

Regarding glaze colour, the preliminary observation carried out using a low magnification microscope evidenced that monochromatic glazed ceramics are generally covered by a honey coloured glaze (with green hues some time). Dichromatic glazes are honey and the decoration was outlined using a black pigment. Only in two cases, the glaze is whitish and green (Figure 81).

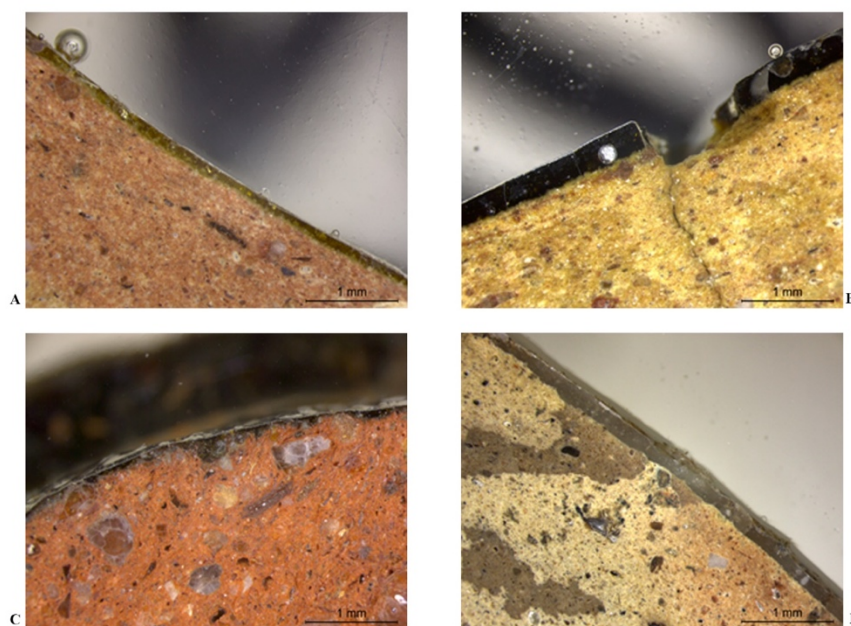


Figure 81: A) SIL 25 (Inner surface). Honey-glazed monochromatic ceramic. B) EVR 11 (Inner surface). Black-decorated honey-glazed ceramic. C) EVR 9 (Outer surface). Green-glazed drop. D) MER 20 (Outer surface).

White glaze.

From the microstructural point of view, the analysis of specimen's BSE images (Figure 82) evidenced that glazes are mostly homogeneous and unaltered. The only exception is the glaze cover of specimens MER 20, which is partly weathered. Rarely air bubbles were observed, and in few cases, vertical fissures were present, suggesting a different glaze-ceramic paste contraction rate during cooling. Small undissolved crystallites might also be observed floating in some specimen glazes.

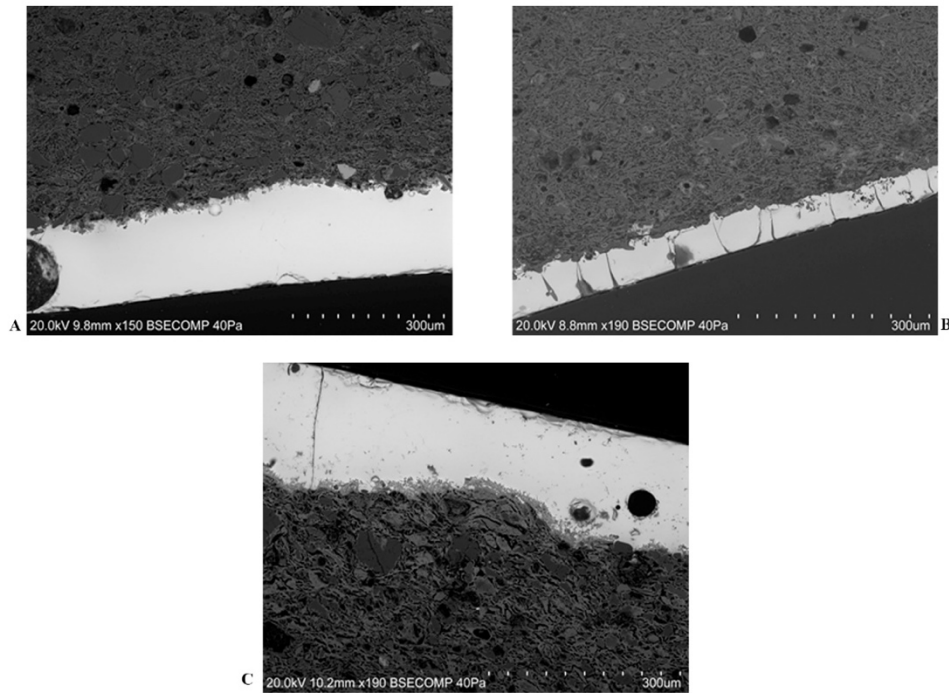


Figure 82: A) EVR 2 (Inner surface). Honey-glazed section of the specimen displaying a limited glaze-body interaction layer and homogeneous and uniform glaze. B) EVR 12 (Inner surface). Honey-glazed section of the specimen characterised by high alkali content. The image displays an absent glaze-body interaction layer and crazing due to the glaze's high thermal contraction. C) SIL 29 (Inner surface). Honey-glazed section of the specimen displaying undissolved Fe-bearing particles.

Firing Technology (single vs double firing)

To evaluate glazed ceramic firing technology, it is important to assess the diffusion during firing of the main glaze components (i.e. mainly PbO) to the ceramic paste. Moreover, different oxides such as Al₂O₃, CaO, MgO, K₂O, Na₂O and FeO can also diffuse from the clay body into the glaze. Therefore, the ceramic paste composition and the firing process applied can influence the final glaze composition. As a consequence, new crystallites form at the glaze-ceramic interface (Molera et al., 2001) and, when a single firing technique is applied, ceramic paste/glaze chemicals exchange is stronger, and the interface is generally more developed and thicker.

The BSE and SE images of each specimen and the elemental distribution point to a limited interaction layer (i.e. interface), accompanied by the formation of overlying new crystalline phases within homogenous and generally uniform glaze formation (Figure 83). These new crystallites are normally rich in potassium or calcium/magnesium and they can be classified as lead rich potassium feldspars and pyroxenes (Molera et al., 1993; Molera et al., 2001).

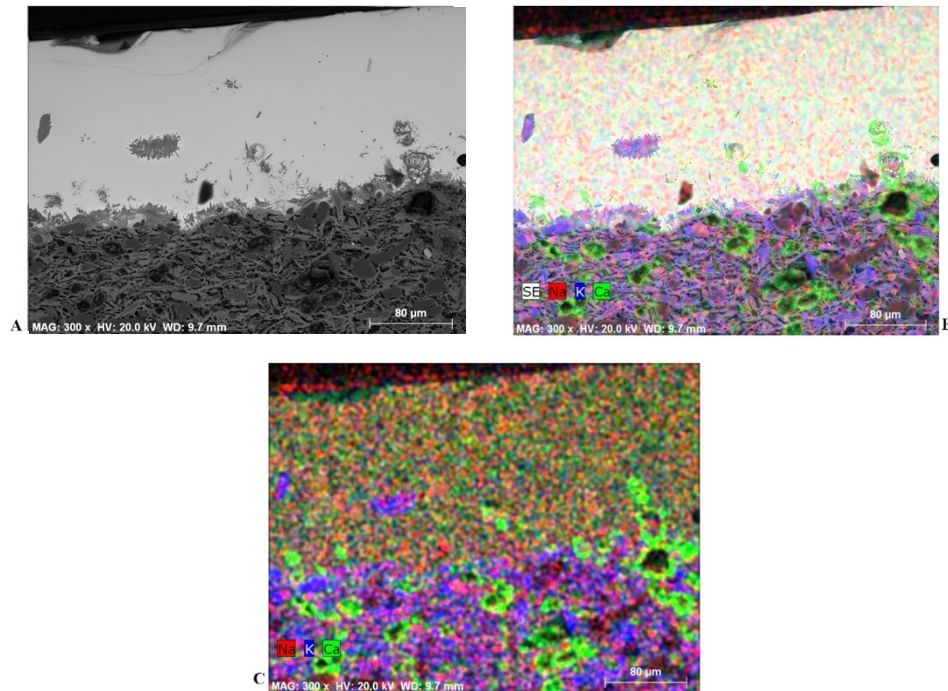


Figure 83: SIL 29 (Inner surface). A) BSE images of the black-decorated section of the specimen displaying new crystallites formation growing from a limited glaze-body interaction layer. B) SE image plus elemental mapping of the black-decorated section displaying the chemical distribution of Na, K and Ca over the glaze, the ceramic body and crystallites. C) Elemental mapping of the black-decorated section displaying the chemical distribution of Na, K and Ca.

In concordance with the literature (Molera et al., 1997a; Molera et al., 1997b; Tite et al., 1998; Molera et al., 2007; Walton & Tite, 2010; Molera et al., 2017; Salinas et al., 2018; Salinas & Pradell, 2018; Matin, 2019; Pradell & Molera, 2020), the formation of limited interaction layers must have been the result of the glaze application over biscuit-fired clay bodies, impeding greater glaze-body reaction during firing.

In those cases where the glaze-body interaction layer was very small or absent, glazes with high alkali contents (i.e. Na_2O and K_2O) were identified (EVR 12, 17, MER 20 and 24). Considering ceramic characteristics, the results obtained are compatible with firing technology applied during the Islamic period in the Iberian Peninsula (Molera et al., 1997a).

Glaze Application Technique

As described, to determine the glaze application technique, the scheme proposed by Walton and Tite (2010) was employed. The result obtained by the comparative analysis of the glaze and ceramic paste “renormalised values” presented in tables 8 and 9 (A-B) indicated that, in all cases, glazes were applied using frits or a mixture of silica plus lead ore, and not by using lead ore by itself on the ceramic surface. Besides, the comparison of Al_2O_3 concentration from specimens’ inner and outer ceramic glazes ceramic paste clearly show that they are different (Figure 84. Plots A-B). Similar results were also obtained considering SiO_2 (Figure 84. Plots C-D). Normally, when lead ore is applied on the ceramic surface and fired, it melts and interacts with the ceramic paste. Thus, the final glaze composition is the result of this interaction, and oxides like SiO_2 and Al_2O_3 (i.e. quartz, plagioclase) are taken from the ceramic paste to form the glaze. In this case, once PbO , colourants and the opacifier are subtracted from the glaze chemical composition and the new values are normalised to 100%, they should reproduce the chemical composition of the ceramic paste after the removal of PbO . This never happened in the samples considered in this thesis.

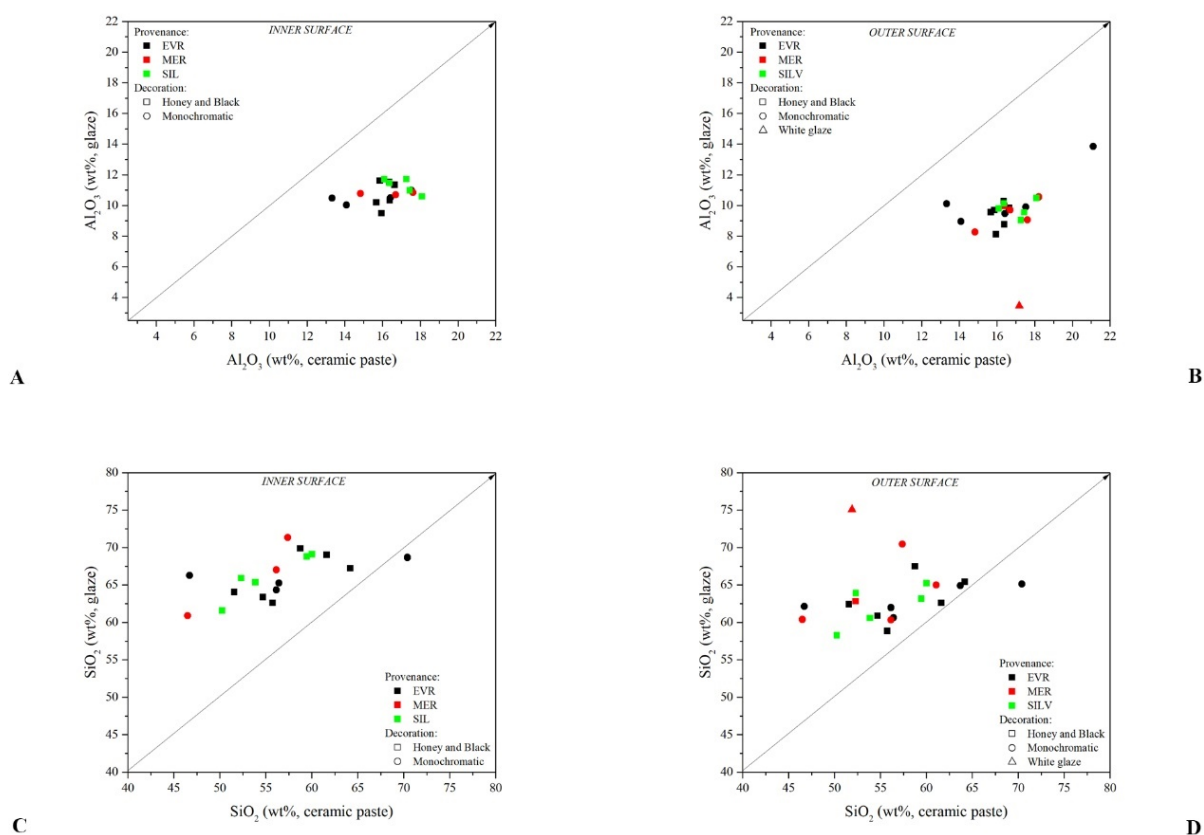


Figure 84: Plots A-B) Al_2O_3 ceramic paste/ Al_2O_3 glaze biplots from the inner and outer surfaces of each glazed specimen. Plots C-D) SiO_2 ceramic paste/ SiO_2 glaze biplots from the inner and outer surfaces of each glazed specimen.

In addition, considering glazes appearance on BSE images, the evidence of a homogeneous and uniform glaze and the lack of unmelted quartz grains dispersed into the glaze can be associated with the use of a homogeneous frit. Thus, probably, in all cases, glazes were applied using frits. This technological option is coherent with the existing bibliography. Actually, since the beginning of glazed ceramic production in the Iberian Peninsula, archaeological and archaeometrical data evidenced that frits were employed in most cases (Molera et al., 1997a; Molera et al., 2007; Salinas et al., 2019; Pradell & Molera, 2020).

Table 8: Renormalised values of the ceramic paste without PbO. Medium values in weight percent (wt%).

Oxides (wt%) renormalised values of the ceramic paste – medium values												
	Na ₂ O	MgO	Al ₂ O ₃	SiO ₂	P ₂ O ₅	SO ₂	K ₂ O	CaO	TiO ₂	MnO	FeO	BaO
EVR-2	0.80	2.22	15.68	58.76	0.30		2.99	12.12	1.15		5.99	
EVR-3	0.73	1.69	15.87	64.20	0.18	0.62	3.08	7.02	0.83		5.78	
EVR-9	1.62	2.38	21.11	63.69			2.54	1.96	0.96		5.73	
EVR-11	1.55	3.02	16.36	55.76		0.51	1.99	14.31	0.73		5.77	
EVR-12	1.87	3.14	15.95	51.58	0.30	0.43	1.56	18.38	1.14		5.64	
EVR-13	0.82	2.72	16.41	56.43	0.27	0.66	2.65	13.04	1.15		5.85	
EVR-14	0.97	1.82	16.40	61.65	0.21	0.17	3.10	8.82	1.09		5.78	
EVR-15	0.78	2.01	13.32	70.38			1.79	6.00	0.94		4.79	
EVR-16	0.97	2.51	14.08	46.71	0.74		2.71	26.18	0.69		5.40	
EVR-17	1.79	2.76	16.65	54.71	0.28	0.82	1.94	13.69	0.86		6.51	
EVR-18	0.88	2.45	17.53	56.13	0.16		2.85	13.56	0.92		5.53	
MER-19	0.70	2.10	16.41	52.31	5.30		3.24	11.76	1.05		7.13	
MER-20	0.76	1.95	17.18	51.90	5.04		3.58	12.04	0.92		6.63	
MER-21	1.71	1.74	17.62	57.38	0.93	0.66	2.79	8.51	1.26	0.53	6.87	
MER-22	1.59	2.05	16.70	56.15	0.84	0.24	1.85	12.93	0.88		6.77	
MER-23	1.99	1.60	18.21	61.06	0.28	0.16	2.12	6.10	1.37	0.04	7.07	
MER-24	1.64	3.23	14.83	46.51	0.81		1.39	25.23	0.98		5.38	
SIL-25	0.93	2.98	16.38	53.88	0.52	0.34	2.42	15.80	0.80		5.95	
SIL-26	1.24	3.29	16.10	50.27	0.29	0.49	1.97	17.28	1.02		8.06	
SIL-27	0.99	2.99	17.28	52.32	0.52	0.38	1.65	16.27	0.94		6.65	
SIL-28	1.13	4.41	17.45	60.04	0.26	0.20	3.48	6.48	0.83		5.71	
SIL-29	0.93	4.48	18.10	59.46	0.08	0.05	3.55	5.87	0.72	0.28	6.21	0.28

Table 9A: Renormalised values of the inner glazes without PbO. Medium values in weight percent (wt%).

Oxides (wt%) renormalised values of the inner glazes – medium values										
	Na ₂ O	MgO	Al ₂ O ₃	SiO ₂	P ₂ O ₅	K ₂ O	CaO	TiO ₂	FeO	BaO
EVR-2	1.24	1.09	10.19	69.85		3.11	8.33	0.23	4.34	1.62
EVR-3	0.90	1.31	11.60	67.21		2.68	9.25	1.17	5.90	
EVR-11	1.37	1.38	11.51	62.60		3.65	11.24	1.04	7.21	
EVR-12	3.20	1.79	9.48	64.02		5.83	10.01	1.39	4.29	
EVR-13	1.56	1.34	10.50	65.26		3.41	11.40	1.49	5.04	
EVR-14	1.77	0.95	10.31	69.01		3.33	8.33	1.63	4.66	
EVR-15	1.08	1.18	10.47	68.66		2.36	9.30	1.18	4.80	0.97

EVR-16	1.11	1.26	10.03	66.26	0.24	3.41	10.02	0.02	4.59	3.06
EVR-17	2.53	1.97	11.33	63.36		4.17	9.88	1.08	5.67	
EVR-18	1.22	1.18	10.99	64.32	0.16	3.54	11.21	1.61	5.76	
MER-21	1.02	1.28	10.84	71.34	0.15	1.54	6.56	1.21	4.72	1.34
MER-22	1.37	1.16	10.71	67.18	0.29	2.40	10.00	1.51	5.38	
MER-24	1.94	1.74	10.78	60.88	0.45	4.11	13.21	2.17	4.71	
SIL-25	1.26	1.26	11.46	65.35	0.18	3.25	10.66	0.30	4.82	1.45
SIL-26	1.53	1.59	11.69	61.57		3.39	11.70	2.45	6.07	
SIL-27	1.55	1.31	11.71	65.91		3.32	10.57	1.19	4.45	
SIL-28	1.19	1.60	10.97	69.08	0.15	2.39	8.36	1.45	4.81	
SIL-29	1.15	1.47	10.57	68.77	0.16	2.75	8.85	0.17	4.44	1.67

Table 9B: Renormalised values of the outer glazes without PbO. Medium values in weight percent (wt%).

Oxides (wt%) renormalised values of the outer glazes – medium values										
	Na ₂ O	MgO	Al ₂ O ₃	SiO ₂	P ₂ O ₅	K ₂ O	CaO	TiO ₂	FeO	BaO
EVR-2	1.39	1.31	9.55	67.47		3.66	9.17	0.33	5.16	1.96
EVR-3	1.19	1.82	9.70	65.39		3.27	11.45	0.98	6.19	
EVR-9	1.62	3.43	13.84	64.89		3.34	3.32	1.43	8.12	
EVR-11	1.34	2.06	10.27	58.82		4.54	13.09	0.05	6.82	3.00
EVR-12	3.98	1.48	8.12	62.39		5.96	11.40	1.46	5.21	
EVR-13	1.85	1.53	9.48	60.63	0.28	4.37	14.21	1.57	6.09	
EVR-14	1.63	1.96	8.76	62.60		4.50	11.58	1.15	6.58	1.24
EVR-15	1.83	1.22	10.11	65.12		3.12	10.64	1.37	6.60	
EVR-16	1.64	1.61	8.94	62.14	0.26	4.19	12.89	0.39	6.36	1.58
EVR-17	3.28	1.66	9.85	60.86		5.91	11.47	1.49	5.48	
EVR-18	1.33	1.69	9.89	61.97	0.22	4.25	13.77	1.37	5.50	
MER-19	1.72	1.51	9.96	62.81	0.23	3.64	11.17	0.17	5.14	3.67
MER-20	4.52	1.32	3.45	75.08	0.66	4.63	6.19	0.85	3.30	
MER-21	1.46	1.56	9.06	70.45	0.09	2.11	8.17	0.89	6.20	
MER-22	1.71	1.61	9.72	60.33	0.24	3.20	14.21	0.26	6.31	2.42
MER-23	1.33	1.44	10.55	64.98		2.62	10.82	1.54	6.71	
MER-24	3.32	1.53	8.27	60.39	0.44	6.12	10.75	0.05	5.74	3.39
SIL-25	1.18	1.74	10.13	60.56	0.23	4.23	12.61	0.08	5.88	3.36
SIL-26	1.27	2.28	9.79	58.25		4.56	15.94	1.53	6.37	
SIL-27	1.79	1.30	9.04	63.90		3.81	12.22	1.55	6.38	
SIL-28	1.04	1.98	9.55	65.20	0.20	2.87	9.96	0.16	5.69	3.35
SIL-29	1.30	2.19	10.48	63.15	0.41	2.95	11.19	0.22	5.96	2.14

Glaze Chemical Composition

The chemical analyses of the glazes revealed that different glaze types are present in the ceramic assemblage, namely high-lead glazes and one case of white-tin opacified lead-alkali glaze. High-PbO content was always observed in most glaze sides (inner and outer surface). Moreover, can also be observed an overall variability of SiO₂ concentration (36-44% inner and 29-39% outer). The SiO₂/PbO ratio is always low (Table 10). Except in specimen MER 22,

where the SiO₂ concentration is higher on both sides (44% inner and 39% outer) (Figure 85. Plots from A to F). Nevertheless, the plots presented in figure 85 (from C to F) show that there is not correlation between SiO₂/PbO ratio and sample origin, decoration style, chronology and fabric (i.e. provenance), indicating that a different SiO₂/PbO ratio could be employed anytime and everywhere.

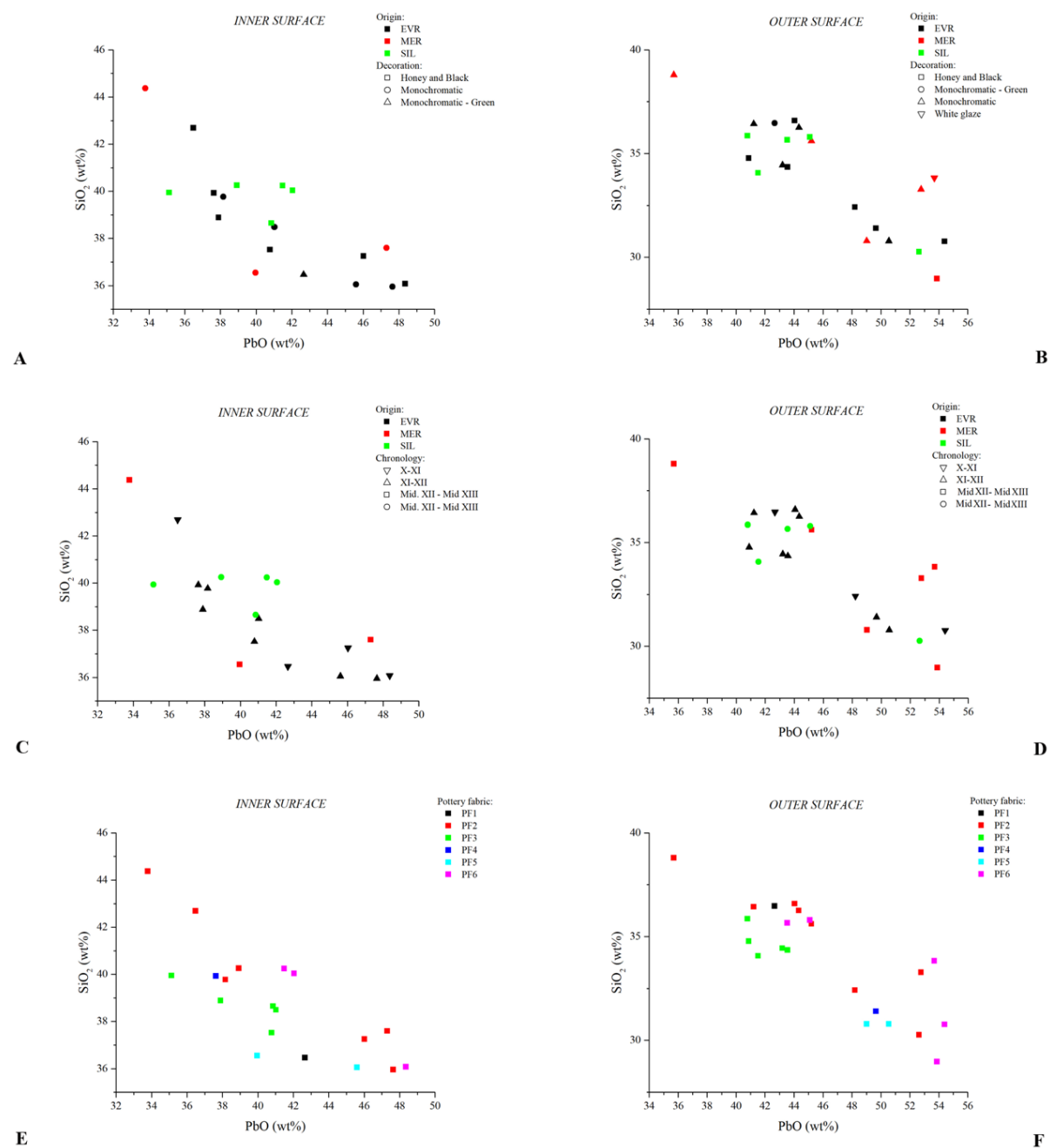
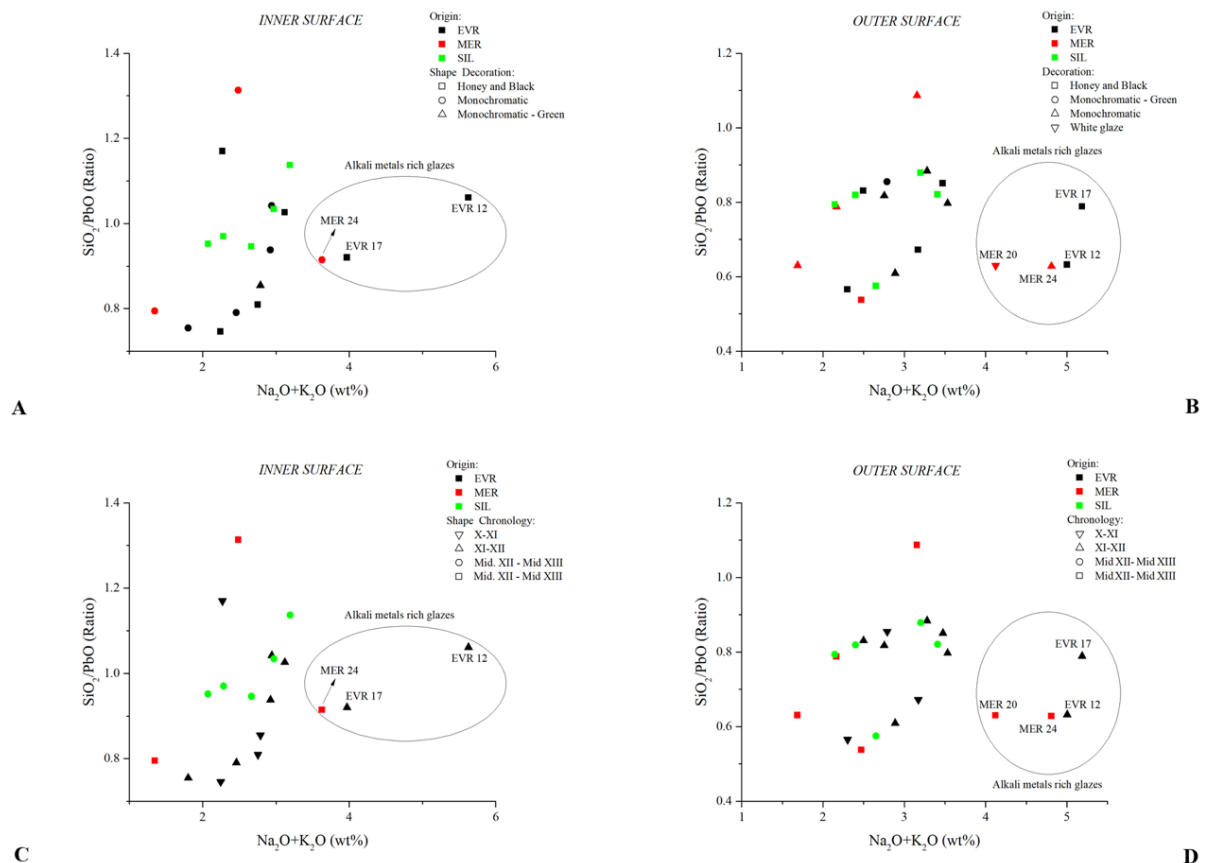
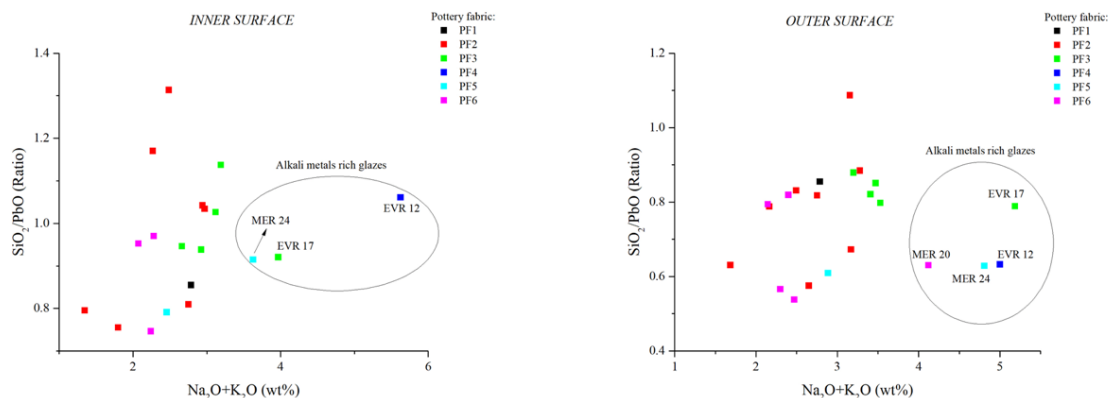


Figure 85: PbO/SiO₂ biplots from the inner and outer glazed surface of each specimen. A-B) PbO/SiO₂ biplots displaying the distribution pattern of specimens according to their decorations. C-D) PbO/SiO₂ biplots displaying the distribution pattern of specimens according to their chronologies. E-F) PbO/SiO₂ biplots displaying the distribution pattern of specimens according to their pottery fabrics.

The evaluation of MER 20 specimen's BSE image determined the presence of well-distributed and undissolved small particles of SnO₂ (i.e. cassiterite) all over the glaze (1.25 wt%), being an example of white tin-opacified glaze within the collection.

The utilization of PbO as the main fluxing agent was assured by the low contribution of alkaline earth metals such as Na₂O and K₂O (1-3% wt% inner and 2-4% wt% outer) (Table 10 and plots presented in figure 86). However, four specimens show an important alkaline earth metal concentration (EVR 12, 17, MER 20 and 24) in the range 4% to 6% and 4% to 5% over the inner and outer glazed surfaces, respectively (Figure 86. Plots from A to F). These specimens are included in different fabrics, and they also have different glaze types. Specimen MER 24 is included in fabric PF5, but it shows a different alkaline earth metal concentration if compared to specimen EVR 16 including in the same fabric. Thus, it was probably produced in a different workshop but using similar raw material in the manufacturing of the ceramic body. The same observation is valid for specimen EVR 17 included in fabric PF3. Nevertheless, these observations are not valid in the case of specimen MER 20. As explained in the background section for the production of lead-alkali tin-opacified glazes, the concentration of alkaline earth metals is generally higher to favour glaze opacity, and the precipitation into the glaze of small cassiterite crystals (Matin et al., 2018; Matin, 2019). So, the glaze is whitish in colour.





E F

Figure 86: Na₂O+K₂O/SiO₂-PbO biplots from the inner and outer glazed surface of each specimen. A-B) Na₂O+K₂O/SiO₂-PbO biplots displaying the groupings of high alkali-content specimens EVR 12, 17, MER 20 and 24, according to their decorations. C-D) Na₂O+K₂O/SiO₂-PbO biplots displaying the groupings of high alkali-content specimens EVR 12, 17, MER 20 and 24, according to their chronologies. E-F) Na₂O+K₂O/SiO₂-PbO biplots displaying the groupings of high alkali-content specimens EVR 12, 17, MER 20 and 24, according to their pottery fabrics.

MgO concentration is generally low in all samples. On the contrary, CaO concentration may vary consistently (Table 6 and 7). This oxide may normally act as a glaze stabiliser. From glaze analysis by SEM-EDS no evidence has been detected to state that a CaO rich component was added to the glaze mixture. Thus, we suppose that glazes CaO concentration might have been the result of the diffusion from the ceramic paste.

Table 10: Comparative chemical elements. Medium values in weight percent (wt%).

Oxides Wt% - Comparative Chemical Elements - Medium Values								
Sample	INNER	OUTER	INNER	OUTER	INNER	OUTER	INNER	OUTER
	PbO		SiO ₂		SiO ₂ /PbO		Na ₂ O+K ₂ O	
EVR-2	48.36	54.40	36.07	30.77	0.75	1.77	2.24	2.30
EVR-3	36.49	44.05	42.68	36.59	1.17	1.20	2.27	2.50
EVR-9		42.66		36.46		1.17		2.79
EVR-11	37.90	40.88	38.88	34.77	1.03	1.18	3.12	3.47
EVR-12	37.64	49.67	39.92	31.40	1.06	1.58	5.63	5.00
EVR-13	41.03	43.20	38.49	34.44	0.94	1.25	2.93	3.53
EVR-14	46.03	48.22	37.25	32.42	0.81	1.49	2.75	3.17
EVR-15	47.64	44.34	35.95	36.25	0.75	1.22	1.80	2.75
EVR-16	45.60	50.55	36.05	30.78	0.79	1.64	2.46	2.89
EVR-17	40.78	43.56	37.52	34.35	0.92	1.27	3.97	5.19
EVR-18	38.17	41.22	39.77	36.43	1.04	1.13	2.94	3.28
MER-19		53.88		28.97		1.86		2.47
MER-20		53.69		33.82		1.59		4.12

MER-21	47.30	52.77	37.59	33.27	0.79	1.59	1.35	1.69
MER-22	33.79	35.70	44.36	38.79	1.31	0.92	2.49	3.16
MER-23		45.21		35.61		1.27		2.17
MER-24	39.97	49.02	36.55	30.79	0.91	1.59	3.63	4.81
SIL-25	40.86	40.79	38.65	35.85	0.95	1.14	2.67	3.20
SIL-26	35.13	41.52	39.94	34.07	1.14	1.22	3.19	3.41
SIL-27	38.93	52.64	40.25	30.26	1.03	1.74	2.97	2.65
SIL-28	42.05	45.10	40.03	35.79	0.95	1.26	2.08	2.15
SIL-29	41.49	43.55	40.24	35.65	0.97	1.22	2.29	2.40

FeO was the main colouring in the inner and outer surface of most specimens (Molera et al., 1997b; Di Febo et al., 2017a). The elevated concentration of FeO might be the result of different factors such as FeO diffusion from the ceramic paste during firing (Molera et al., 2001; Chapoulie et al., 2005) or the deliberate addition of some FeO rich clay to the glaze mixture during glaze application (Tite et al., 1998; Chapoulie et al., 2005; Beltrame et al., 2021).

Considering that in sample MER 20 (i.e. the white tin-opacified glaze), the FeO concentration is 1.49 wt%, it is possible to state that the ceramist did not want any interference from different pigments to obtain a white glaze, and that the presence of FeO in the glaze is mainly the result of diffusion from the ceramic paste.

In the majority of the glazes analysed FeO concentration is high in both the inner and in the outer glaze (see Table 6 and 7). In addition, considering the plot presented in figure 87, it is possible to observe that Al₂O₃ and FeO are linearly correlated, and they were probably included in the same component. Thus, some FeO was surely diffused from the ceramic paste, but such an elevated concentration of FeO can only be explained with the addition of some Fe-bearing compounds to the glaze mixture (i.e. clay powder).

The only specimen that presents a green glaze is EVR 9 (i.e. the tripod). In this case, the main colouring agent is CuO.

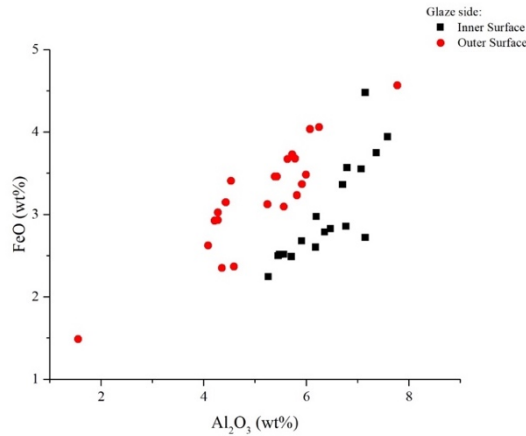


Figure 87: Al₂O₃/FeO biplot displaying the linear correlation between the chemical elements.

Table 6: Calculate Medium Values (Avr.) with Standard Deviation (SD). Inner glazed surface. Oxides Wt%.

Calculate Medium Values with Standard Deviation - Inner Glazed Surface - Oxides Wt%													
Sample		Na ₂ O	MgO	Al ₂ O ₃	SiO ₂	P ₂ O ₅	K ₂ O	CaO	TiO ₂	Mn O	FeO	BaO	PbO
EVR-2	Avr.	0.64	0.56	5.26	36.07		1.60	4.30	0.12		2.24	0.84	48.36
	SD	0.05	0.10	0.12	0.91		0.05	0.10	0.12		0.06	0.22	0.86
EVR-3	Avr.	0.57	0.83	7.37	42.68		1.70	5.87	0.74		3.75		36.49
	SD	0.08	0.09	0.09	0.25		0.10	0.17	0.18		0.42		0.11
EVR-9	.	Outer surface											
EVR-11	Avr.	0.85	0.86	7.15	38.88		2.27	6.98	0.64		4.48		37.90
	SD	0.07	0.12	0.13	0.65		0.05	0.24	0.21		0.19		0.42
EVR-12	Avr.	1.99	1.11	5.91	39.92		3.63	6.24	0.86		2.68		37.64
	SD	0.18	0.10	0.29	0.34		0.12	0.19	0.14		0.43		0.36
EVR-13	Avr.	0.92	0.79	6.19	38.49		2.01	6.72	0.88		2.97		41.03
	SD	0.03	0.04	0.15	0.35		0.08	0.19	0.36		0.16		0.44
EVR-14	Avr.	0.95	0.51	5.57	37.25		1.80	4.50	0.88		2.52		46.03
	SD	0.12	0.10	0.13	0.20		0.08	0.08	0.11		0.09		0.08
EVR-15	Avr.	0.57	0.62	5.48	35.95		1.24	4.87	0.62		2.51	0.51	47.64
	SD	0.09	0.08	0.07	1.07		0.06	0.11	0.33		0.27	0.72	1.20
EVR-16	Avr.	0.61	0.68	5.46	36.05	0.13	1.85	5.45	0.01		2.50	1.66	45.60
	SD	0.09	0.10	0.54	0.90	0.10	0.08	0.08	0.02		0.38	0.21	1.30
EVR-17	Avr.	1.50	1.17	6.71	37.52		2.47	5.85	0.64		3.36		40.78
	SD	0.13	0.28	0.16	0.34		0.24	0.25	0.45		1.31		0.58
EVR-18	Avr.	0.76	0.73	6.80	39.77		2.19	6.93	1.00		3.56		38.17
	SD	0.14	0.13	0.09	0.74	0.08	0.12	0.22	0.08		0.75		0.66
MER-19		Outer surface											
MER-20		Outer surface											
MER-21	Avr	0.54	0.67	5.71	37.59	0.08	0.81	3.46	0.64		2.49	0.71	47.30
	SD	0.22	0.06	0.13	0.52	0.09	0.06	0.04	0.51		0.12	0.51	0.36
MER-22	Avr.	0.90	0.77	7.07	44.36	0.19	1.59	6.60	1.00	0.18	3.55		33.79

	SD	0.02	0.10	0.14	0.24	0.03	0.11	0.06	0.40	0.25	0.16		0.32
MER-23		Outer surface											
MER-24	Avr.	1.17	1.04	6.47	36.55	0.27	2.46	7.93	1.30		2.83		39.97
	SD	0.06	0.14	0.14	0.29	0.08	0.10	0.38	0.72		0.38		1.07
SIL-25	Avr.	0.75	0.74	6.78	38.65	0.11	1.92	6.31	0.18		2.85	0.86	40.86
	SD	0.02	0.07	0.17	0.18	0.01	0.06	0.12	0.10		0.11	0.09	0.41
SIL-26	Avr.	0.99	1.03	7.59	39.94		2.20	7.59	1.59		3.94		35.13
	SD	0.21	0.38	0.33	0.49		0.09	0.37	0.07		0.20		0.93
SIL-27	Avr.	0.95	0.80	7.15	40.25		2.03	6.46	0.72		2.72		38.93
	SD	0.10	0.10	0.10	0.50		0.19	0.13	0.11		0.26		0.51
SIL-28	Avr.	0.69	0.93	6.36	40.03	0.09	1.38	4.84	0.84		2.78		42.05
	SD	0.17	0.16	0.29	0.54	0.06	0.08	0.24	0.05		0.26		0.69
SIL-29	Avr.	0.68	0.86	6.18	40.24	0.09	1.61	5.18	0.10		2.60	0.97	41.49
	SD	0.11	0.16	0.20	0.09	0.07	0.06	0.08	0.06		0.02	0.21	0.06

Table 7: Calculate Medium Values (Avr.) with Standard Deviation (SD). Outer glazed surface. Oxides Wt%.

Calculate Medium Values with Standard Deviation - Outer Glazed Surface - Oxides Wt%														
Sample		Na ₂ O	MgO	Al ₂ O ₃	SiO ₂	P ₂ O ₅	K ₂ O	CaO	TiO ₂	FeO	BaO	CuO	SnO ₂	PbO
EVR-2	Avr	0.63	0.60	4.36	30.77		1.67	4.18	0.15	2.35	0.89			54.40
	SD	0.11	0.08	0.56	2.20		0.10	0.38	0.04	0.16	0.20			2.15
EVR-3	Avr	0.67	1.02	5.43	36.59		1.83	6.41	0.55	3.46				44.05
	SD	0.02	0.03	0.04	0.35		0.10	0.18	0.08	0.08				0.04
EVR-9	Avr	0.91	1.93	7.78	36.46		1.88	1.87	0.80	4.56		1.15		42.66
	SD	0.11	0.06	0.40	1.01		0.06	0.19	0.06	0.25		0.25		1.57
EVR-11	Avr	0.79	1.22	6.07	34.77		2.68	7.74	0.03	4.03	1.77			40.88
	SD	0.12	0.14	0.17	0.36		0.06	0.16	0.02	0.19	0.18			0.45
EVR-12	Avr	2.00	0.75	4.08	31.40		3.00	5.74	0.74	2.62				49.67
	SD	0.16	0.16	0.04	0.16		0.13	0.36	0.39	0.47				0.10
EVR-13	Avr	1.05	0.87	5.38	34.44	0.16	2.48	8.07	0.89	3.46				43.20
	SD	0.05	0.13	0.10	0.34	0.12	0.05	0.08	0.24	0.17				0.49
EVR-14	Avr	0.84	1.02	4.54	32.42		2.33	6.00	0.60	3.41	0.64			48.22
	SD	0.15	0.22	0.13	0.45		0.06	0.13	0.21	0.69	0.91			0.60
EVR-15	Avr	1.02	0.68	5.63	36.25		1.73	5.92	0.76	3.67				44.34
	SD	0.05	0.03	0.13	0.36		0.04	0.16	0.13	0.09				0.42
EVR-16	Avr	0.81	0.80	4.43	30.78	0.04	2.08	6.39	0.19	3.15	0.78			50.55
	SD	0.05	0.09	0.11	0.21	0.06	0.05	0.40	0.06	0.39	0.57			0.35
EVR-17	Avr	1.85	0.94	5.56	34.35		3.34	6.47	0.84	3.09				43.56
	SD	0.10	0.13	0.06	0.81		0.13	0.32	0.16	0.35				0.35
EVR-18	Avr	0.78	0.99	5.82	36.43	0.13	2.50	8.10	0.81	3.23				41.22
	SD	0.14	0.08	0.04	1.24	0.04	0.31	0.30	0.10	0.58				1.40
MER-19	Avr	0.79	0.70	4.59	28.97	0.11	1.68	5.15	0.08	2.37	1.69			53.88
	SD	0.09	0.08	0.20	1.04	0.02	0.06	0.37	0.02	0.57	0.57			1.39
MER-20	Avr	2.04	0.59	1.56	33.82	0.30	2.08	2.79	0.38	1.49			1.25	53.69

	SD	0.22	0.07	0.57	0.38	0.09	0.28	0.04	0.16	0.74			0.08	1.83
MER-21	Avr	0.69	0.74	4.28	33.27	0.04	1.00	3.86	0.42	2.93				52.77
	SD	0.03	0.06	0.13	0.34	0.03	0.07	0.27	0.09	0.33				0.31
MER-22	Avr	1.10	1.04	6.25	38.79	0.16	2.06	9.14	0.17	4.06	1.55			35.70
	SD	0.04	0.05	0.29	0.40	0.11	0.11	0.26	0.05	0.46	0.14			0.44
MER-23	Avr	0.73	0.79	5.78	35.61	0.00	1.44	5.93	0.84	3.68				45.21
	SD	0.07	0.11	0.40	0.85		0.07	0.09	0.09	0.15				1.49
MER-24	Avr	1.69	0.78	4.22	30.79	0.23	3.12	5.48	0.03	2.92	1.73			49.02
	SD	0.12	0.12	0.05	0.70	0.13	0.19	0.34	0.02	0.06	0.34			0.33
SIL-25	Avr	0.70	1.03	6.00	35.85	0.14	2.50	7.47	0.05	3.48	1.99			40.79
	SD	0.06	0.12	0.19	0.46	0.07	0.07	0.27	0.01	0.05	0.59			1.16
SIL-26	Avr	0.74	1.34	5.72	34.07		2.66	9.32	0.89	3.73				41.52
	SD	0.13	0.03	0.16	0.54		0.07	0.31	0.10	0.72				0.64
SIL-27	Avr	0.85	0.61	4.28	30.26		1.80	5.79	0.74	3.02				52.64
	SD	0.15	0.09	0.20	1.19		0.18	0.19	0.07	0.29				1.86
SIL-28	Avr	0.57	1.09	5.24	35.79	0.11	1.57	5.47	0.09	3.12	1.84			45.10
	SD	0.05	0.14	0.11	0.41	0.06	0.10	0.24	0.05	0.55	0.80			0.34
SIL-29	Avr	0.74	1.24	5.91	35.65	0.23	1.67	6.32	0.12	3.37	1.21			43.55
	SD	0.16	0.12	0.12	0.30	0.08	0.07	0.38	0.09	0.14	0.54			0.51

Black Decoration

Black decorations were analysed on twelve specimens in total (Table 5). The glaze could appear mostly homogeneous (8 out of 12 specimens), and the pigment is generally completely dissolved into the glaze, or heterogeneous (Figure 88 A and C). In other cases different crystallites enriched in FeO and/or MnO (4 out of 12 specimens – EVR 2, 11/SIL 25, 26) were observed inside the glaze (Figure 88 B and D).

In all cases the pigment was applied overglaze mixing colouring agents with some frit, and applied on top the raw glaze (i.e. overglaze) prior to a second firing (Pradell & Molera, 2020). This is particularly evident on black decorated samples enriched in new crystallites. Besides, the developments of new crystalline phases, are observed from the upper glaze surface to the lower part or filling the whole glaze area when the mineral colourants were applied in high quantities (Figure 88 B and D). On the contrary, on homogeneous glazes the pigment is completely dissolved (Figure 88 A and C) because it was added probably in low amounts (Molera et al., 2013).

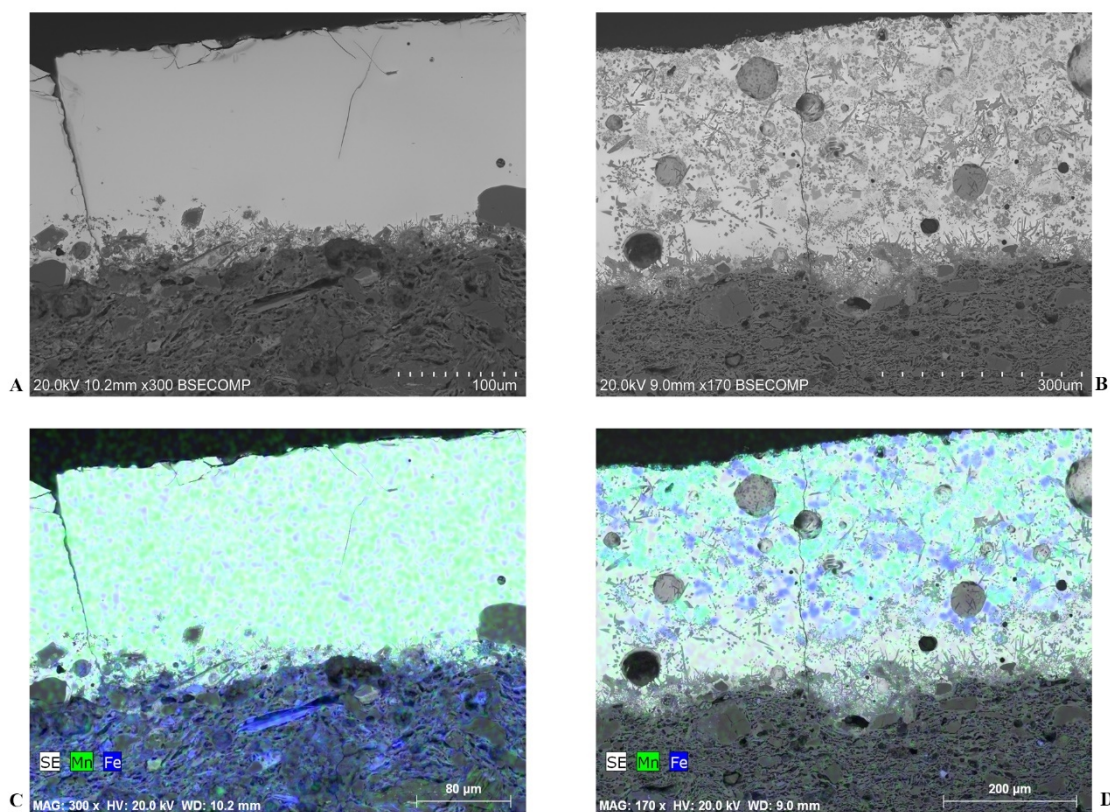


Figure 88: MER 19 displaying the absence of crystallites due to they were dissolved into the glaze (A-C).
SIL 26 displaying Fe- and Mg-bearing crystallites undissolved into the glaze (B-D).

The chemical composition of clean (i.e. without any crystallite when present) black-decorated areas (Table 11) on homogeneous and heterogeneous glazes determined the variable contribution of FeO (1-10%) and MnO (1-3%), indicating that different pigments could be mixed together and applied.

Nevertheless, on homogeneous glazes, considering that the black decoration was applied over a honey-coloured glaze (see previous section) it is not always possible to determine to which extent FeO rich raw material was utilized as pigment. In any case it is possible to affirm that a MnO-rich raw material was surely added to the decoration, as it was never detected on the honey glaze.

Table 11: Medium values of the chemical composition of the black decoration.

Oxides Wt% - Black Glaze - Medium Values														
Specimen	Media / St Dev	Glaze look	Na ₂ O	MgO	Al ₂ O ₃	SiO ₂	P ₂ O ₅	K ₂ O	CaO	TiO ₂	MnO	FeO	BaO	PbO
EVR-2	Media	HET	0.43	0.55	6.08	35.50	0.16	2.39	4.38	0.32	2.51	1.34	0.57	45.78
	St dev		0.09	0.07	0.43	0.55	0.19	0.25	0.30	0.30	0.43	0.26	0.49	1.08
EVR-3	Media	HOM	0.53	1.06	7.71	42.01	0.06	2.00	5.23	1.08	0.50	2.56		37.25
	St dev		0.12	0.22	0.17	0.98	0.03	0.10	0.11	0.24	0.14	0.22		1.61

EVR-11	Media	HET	0.63	0.86	5.86	34.93	0.00	1.72	6.31	0.10		7.12	1.82	40.64
	St dev		0.23	0.14	0.64	1.22	0.00	0.29	0.41	0.07		0.64	0.39	2.50
EVR-12	Media	HOM	1.52	0.93	4.80	34.76	0.31	2.25	5.22	0.84	3.14	2.18		44.06
	St dev		0.02	0.16	0.27	0.74	0.15	0.16	0.65	0.24	1.07	0.37		0.82
EVR-14	Media	HOM	0.51	0.75	8.09	41.56	0.07	2.68	4.36	0.06	2.46	1.84	1.59	36.04
	St dev		0.12	0.26	0.16	0.10	0.02	0.14	0.27	0.07	0.32	0.22	0.63	0.96
EVR-17	Media	HOM	1.46	0.93	6.28	35.01	0.28	2.06	5.95	0.50	1.51	3.78	0.45	41.80
	St dev		0.20	0.30	0.30	0.90	0.02	0.02	0.43	0.40	0.13	0.46	0.63	1.26
MER-19	Media	HOM	0.68	0.78	6.00	36.27	0.17	1.73	5.13	0.15	1.80	2.80	1.00	43.49
	St dev		0.15	0.09	0.12	0.35	0.09	0.18	0.03	0.08	0.38	0.32	0.67	1.99
SIL-25	Media	HET	0.48	0.84	7.23	38.48	0.19	3.05	5.67	0.09	0.90	3.54	0.91	38.63
	St dev		0.07	0.09	0.24	0.61	0.12	0.15	0.25	0.09	0.08	0.24	0.36	0.31
SIL-26	Media	HET	0.55	0.93	5.85	33.05	0.08	1.81	6.12	0.39	2.67	10.37	1.32	36.87
	St dev		0.21	0.22	0.38	2.56	0.13	0.32	0.53	0.16	0.75	2.19	0.24	1.87
SIL-27	Media	HOM	0.85	0.96	6.84	40.34	0.06	2.14	6.03	0.29	1.12	2.01	0.63	38.73
	St dev		0.06	0.22	0.70	1.51	0.09	0.20	0.14	0.08	0.43	0.34	0.17	1.20
SIL-28	Media	HOM	0.52	0.83	5.37	36.49	0.13	1.13	4.83	0.19	0.59	3.35	1.29	45.29
	St dev		0.07	0.05	0.48	0.77	0.10	0.15	0.13	0.23	0.42	0.16	0.92	1.48
SIL-29	Media	HOM	0.75	0.84	6.26	38.14	0.25	1.65	5.08	0.29	0.52	3.81	0.95	41.44
	St dev		0.05	0.07	0.48	0.58	0.05	0.19	0.05	0.00	0.40	0.44	0.19	0.74

On heterogeneous glazes, on the contrary, it was possible to suggest the kind of pigment was employed in the black decoration. Nevertheless, it was difficult to classify with certainty any of these inclusions, and more analyses such as μ Raman and/or μ XRD are necessary. Spot analyses results by SEM-EDS are reported in table 12.

In two cases, EVR 2 and EVR 11, the black decoration was developed just using MnO- or FeO-rich pigments, respectively.

On the black decoration of specimen EVR 2, spots analyses (Table 12) and elemental mapping distribution (Figure 89 A and C) evidenced that inclusions are MnO rich. Considering low particle contrast on BSE image, and the elevated concentration of MnO if compared to PbO and SiO₂ in the microanalysis results, crystallites can be classified as braunite (Mn²⁺Mn³⁺₆SiO₁₂) (Molera et al., 2013). Thus, pyrolusite (MnO₂) was probably the original pigment.

On the contrary, the black decoration of specimen EVR-11 is the only case where MnO was not detected, neither during area analyses (Table 11) nor by spots analyses (Table 12), and elemental mapping distribution (Figure 89 B and D). In this case, only FeO was detected in crystallites. Moreover, considering their low contrast on the BSE image and the chemical composition obtained by spot analyses (i.e. the inclusion is extremely rich in FeO and poor in

PbO), they cannot be classified as melanotekite ($\text{Pb}_2\text{Fe}_2\text{Si}_2\text{O}_9$) and they are most probably hematite (Fe_2O_3) crystals.

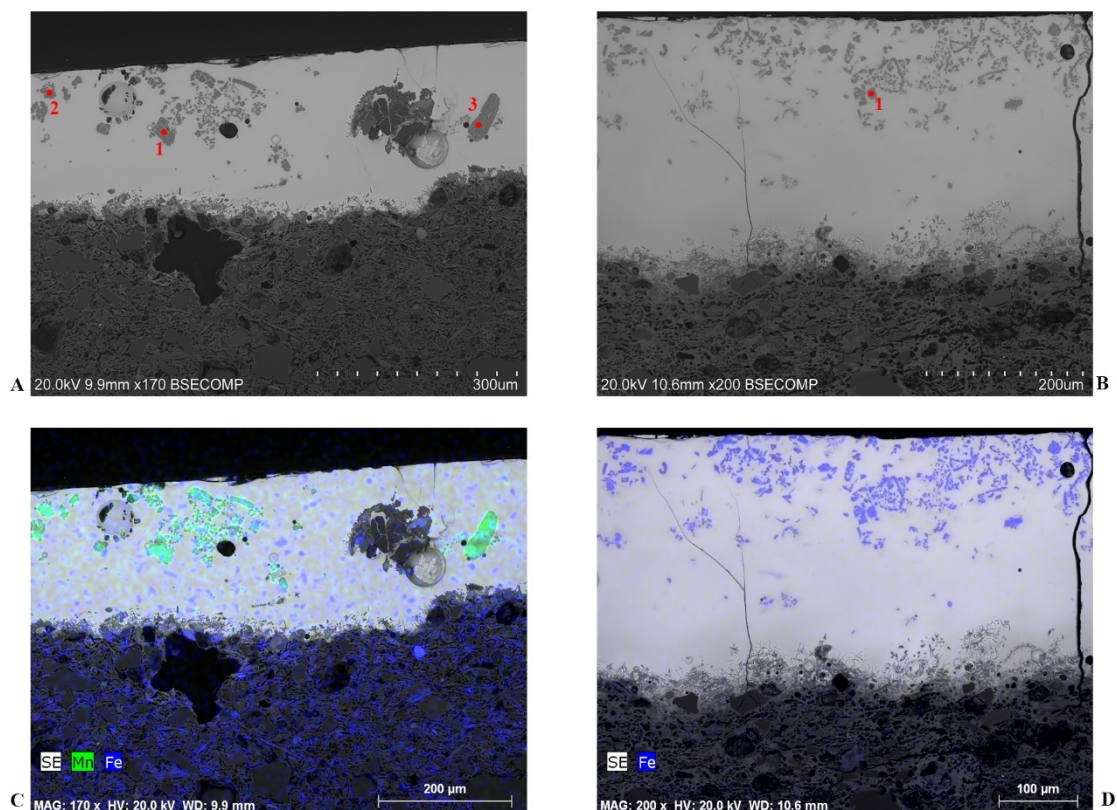


Figure 89: EVR 2, Mn-bearing components present in high amount within the black decoration as they did not dissolved during the firing process, developing new crystalline compounds (A-C). EVR 11, Fe-bearing components as a main mineral pigment for black decoration colouring (i.e. hematite) (B-D). The mineral colourants were applied overglaze and grew towards the glaze-body interface during the firing process.

Conversely to specimens EVR 2 and EVR 11, on the black decoration of SIL 25 and SIL 26 a slightly different situation has been detected. In both cases MnO and FeO were always detected during elemental mapping distribution, area and spot analyses (Figure 90, Table 12). In both cases, FeO is always more represented, suggesting that the pigment was mainly enriched in this oxide.

On specimen SIL 25, MnO and FeO are generally dissolved in the glaze. Nevertheless, two different kinds of crystallites have been analysed by SEM-EDS. The first one (Figure 90A, spot 1) probably represent the raw material (i.e. the pigment) applied on the glaze surface. The high concentration of SiO_2 (42.47 wt%) suggest it was a clayey material enriched in MnO (1.71 wt%) and FeO (11.88 wt%). The second one considering the high concentration of FeO (80 wt%) is most probably an hematite crystal (Fe_2O_3) (Figure 90A, spot 2).

On specimen SIL 26 a high amount of colouring agent was applied on the glaze surface, and many crystallites almost completely cover the glaze in its all thickness. Elemental mapping distribution (Figure 90 B and D) and spot analyses (Figure 90B, spot 2) evidence that some crystallites are FeO rich (80 wt%), they show low contrast on BSE image, and they can be probably classified as hematite crystals (Fe_2O_3).

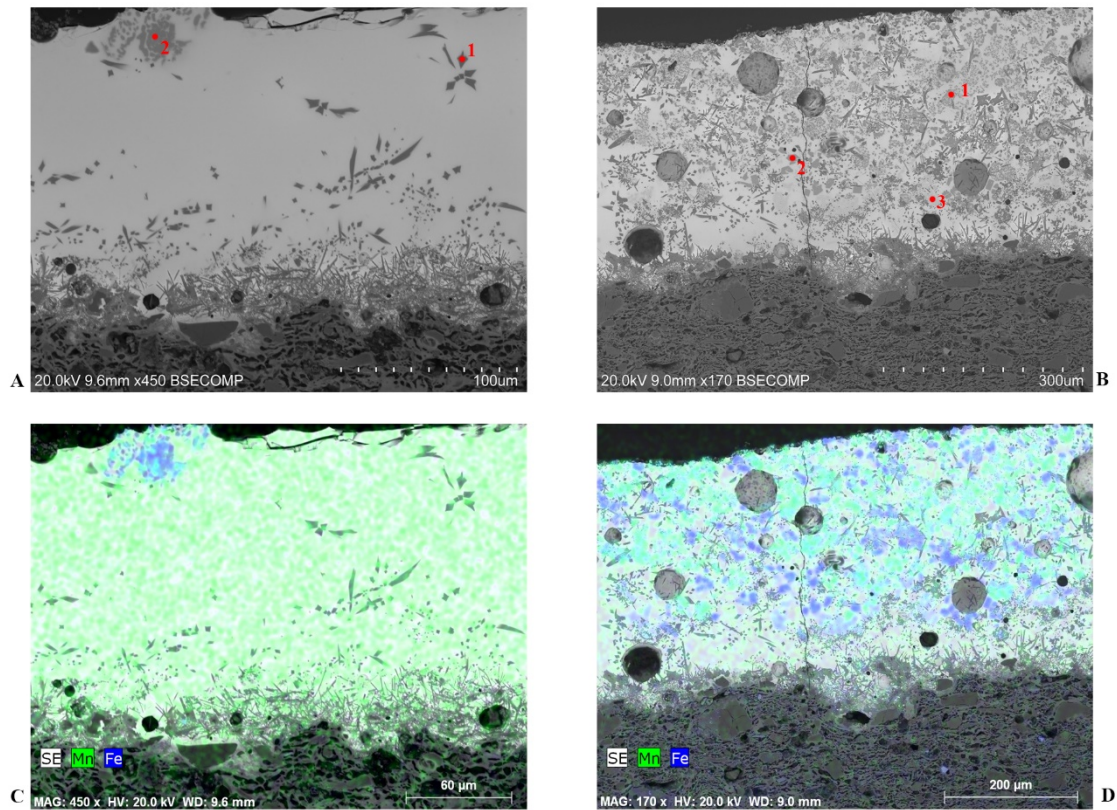


Figure 90: SIL 25 possibly displaying undissolved particles of the raw materials and from the Fe-bearing metallic pigments (A-C). SIL 26 displaying Fe-bearing undissolved particles (i.e. Hematite) (B-D).

Moreover, also other small inclusions, which are scattered all over the glaze surface, show low contrast on BSE image (Figure 90B, spot 1, 2 and 3), in addition to FeO and MnO superimposition in elemental mapping distribution (Figure 90D). Micro-analysis determined their chemical composition, evidencing that FeO (44.68 wt%) is more represented than MnO (15.63 wt%). Basing on these observations, the inclusions are probably an iron and manganese oxide, and they can possibly classified as jacobite (MnFe_2O_4) (Figure 90B, spot 1). This inclusion type probably crystallized during firing by the combination of manganese- and iron-rich raw material (Molera et al., 2013).

The last inclusion identified in the decoration (Figure 90B, spot 3) shows high contrast on the BSE image. Thus, PbO was surely included in the internal crystallite structure. Moreover, also in this case, elemental mapping distribution indicate Fe and Mn superimposition in the same

position. Considering the crystallite chemical composition (Table 12), this mineral can be probably included in the solid solution which normally include melanotekite ($\text{Pb}_2\text{Fe}_2\text{Si}_2\text{O}_9$) and Kentrolite ($\text{Pb}_2\text{Mn}_2\text{Si}_2\text{O}_9$) (Pradell et al., 2013).

Table 12: Chemical composition of analysed crystallites by means of point analysis.

Oxides Wt% - Black Decoration - Spot Analyses													
Samples	Points	Na₂O	MgO	Al₂O₃	SiO₂	P₂O₅	K₂O	CaO	TiO₂	MnO	FeO	BaO	PbO
EVR-2	1	0.52	0.71	4.75	20.63		1.01	3.22	0.82	56.21	0.44		11.69
	2	0.41	0.36	2.55	16.04		0.23	1.17	1.04	68.31	1.43		8.45
	3	0.20	0.34	2.72	14.40		0.41	2.03	1.27	67.96	1.20		9.46
EVR-11	1	0.53	0.55	2.90	11.86		0.43	1.73	1.61		68.87		11.52
SIL-25	1	0.71	4.90	5.64	42.47	0.33	1.57	19.86		1.71	11.88	1.27	9.66
	2	0.43	0.12	2.76	6.76	0.14	0.33	0.91	0.02	1.98	80.02	1.59	4.93
SIL-26	1	0.70	3.70	3.08	12.77		0.82	2.53	1.04	15.63	44.68		15.06
	2	0.00	0.43	2.08	6.62		0.31	1.28	0.81	3.54	80.04		4.88
	3	0.73	0.55	3.58	13.00		0.53	2.53	1.60	5.01	47.80		24.67

CHAPTER 7: FINAL REMARKS

The present thesis studies the Islamic glazed pottery found in Évora, and its comparison with other cities such as Mértola and Silves. The analysed specimens belong to these three sites and they consist of monochromatic and black-decorated dichromatic honey glazes and coarsewares.

The chemical and mineralogical analyses were carried out in order to answer four main questions related to the production technology, provenance and trade. The following description is the response to those matters, based on the analytical results obtained.

1. To establish whether monochromatic and honey and black ceramics were produced in the city of Évora during the Islamic time or were imported in the city.

It was reported that the Pottery Fabric 1 is the local production from the city of Évora. It coincides with the regional geology. It was documented the manufacture of coarsewares, namely, unglazed cookwares and tablewares. The glazed collection of the city underwent to a comparison with the glazed ceramic from Mértola and Silves, giving rise to their similarities regarding the clay and tempering material used. Thus, none of the remaining five pottery fabrics identified were produced locally. This statement does not rule out the local production of glazed ceramic but the results point out to the relationship of Évora with other cities during the Islamic time, being an important crossroad towards some harbour cities such as Lisbon and Alcácer do Sal (Galiza, 2012).

2. To analyse glazed ceramic production recovered in Silves and Mértola to establish whether monochromatic and/or honey and black ceramic show similar characteristics to Évora glazed ceramics.

The comparative analysis of the glaze from the cities of Évora, Mértola and Silves corroborated the traditional glazing technique in the *al-Andalus*. It consisted of transparent high-lead glaze, obtained by the use of frits and applied over biscuit-fired calcareous-rich ceramic bodies.

Every step of the traditional glaze recipe was corroborated in the entire glazed collection. The exclusive use of lead and its benefits were checked in the final glaze appearance. Evenly, the extensive use of frits, documented from the beginning of the glazed pottery production over a pre-fired calcium-rich bodies (Salinas et al., 2019), was corroborated by the limited glaze-body interaction layer and the uniform and homogenous glaze formation. Additionally, the beneficial

properties of calcareous clay were confirmed. Thereby, the glazed ceramic pieces retrieved from Évora, Mértola and Silves are an example of a recurrent glazing practice based on their constituent processes, in spite of being identified some differences.

The results demonstrated particular differences in the preferential and variable use of raw materials, which reflect a particular way to manufacture glaze and ceramic during the Islamic period. On one hand, it was able to identify two types of clayey material employed for glaze production, namely, calcareous and non-calcareous clays. This differentiated use of clay materials seems to be related to different workshops, the vessel function and its fate in term of a local or non-local market. Also, the high-calcium content variability observed in ceramic bodies reflect a workable clay paste's preparation process in which the desirable calcium-bearing components were added (Molera et al., 1996).

It was possible to distinguish another glazing technique by the application of alkali materials as fluxes. One of them was the white tin-opacified glaze, in which the addition of alkali component was part of the recipe for obtaining whitish colours. The rest seems to be part of experimentation (EVR 17) and/or the production of particular workshops from the southernmost area of the Iberian Peninsula, such as it can see in EVR 12 and MER 24.

3. To establish whether some glazed ceramics were imported from a different area of the al-Andalus.

None of the glazed specimens come from the city of Évora. The identification of different raw materials into the ceramic paste, especially temper inclusions, were determinant for such a statement. All the glazed pottery, made up of calcareous clay, belongs to the south towards Mértola and Silves. However, two specimens not only represent a distinctive glaze production (i.e. alkali content) but, due their higher calcareous clay bodies, may point out a provenance area rich in calcium clay sources.

In the case of Mértola, most of the glazed specimens were locally produced. However, the presence of an alkali-bearing glazed specimen with a higher calcareous ceramic body, reflects an introduction (i.e. imported) from areas with Ca-rich clay sources, similar to the situation of Évora. Although, the possibility was much more prone in Mértola owing to their function as a riverine port during the Islamic period.

The glazed specimens from Silves, according to the underlying ceramic body, is compatible with the geological setting of the city. The production was local and the overland trading was directed to inland markets such an Évora.

4. To evaluate glaze technology over time.

The established time framework for the collection goes from 10th to mid-13th centuries AD, corresponding to the Islamic period. In this timelapse, the glazed pottery production was characterized by high lead contents, with a decrease in its quantity over time being clearly notified in a subsequent glazed pottery technology called Hispano Moresque.

The series of analyses carried out upon the glazed coating and the underlying clay body demonstrated a continuity not only by the use of high lead as a main flux, but also in other typical signatures of the Islamic production technology.

Islamic glazed pottery production was characterized for using frits and calcareous ceramic bodies which, due to all the benefits during the glaze forming, were previously fired. Evenly, in the case of metallic pigments, the persistence of iron and manganese as main colourants were still being used into the glaze mixture and black decoration, respectively.

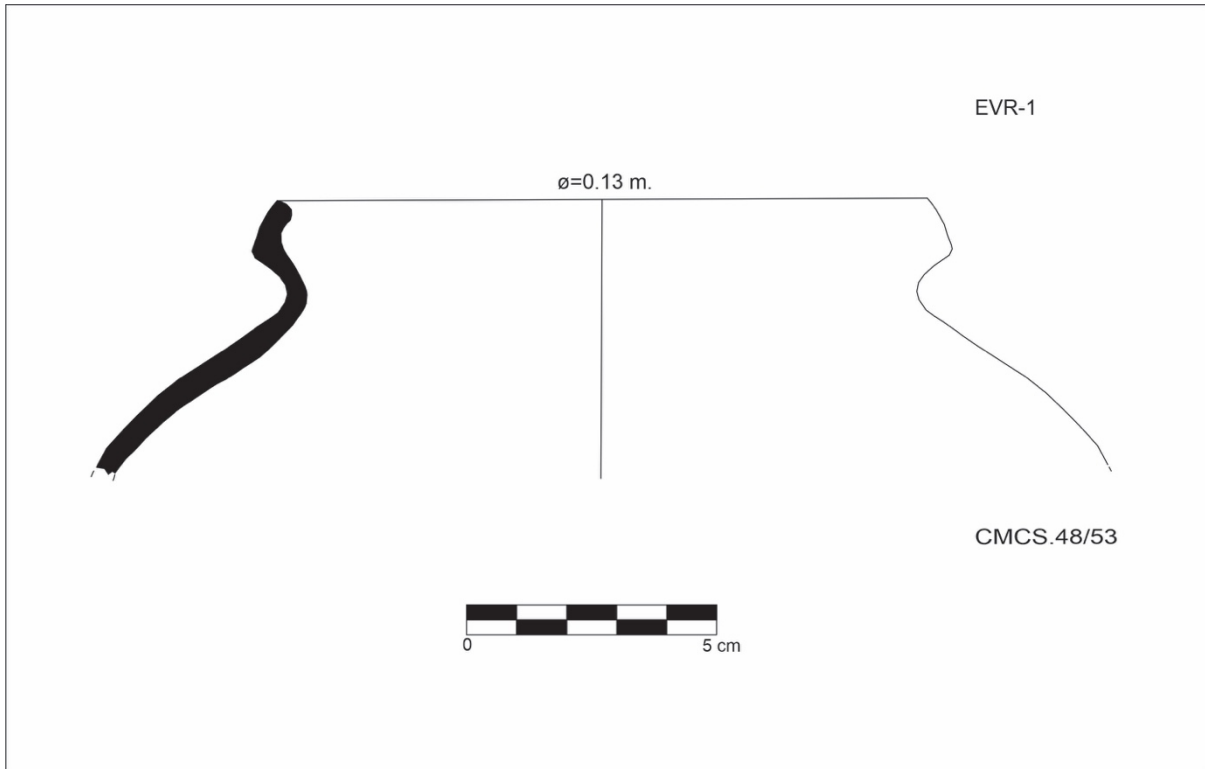
In the case of tin-opacified glazed pottery, the traditional glaze recipe for making white glazes was similar from the onset of this technique, using frits over fired-biscuit calcareous clay bodies.

Therefore, despite the reduced number of specimens, it can say that the analysed collection represents the Islamic glazed pottery production and, yet some variations were observed, the traditional recipe for making glazes and ceramic bodies was preserved.

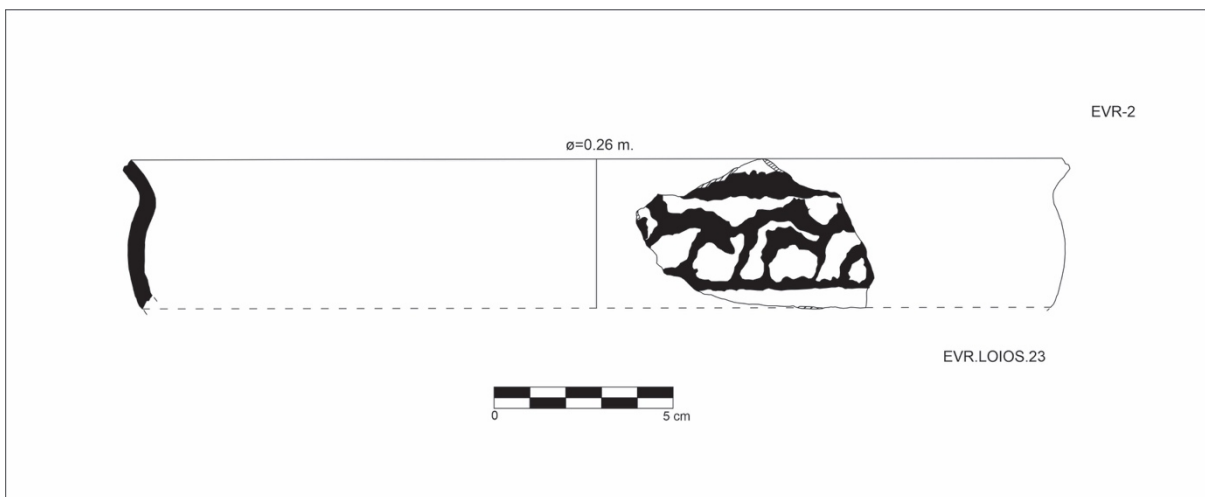
CHAPTER 8: APPENDICES

Appendix I

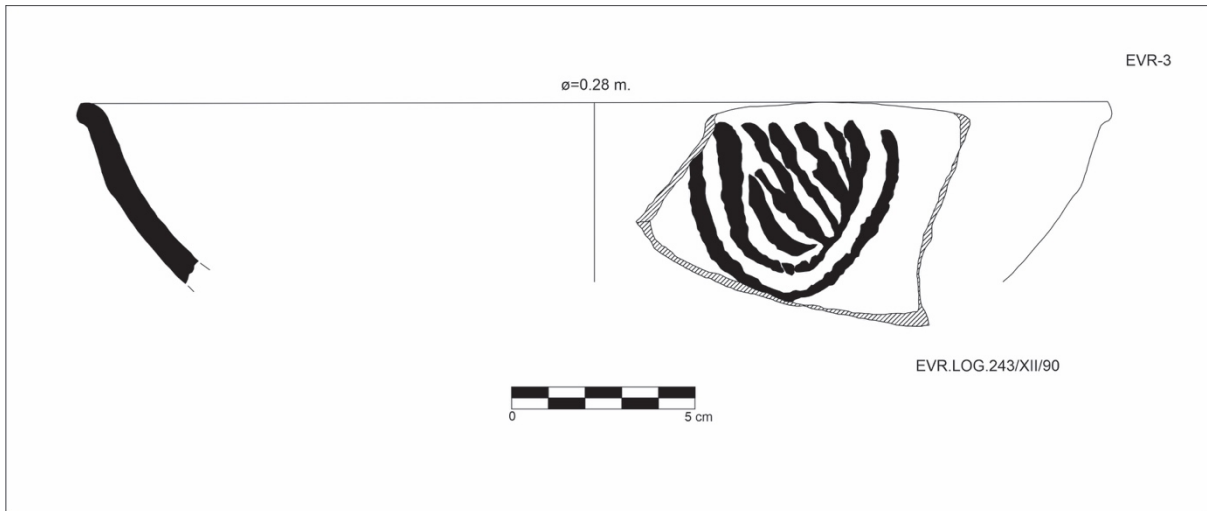
EVR 1



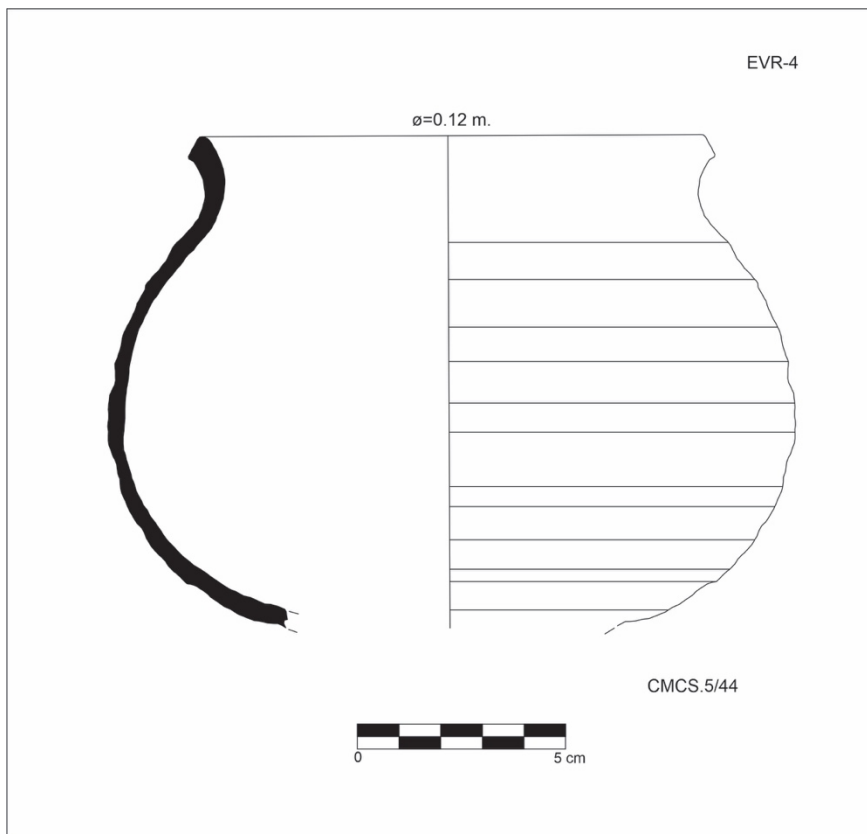
EVR 2



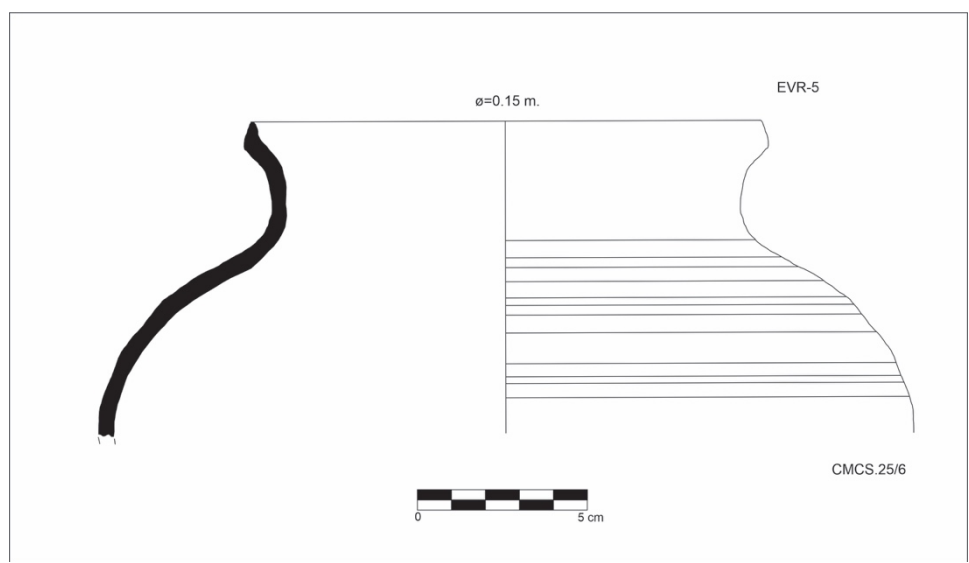
EVR 3



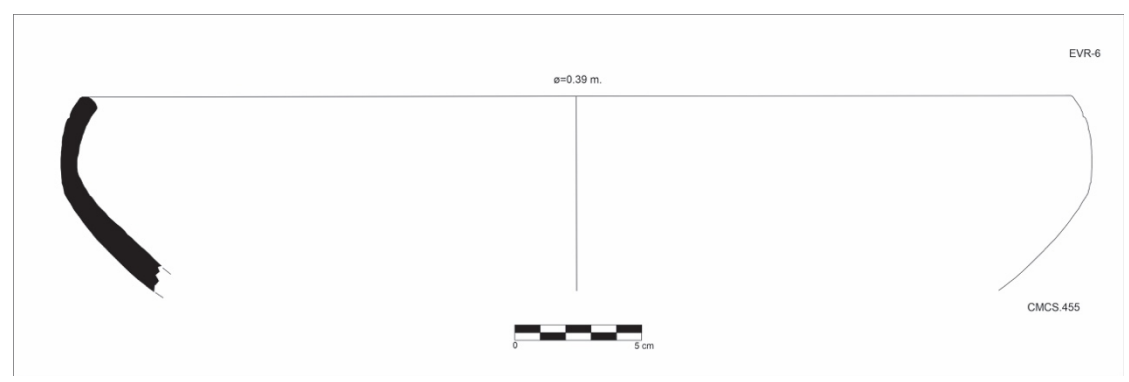
EVR 4



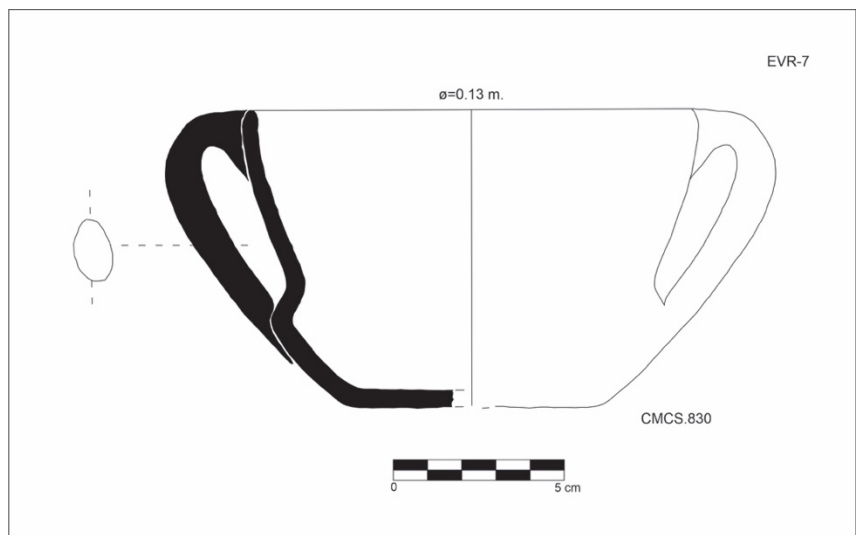
EVR 5



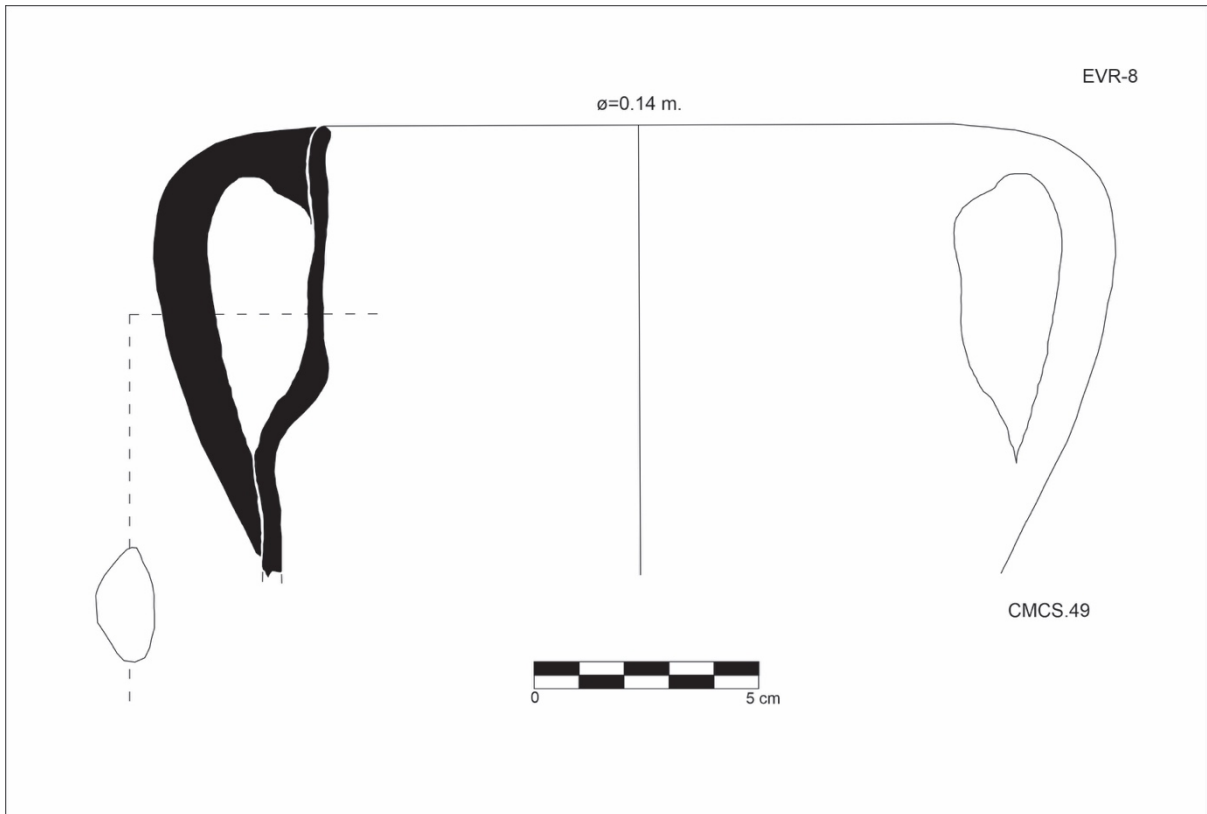
EVR 6



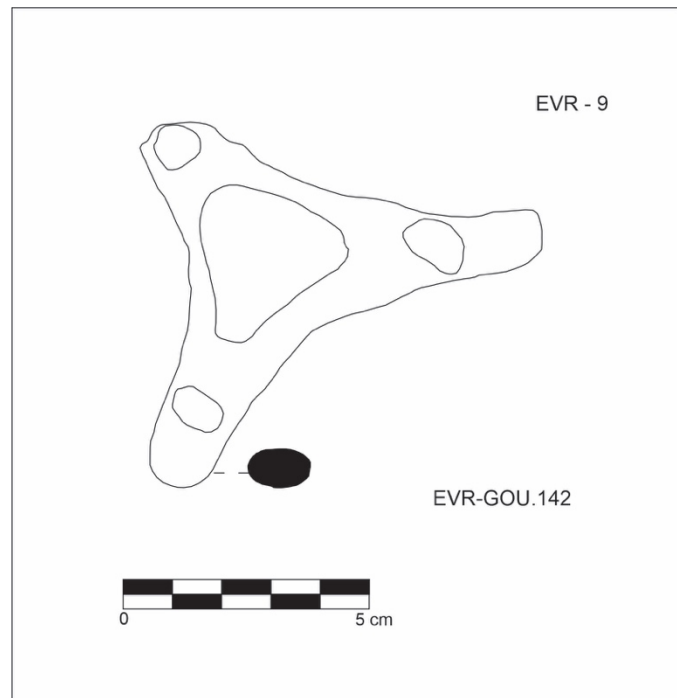
EVR 7



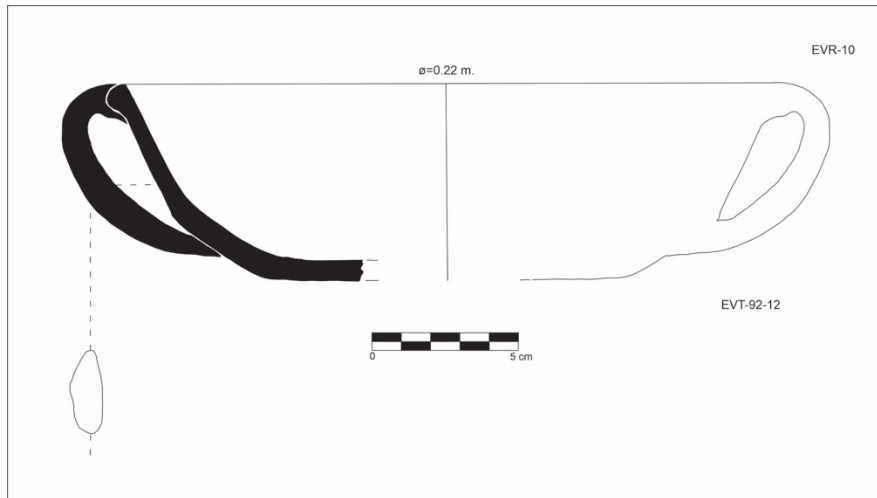
EVR 8



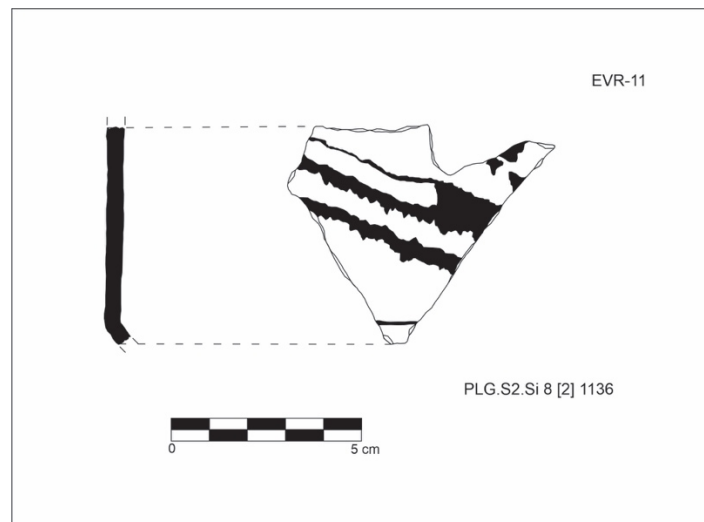
EVR 9



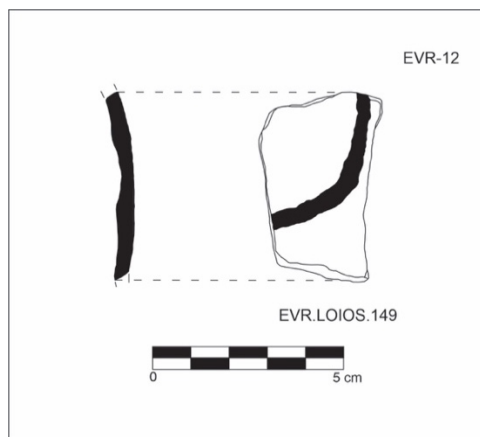
EVR 10



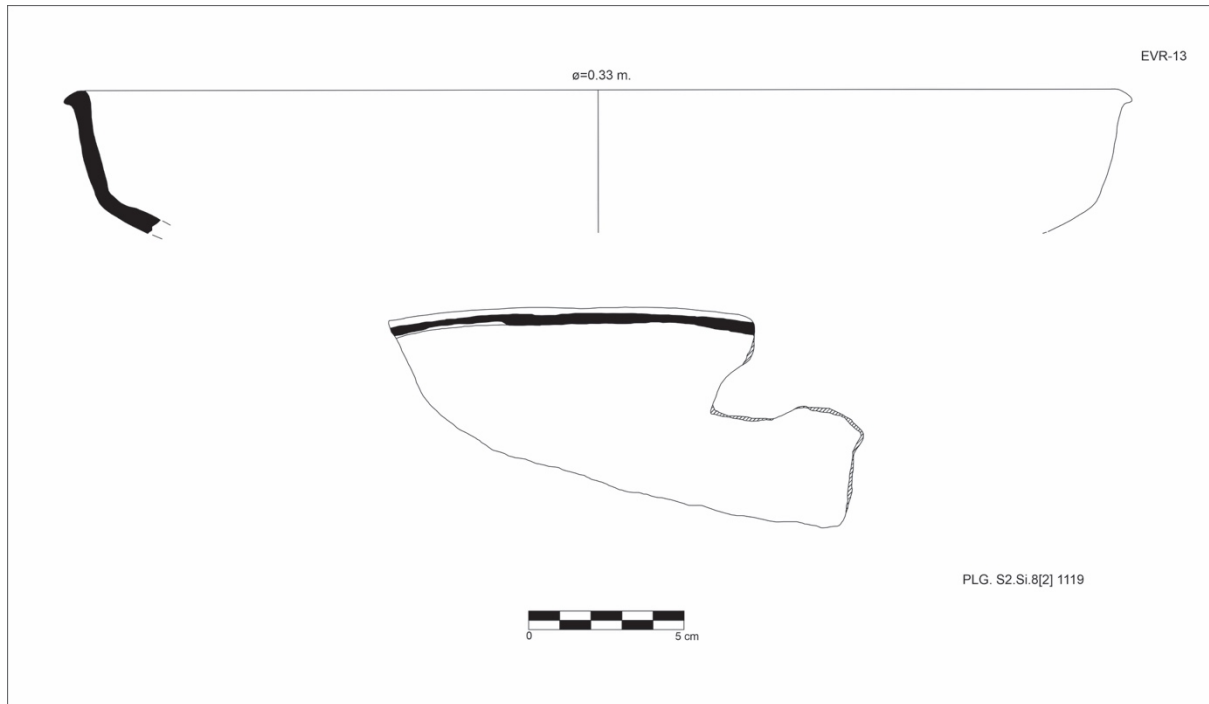
EVR 11



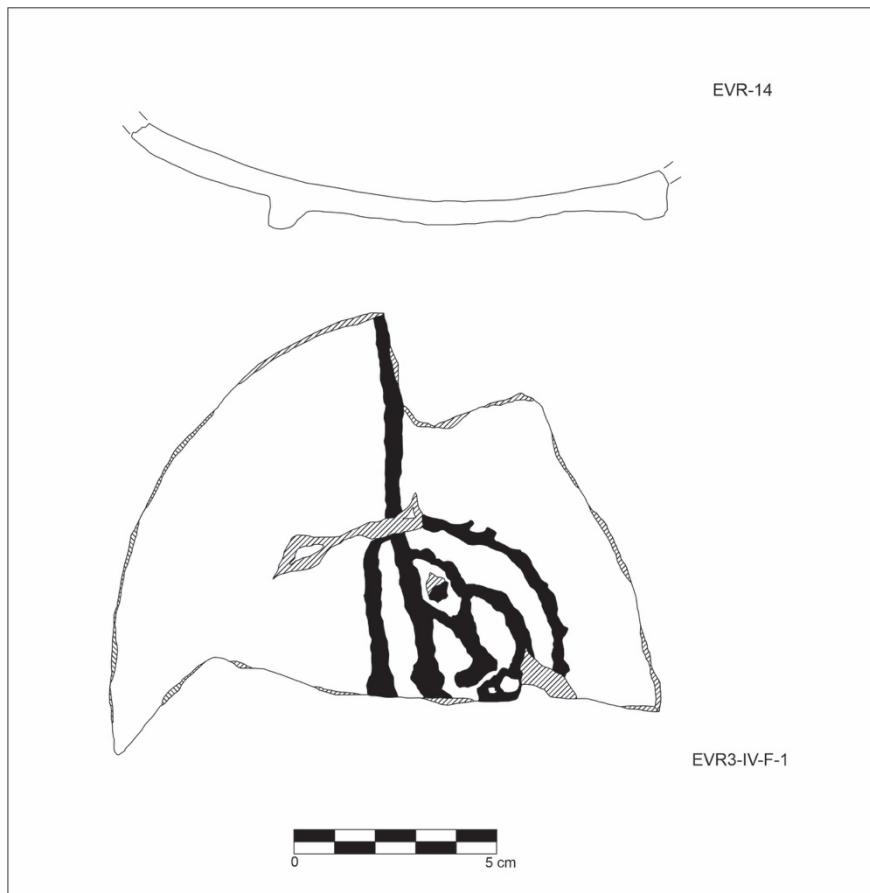
EVR 12



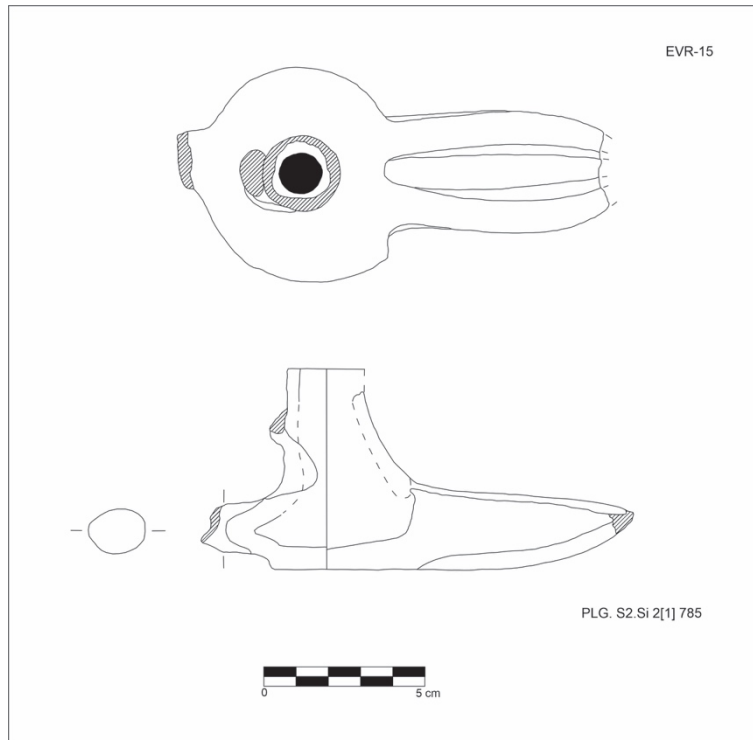
EVR 13



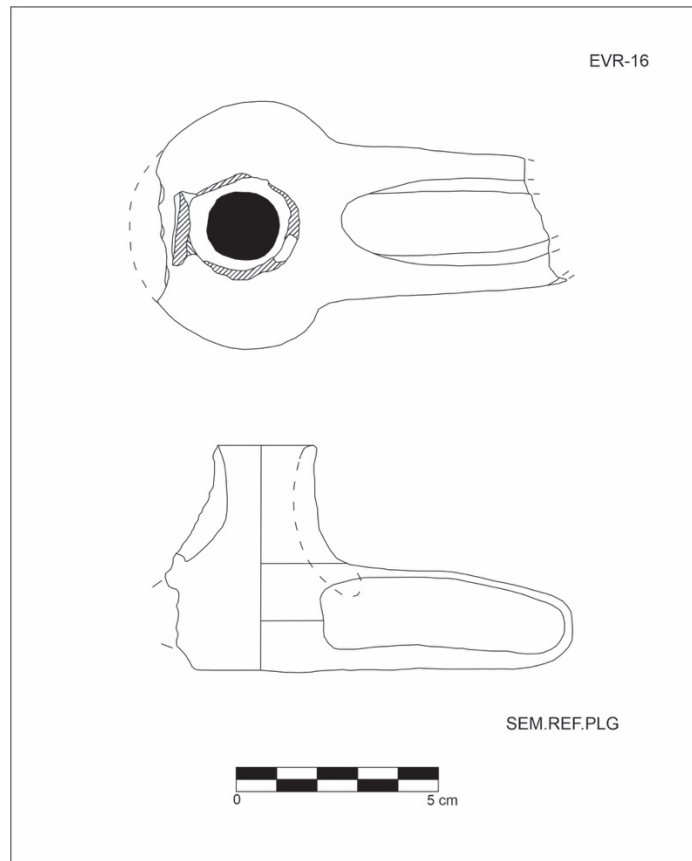
EVR 14



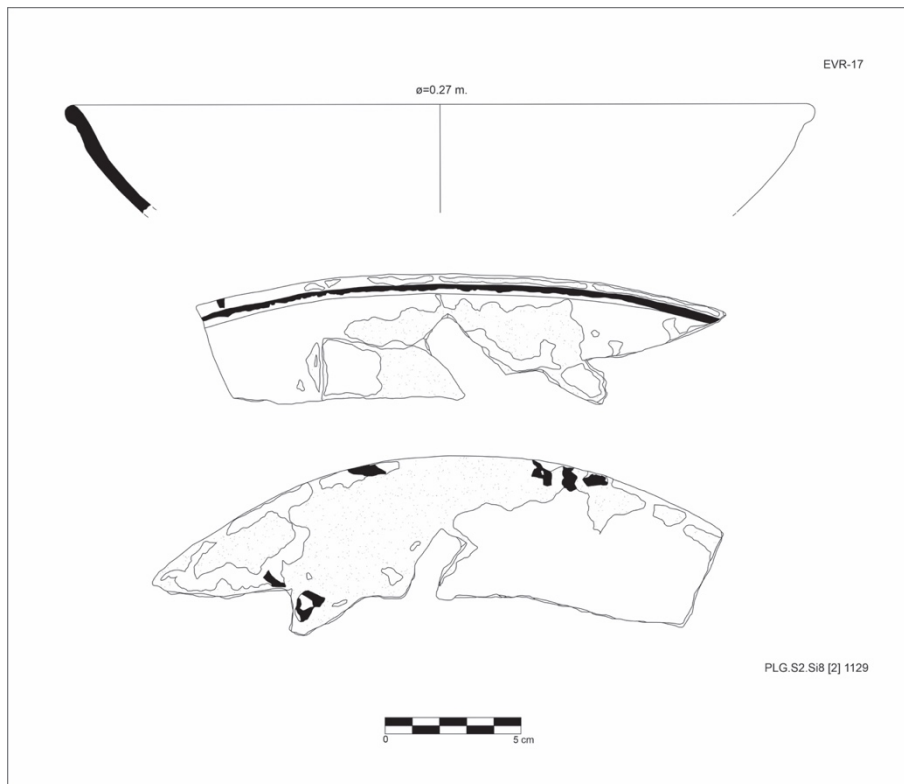
EVR 15



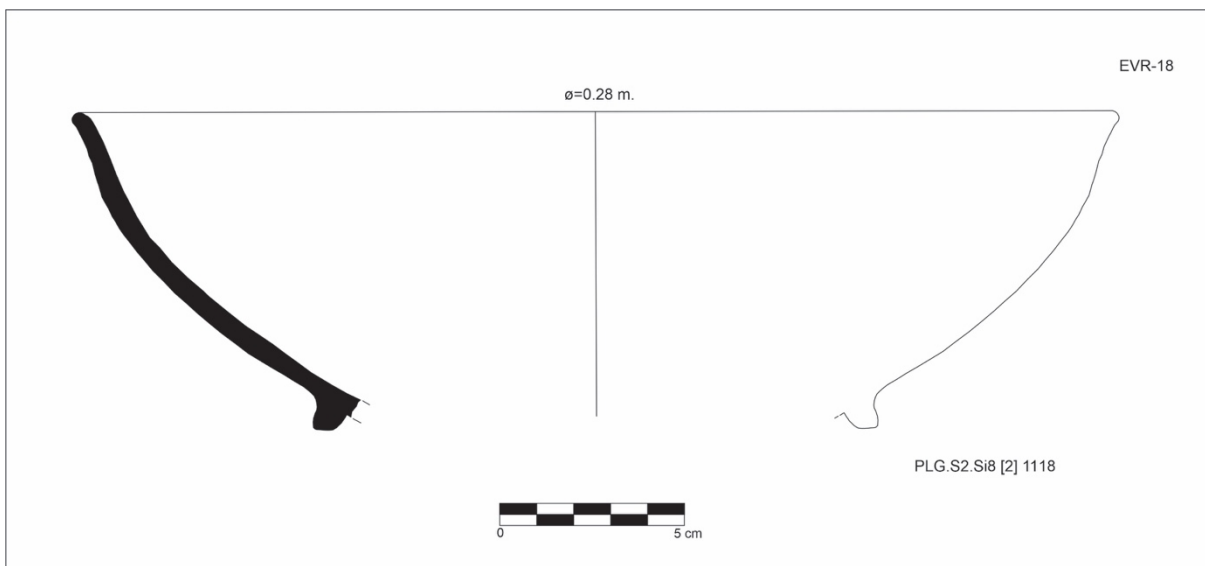
EVR 16



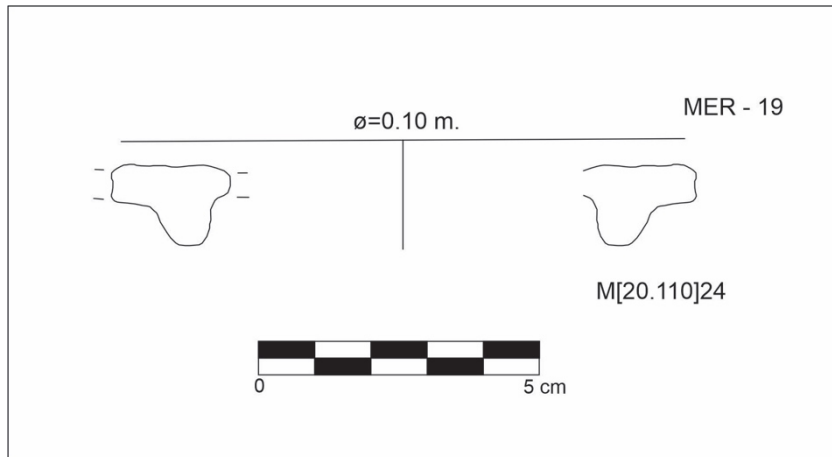
EVR 17



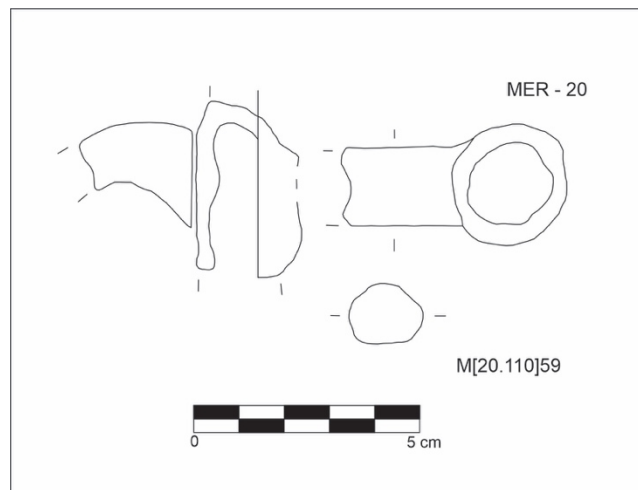
EVR 18



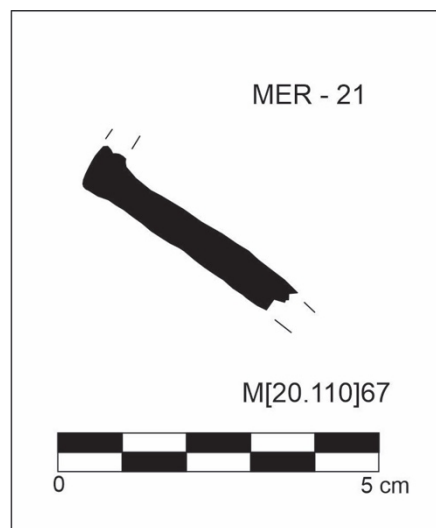
MER 19



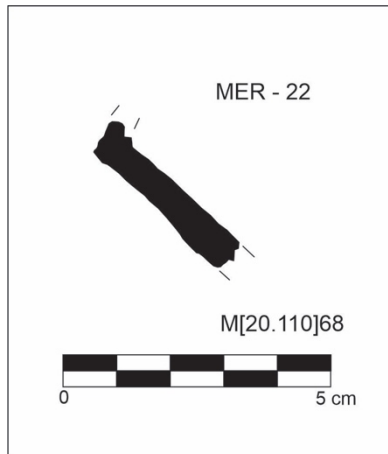
MER 20



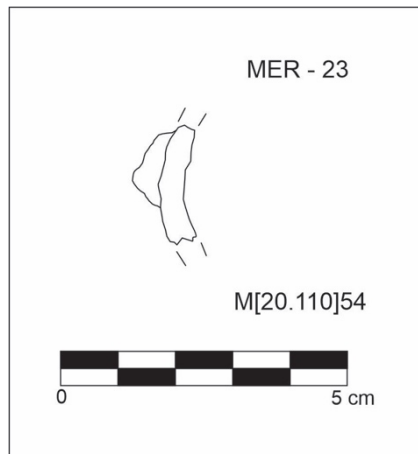
MER 21



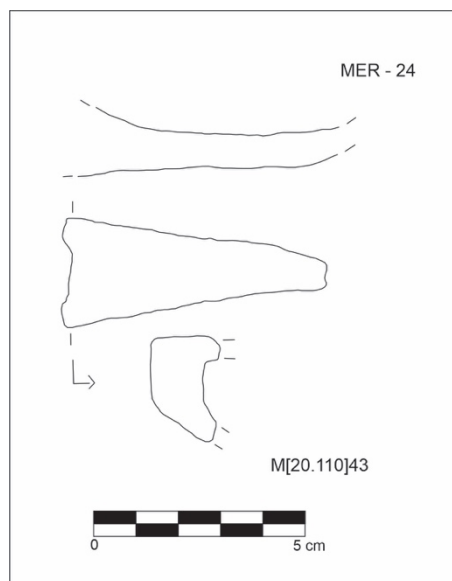
MER 22



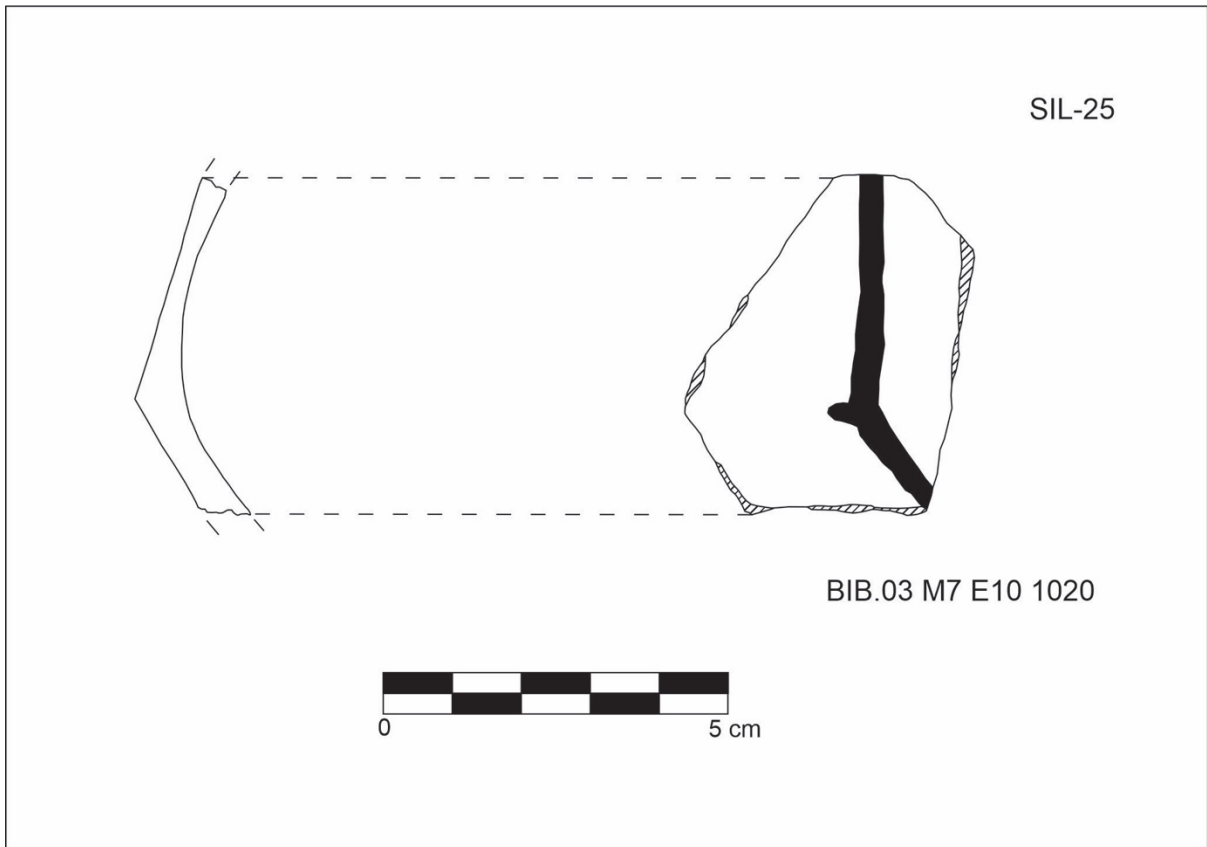
MER 23



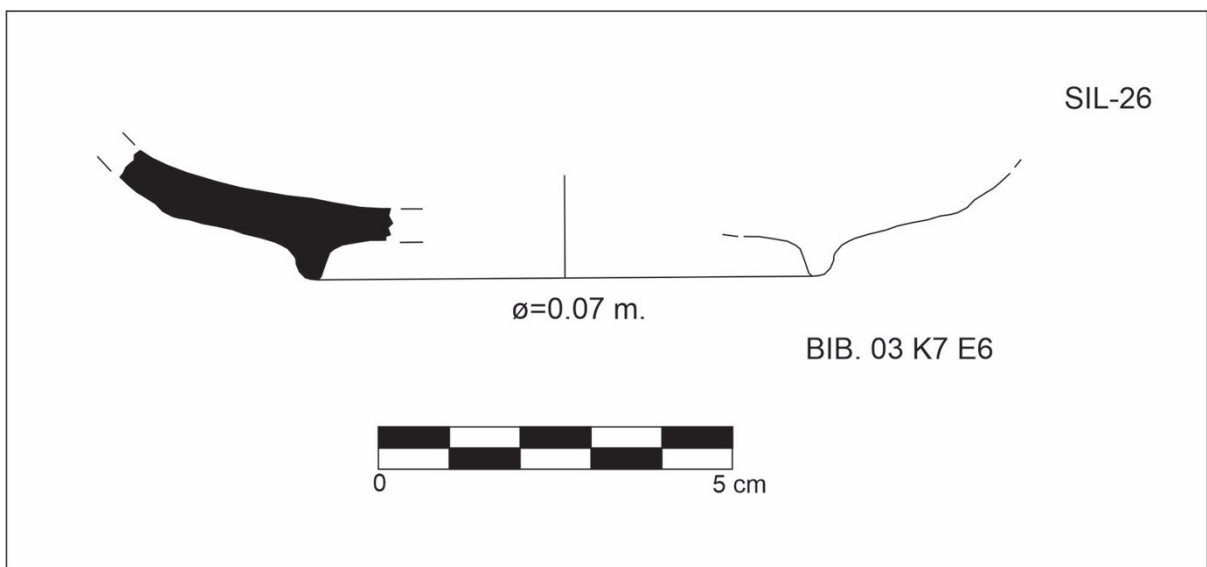
MER 24



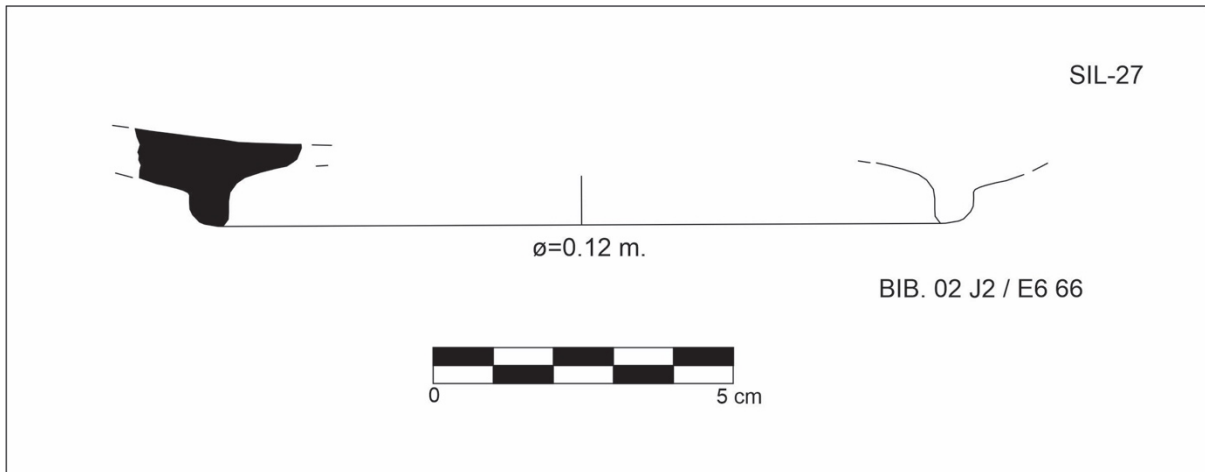
SIL 25



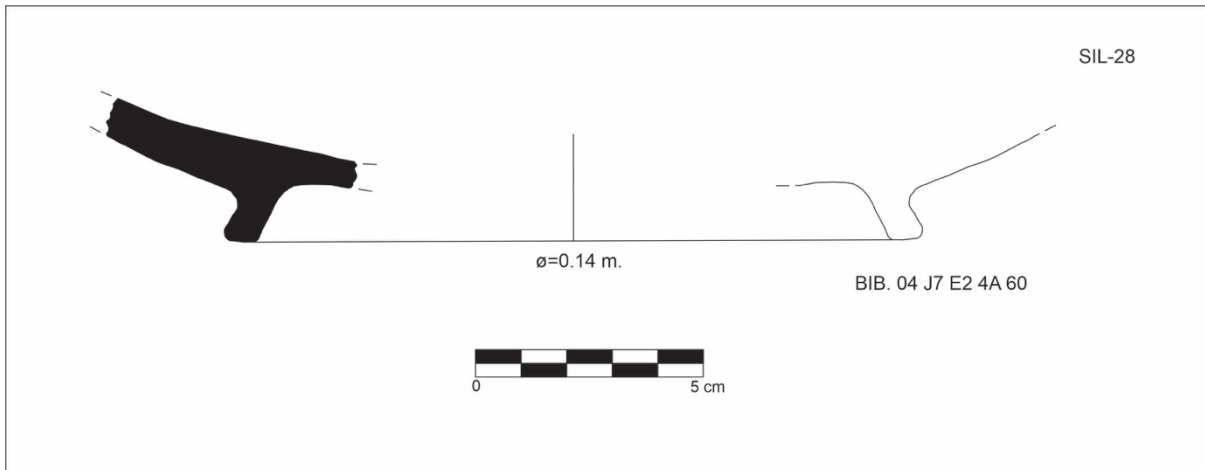
SIL 26



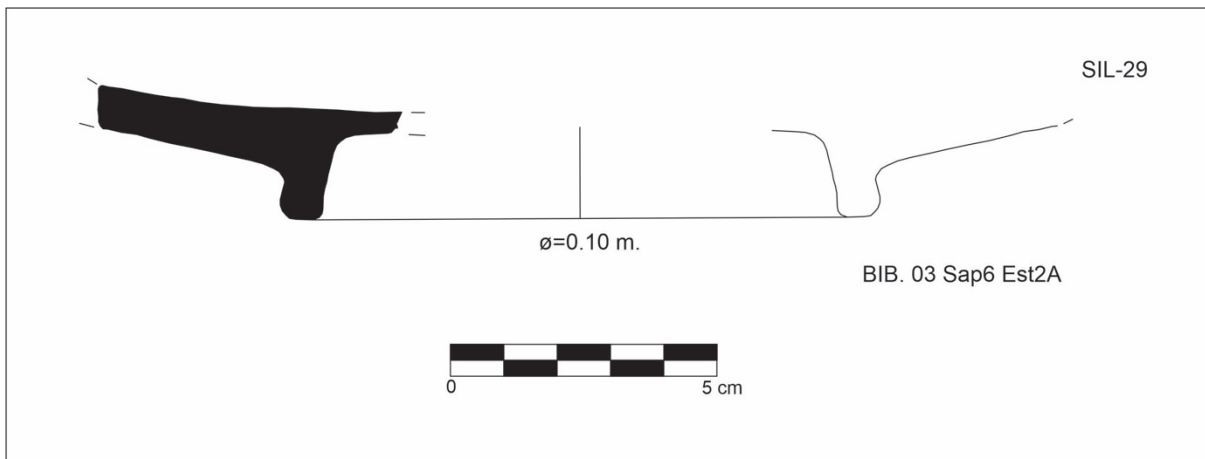
SIL 27



SIL 28



SIL 29



CHAPTER 9: REFERENCES

- Acien, A. et al. (1991). Evolución de los tipos cerámicos en el S.E. de Al-Andalus. In *Actes du 5eme Colloque sur la ceramique medieval en Mediterranee occidentale* (pp. 125-139).
- Almodóvar, G. et al. (2019). Massive sulfide ore in the Iberian Pyrite Belt: mineralogical and textural evolution. In *Minerals* 9 (653) (pp. 1-20).
- Aras, A. (2003). The change of phase composition in kaolinite- and illite-rich clay-based ceramic bodies. In *Applied Clay Science* 24 (pp. 257-269).
- Arai, T. (2006). Introduction. In B. Beckhoff, B. Kanngießer, N. Langhoff, R. Wedell, & H. Wolff (Eds.), *Handbook of practical X-ray fluorescence analysis* (pp. 1-31).
- Arkadiev, V., Knüpfer, W., & Langhoff, N. (2006). X-ray tubes. In B. Beckhoff, B. Kanngießer, N. Langhoff, R. Wedell, & H. Wolff (Eds.), *Handbook of practical X-ray fluorescence analysis* (pp. 36-54).
- Beltrame, M. et al. (2020). Comparative pottery technology between the middle ages and modern times (Santarém, Portugal). In *Archaeological and Anthropological Sciences* 12 (130) (pp. 1-31).
- Beltrame, M. et al. (2021). The Islamic ceramic of the Santarém *Alcaçova*: raw material, technology, and trade. In *Archaeometry* 63 (7) (pp. 1-21).
- Braekmans, D. & Degryse, P. (2017). Petrography. Optical Microscopy. In M. Alice & W. Hunt (Eds.), *The Oxford handbook of archaeological ceramic analysis* (pp. 233-265). Oxford: University Press.
- Bugalhão, J. et al. (2010). CIGA: projecto de sistematização para a cerâmica islâmica do Gharb al-Ândalus. In *XELB* 10 (pp. 455-476).
- Chapoulie, R. et al. (2005). Cuerda seca ceramics from Al-Andalus, Islamic Spain and Portugal (10th-12th centuries AD): investigation with SEM-EDX and cathodoluminescence. In *Archaeometry* 47 (3) (pp. 519-534). University of Oxford.
- Coradeschi, G. (2017). Investigação arqueobotânica dos sedimentos arqueológicos de Paço dos Lobos da Gama: um arrabalde islâmico da cidade de Évora (séculos XI-XII). In *digitAR* 4 (pp. 33-40).
- Cultrone, G. et al. (2001). Carbonate and silicate phase reactions during ceramic firing. In *European Journey of Mineralogy* 13 (pp. 621-634).
- Cullum, B. & Vo-Dinh, T. (2003). Sample collection and preparation of liquid and solids. In G. Gauglitz & T. Vo-Dinh (Eds.), *Handbook of Spectroscopy* (pp. 17-35).
- Di Febo, R. et al., (2017a). Technological implication of neo-formed hematite crystals in ceramic leas glazes. In *Star: Science & Technology of Archaeological Research* 3 (2) (pp. 366-375).

- Di Febo, R. et al. (2017b). Thin-section petrography and SR- μ XRD for the identification of microcrystallites in the brown decorations of ceramic lead glazes. In *European Journal of Mineralogy* 29 (pp. 861-870).
- Di Febo, R. et al. (2017c). the production of a lead glaze with galena: Thermal transformations in the PbS-SiO₂ system. In *Journal of the American Ceramic Society* 101 (pp. 2119-2129).
- Duminuco, P., Messiga, B., Riccardi, M. (1998). Firing process of natural clays. Some microtextures and related phase compositions. In *Thermochimica Acta* 321 (pp. 185-190).
- El Ouahabi, M. et al., (2015). Modified mineral phases during clay ceramic firing. In *Clays and Clay Minerals* 63 (5) (pp. 404-413).
- Fabbri, B., Gualtieri, S., Shoval, S. (2014). The presence of calcite in archaeological ceramics. In *Journal of the European Ceramic Society* 34 (pp. 1899-1911).
- Lopes, G. & Santos, J. (2015). Cerâmicas islâmicas da Natatio das Termas Romanas de Évora. In *X Actas do Congresso Internacional a cerâmica medieval no Mediterrâneo* (pp. 346-352).
- Galiza, V. (2012). Contributo para o conhecimento da presença islâmica em Yābura. Dissertação de Mestrado em Arqueologia. Univesidade Nova de Lisboa.
- Gonçalves, M. (2008). Silves Islâmico. A muralha do arravalde oriental e a dinâmica de ocupação do espaço adjacente. Mestrado em Teoria e Métodos da Arqueologia. Univesidade do Algarve.
- Gonçalves, M., Pires, A., Mendonça, C. (2009). Utensílios do quotidiano de um arrabalde Islâmico de Silves: análise preliminar da louça de cozinha. In *XELB* (9) (pp. 695-706).
- Gómez S. (2004). La ceramica Islamica de Mértola: produccion y comercio. Memoria para optar al grado de doctor. Univerisidad Complutense de Madrid.
- Gómez S., Grange, M., Lopes, G. (2012). A cerâmica islâmica no Alentejo. In *Arqueologia Medieval* 12 (pp. 109-119).
- Gómez, S. et al. (2015). A cidade e o seu território no Gharb Al-Andalus através da cerâmica. In *X Actas do Congresso Internacional a cerâmica medieval no Mediterrâneo* (pp. 19-50).
- Hall, M. (2017). X-ray fluorescence-energy dispersive (ED-XRF) and wavelength dispersive (WD-XRF) spectrometry. In M. Alice & W. Hunt (Eds.), *The Oxford handbook of archaeological ceramic analysis* (pp. 342-362). Oxford: University Press.
- Heimann, R. (2017). X-ray powder diffraction (XRPD). In M. Alice & W. Hunt (Eds.), *The Oxford handbook of archaeological ceramic analysis* (pp. 337-341). Oxford: University Press.
- Heimann, R. & Maggetti, M. (2019). The struggle between thermodynamics and kinetics: phase evolution of ancient and historical ceramics. In *EMU Notes in Mineralogy* 20 (6) (pp. 233-281).
- Injuk, J., Van Grieken, R., Blank, A., Eksperiandova, L., & Buhrke, L. (2006). Specimen preparation. In B. Beckhoff, B. Kanngießer, N. Langhoff, R. Wedell, & H. Wolff (Eds.), *Handbook of practical X-ray fluorescence analysis* (pp. 411-432).

- Janssens, K. (2003). X-ray fluorescence analysis. In G. Gauglitz & T. Vo-Dinh (Eds.), *Handbook of Spectroscopy* (pp. 365-420).
- Janssens, K. & Van Grieken, R. (2004). Introduction and overview. In K. Janssens & R. Van Grieken (Eds.), *Non-destructive microanalysis of cultural heritage* (pp. 1-11). Belgium: University of Antwerp.
- Janssens, K. (2004). X-ray based methods of analysis. Introduction and overview. In K. Janssens & R. Van Grieken (Eds.), *Non-destructive microanalysis of cultural heritage* (pp. 129-226). Belgium: University of Antwerp.
- Jenkins, R. (1999). X-ray fluorescence spectrometry. New York: Willey Interscience.
- Langhoff, N. & Simionovici, A. (2006). X-ray sources. In B. Beckhoff, B. Kanngießer, N. Langhoff, R. Wedell, & H. Wolff (Eds.), *Handbook of practical X-ray fluorescence analysis* (pp. 33-36).
- Longoni, A. & Fiorini, C. (2006). X-ray detectors and signal processing. In B. Beckhoff, B. Kanngießer, N. Langhoff, R. Wedell, & H. Wolff (Eds.), *Handbook of practical X-ray fluorescence analysis* (pp. 203-262).
- Macias, S. (2014). Casas urbanas e quotidiano no Gharb al-Ândalus. In *Portugal Islâmico. Os últimos sinais do Mediterrâneo* (pp.109-120).
- Malek, Z. et al. (1997). The study of the dehydration and dehydroxylation of smectites by emanation thermal analysis. In *Journal of Thermal Analysis* 48 (pp. 83-92).
- Markowicz, A. (2002). X-ray physics. In R. Van Grieken & A. Markowicz (Eds.), *Handbook of X-ray spectrometry* (pp. 1-94).
- Matin, M., Tite, M., Watson, O. (2018). On the origins of tin-opacified ceramic glazes: New evidence from early Islamic Egypt, the Levant, Mesopotamia, Iran, and Central Asia. In *Journal of Archaeological Science* 97 (pp. 42-66).
- Matin, M. (2019). Tin-based opacifiers in archaeological glass and ceramic glazes: a review and new perspectives. In *Archaeological and Anthropological Sciences* 11 (pp. 1155-1167).
- Molera, J. et al. (1993). The growth of sanidine crystals in the lead of glazes of Hispano-Moresque pottery. In *Applied Clay Science* 7 (pp. 483-491).
- Moita, P. (2008). Granitóides no SW da zona de Ossa-Morena (Montemos-o-Novo – Évora): pretrogénese e processos geodinâmicos. Doctoral thesis. Universidade de Évora.
- Moita, P. et al. (2009). Layered granitoids: interaction between continental crust recycling processes and mantle-derived magmatism. Examples from the Évora Massif (Ossa-Morena zone, southwest Iberia, Portugal). In *Lithos* 111 (pp. 125-141).
- Molera, J. et al. (1996). Hispano-Moresque pottery production of the fourteenth-century workshop of Testar del Moli (Paterna, Spain). In *Archaeometry* 38 (1) (pp. 67-80).
- Molera, J. et al. (1997a). La tecnología de la cerámica Islámica y Mudéjar. In *Caesaraugusta* 73 (pp. 15-41).

- Molera, J., Vendrell-Saz, M., Garcia-Valles, M., Pradell, T. (1997b). Technology and colour development of Hispano-Moresque lead-glazed pottery. In *Archaeometry* 39 (1) (pp. 23-39).
- Molera, J., Pradell, T., Vendrell-Saz, M. (1998). The colours of Ca-rich ceramic paste: origin and characterization. In *Applied Clay Science* 13 (pp. 187-202).
- Molera, J. et al., (1999). Evidence of tin oxide recrystallization in opacified lead glazes. In *Journal of the American Ceramic Society* 82 (10) (pp. 2871-2875).
- Molera, J. et al. (2001). Interactions between clay bodies and lead glazes. In *Journal of the American Ceramic Society* 84 (5) (pp. 1120-1128).
- Molera, J. et al. (2007). Lead frits in Islamic and Hispano-moresque glazed productions. In *From Mine to Microscope: Advances in the Study of Ancient Technology* (pp. 11-22).
- Molera, J. et al. (2013). Manganese brown decorations in 10th to 18th century Spanish tin glazed ceramics. In *Applied Clay Science* 82 (pp. 86-90).
- Molera, J. et al. (2017). Glazes, colourants and decorations in early Islamic glazed ceramics from the Vega of Granada (9th to 12th centuries CE). In *Journal of Archaeological Science* 21 (pp. 1141-1151).
- Nodari, L. et al. (2007). Hematite nucleation and growth in the firing of carbonate-rich clay for pottery production. In *Journal of the European Ceramic Society* 27 (pp. 4665-4673).
- Oliveira, J., Silva, J. (1990). Carta Geológica de Portugal à escala 1:50000, Folha 46-D, Mértola. Serviços Geológicos de Portugal.
- Oliveira, J., Silva, J. (2007). Notícia Explicativa de Folha 46-D, Mértola. Dep. Geologia. INETI.
- Pollard, M. & Heron, C. (1996). *Archaeological chemistry*. Cambridge: Royal Society of Chemistry.
- Pollard, M., Batt, C., Stern, B., & Young, S. M. M. (2006). *Analytical chemistry in archaeology*. Cambridge: Cambridge University Press.
- Pradell, T. & Molera, J. (2020). Ceramic technology. How to characterize ceramic glazes. In *Archaeological and Anthropological Sciences* 12 (189) (pp. 1-28).
- Price, T. D. & Burton, J. H. (2011). *An introduction to archaeological chemistry*.
- Quinn, P. S. (2013). *Ceramic petrography: The interpretation of archaeological pottery & related artefacts in thin section*. Oxford: Archaeopress.
- Riccardi, M., Messiga, B., Duminuco, P. (1999). An approach to the dynamics of clay firing. In *Applied Clay Science* 15 (pp. 393-409).
- Robinson, C. (2011). *The new Cambridge history of Islam*. Cambridge: Cambridge University Press.

Salinas E., Pradell, T., Molera, J. (2019). Glaze production at early Islamic workshop in al-Andalus. In *Archaeological and Anthropological Sciences* 11 (pp. 2201-2213).

Salina, E. & Pradell, T. (2018). The transition from lead transparent to tin-opacified glaze productions in the western Islamic lands: al-Andalus, c. 875-929 CE. In *Journal of Archaeological Science* 94 (pp. 1-11).

Santos, J. (2015). Um olhar sobre o quotidiano de Évora no período medieval – Islâmico. Séculos VIII – XI. Mestrado em Arqueologia e Ambiente. Universidade de Évora.

Santos, J. (2018). Évora durante os séculos VIII-XII, das fontes literárias à materialidade arqueológica. In *Arqueologia Urbana em Centros Históricos* (pp. 212-225).

Santos, J. (2016). Conjunto de cerâmica Omíada (séculos X-XI) do Colégio Dos Meninos do Coro da Sé de Évora. In *Arqueologia Medieval* 13 (pp. 91-100).

Schwedt, A. et al. (2006). Analcime crystallization and compositional profiles. Comparing approaches to detect post-depositional alterations in archaeological pottery. In *Archaeometry* 48 (2) (pp. 237-251). University of Oxford.

Schibille, N. et al. (2020). Ex novo development of lead glassmaking in early Umayyad Spain. In *PNAS Latest Articles* (pp. 1-7).

Shackley, M. (2011). An introduction to X-ray fluorescence (XRF) analysis in archaeology. In M.S. Shackley (Eds.), *X-ray fluorescence spectrometry (XRF) in geoarchaeology* (pp. 7-44).

Schermerhorn, L. (1971). An outline stratigraphy of the Iberian Pyrite Belt. In *Boletim Geológico Mineiro* (82) (pp. 239-268).

Schmeling, M. & Van Grieken, R. (2002). Sample preparation for X-ray fluorescence. In R. Van Grieken & A. Markowicz (Eds.), *Handbook of X-ray spectrometry* (pp. 933-976).

Skoog, D., Holler, F., Crouch, S. (2018). *Principles of instrumental analysis*. Australia.

Teichner, F. (1998). A ocupação do centro da cidade de Évora da época romana à contemporânea. Primeiros resultados da intervenção do Instituto Arqueológico Alemão (lisboa). In *Actas das 2^{as} Jornadas de Cerâmica Medieval e pós-Medieval* (pp. 17-31).

Tite, M. et al. (1998). Lead glazes in antiquity. Methods of production and reason for use. In *Archaeometry* 40 (2) (pp. 241-260).

Tite, M., Wolf, S., Mason, R. (2011). The technological development of stonepaste ceramics from the Islamic Middle East. In *Journal of Archaeological Science* 38 (pp. 570-580).

Tite, M. et al. (2015). Revisiting the beginnings of tin-opacified Islamic glazes. In *Journal of Archaeological Science* 57 (pp. 80-91).

Trindade, M. et al. (2009). Mineral transformation of calcareous rich clays with firing: A comparative study between calcite and dolomite rich clays from Algarve, Portugal. In *Applied Clay Science* 42 (pp. 345-355).

Trindade, M. et al. (2013). Mineralogy and grain-size distribution of clay-rich units of the Algarve basin (south Portugal). In *Clay Minerals* 48 (1) (pp. 59-83).

Trindade, M. et al., (2018). Geochemistry of mudrock units from the Meso-Cenozoic Algarve basin, Portugal. In *Geosciences Journal* (22) (pp. 1-17).

Walton, M. & Tite, M. (2010). Production technology of roman lead-glazed pottery and its continuance into late antiquity. In *Archaeometry* 52 (5) (pp. 733-759).

Whitbread, I. (2017). Fabric description of archaeological ceramics. In M. Alice & W. Hunt (Eds.), *The Oxford handbook of archaeological ceramic analysis* (pp. 200-216). Oxford: University Press.